Peer Review File

Manuscript Title: Pivotal role of reversible NiO6 geometric conversion in oxygen evolution

Reviewer Comments & Author Rebuttals

Reviewer Reports on the Initial Version:

===== Referees' comments =====

Referee #1 (Remarks to the Author):

Wang et al. report the light-induced activation of Ni oxide for the oxygen evolution reaction.
A. The key results are
R1 NR-NiOOH and also the well known NiFe LDH activate over the course of hours (on carbon cloth) or about a minute (ITO) under simulated sunlight irradiation (at 300 W).
R2 The active state differs when exposed to light as Ni valence and oxygen coordination are reduced under simulated sunlight irradiation (at 300 W).
R3. The mechanism differs when exposed to light as the Tafel slope becomes susceptible to an O2 scavenger probe in light and the reaction order with respect to pH differs in light and dark conditions.
R4. Metal bands are close to the Fermi level in octahedral coordination and oxygen bands in square planar coordination as calculated by DFT
The results are clearly visible in the data or calculations. However, I disagree with some interpretations as detailed below. The mechanistic concept to take electrons from different sites during the mechanistic sequence is exciting but I have some doubts whether this is a truly novel proposal. Nonetheless, I find the discussion is an important one for the field of electrocatalysis.

B. Originality and significance
Discussion about the important of orbital energy level such as this one is urgently needed to advance the understanding of electrocatalysis where often arguments are made on occupancy (e.g., of the eg orbital) alone.
Catalyzing the evolution of oxygen is demanding due to the need to transfer four electrons (and protons/hydroxide). This work provides an attractive concept where two electrons come from a metal side and two electrons come from oxygen sites. A clear increase of the current is demonstrated under the conditions where the new mechanism can operate.
A light induced trigger is certainly of highest interest to the academic community for model studies, e.g., of the mechanism such as this one. Could the authors comment on whether they see any commercial relevance of the light activation of Ni oxide? I have hard times imagining a complete redesign of electrolyzer stacks and sun roof in the facilities where they are housed. Yet, the property of light activation may be an advantage for artificial photosynthesis devices. However, these operate at near neutral conditions (e.g in phosphate buffer at pH 7). Does the catalyst show the same behavior under these conditions?
The activation of a Ni-containing oxide has been reported recently:
https://www.degruyter.com/document/doi/10.1515/zpch-2019-1431/html

It should be cited and clearly stated how this work goes beyond the previous report.
A new type of mechanism (COM) is proposed as involving both metal and oxygen redox. There is not much discussion of it in ref. 10 but the "LOM"-type mechanisms in this paper also include metal redox ("It is postulated here that the rate-limiting step in the concerted mechanism (Fig. 4c,e)—deprotonation of hydroxyl groups O–Mn+–OH + OH− → O–M(n−1)+–O + H2O (highlighted in green)—has become non-concerted and decoupled from subsequent electron transfer during the evolution of molecular oxygen, O–M(n−1)+–OO → O–Mn+–□ + O2 + e− (highlighted in yellow)."). The distinction from previous LOM proposals must be improved.
Finally, I am wondering, if the described effect can be observed in many oxides or just NR-NiOOH and the related NiFe LDH. Please comment on how general the concept is, ideally with a Table of other selected non-Ni materials that also have suitable electronic structure.

C. Data and methodology
The data clearly shows the ascribed effects and is of high quality. The data and concepts are very well presented. I like the cartoons of the band diagram to support the author's arguments. In a few cases, I would prefer more explanation and motivation of the experiments for non-experts, perhaps as supporting discussion.

C1. Please give the details of the FT of the EXAFS data. What energy range was used? What window function and which parameters? The fitting parameters are also not documented? How (method) was the fit performed? In R or k-space or filtered space? What E/k/R range was used? What software was used? What model or sample was used to obtain phase functions? What was the amplitude reduction factor, S02, and energy shift E0? What energy value was used to convert to k-space? Without these experimental details, the EXAFS analysis is not reproducible by others.

C2. Please give more details on the experiment in Fig. S4e? What was the pre-treatment? What were the conditions during the experiment? Please add a sentence about the connection between hole scavenger and oxygen evolution for non-experts.

C3. Fig. S4c. Please plot with equal scaling on the x and y-axis (as per EIS convention). Which resistance is indicated in the figure? Ru (uncompensated resistance of the electrolyte and material)?

C4. How can the analysis in Fig. 3b be done with only one experimental reference (b-Ni(OH2))? One needs at least two points or a point and slope for the calibration.

D. Statistics
No statistic analysis of the results is performed. The manuscript could be significantly improved if the (photo)electrochemical experiments were repeated to calculate standard deviations. It is unclear if the experiments were repeated by the authors and if the given electrochemical values are representative.

E. Conclusions
The main conclusions

(1) light activation enables a mechanism with both metal and oxygen redox whereby the rate-liming steps with a single type of redox are improved upon
(2) superior oxygen evolution activity compared to previously reported electrocatalysts
Could be further supported by additional data and more direction measurements (see points F below). Conclusion 1 is speculative as only metal redox is supported directly by measurements. Furthermore, no statement can be made about the activity of the electrocatalyst with the used metric. I expect that this can be easily improved by revision. .

There are some statements and interpretations that I disagree with or that need to be clarified
E1 The lifetime of photoexcited holes not of the order of hours as claimed. They are typically ~<10s in other oxides: https://pubs.acs.org/doi/10.1021/ja412058x. Clearly there is a structural change which is a much more straightforward explanation for the observations than an excited state that lasts hours.

E2. The coordination number of Ni-O (Table S2) in the dark (5.1±0.5
) and in light (4.2±0.9) are identical within the fit error. This contradicts the statement on P9 that "the Ni-O coordination number in NR-NiOOH is greatly reduced when subjected to light"

E3. P16. "which results in the COM route during the OER process. These calculations agree well with the experimental results (Fig. 2a)." It is unclear how exactly the COM route is visible in Fig 2a. I ask below to discuss the values of the Tafel slope and reaction order to support such a statement.

F. Suggested improvements
F1. The "catalyst activity" is given as overpotential at 10 mA/cm2 by normalization of the electrode area. This metric measures the activity of a composite electrode, not solely of the catalyst material, refer to e.g. https://onlinelibrary.wiley.com/doi/abs/10.1002/adma.201806296. This reference also provides state-of-the art intrinsic activities of electrocatalyst materials.
Please normalize by a catalyst property such as loading or surface area of the catalyst or the turnover frequency and compare those to literature.
Table S1 contains few entries. More active NiFe LDH electrodes are known:
https://onlinelibrary.wiley.com/doi/10.1002/aenm.201600621
Please also show the iR corrected data that is mentioned on P6.

F2. LOM in Fig 1b is based on ref 11 but in ref 10, the authors propose both metal and oxygen redox. A more comprehensive discussion of previous LOM proposals would improve the manuscript and help to highlight the novelty of this work.

F3. Are the mechanisms in Fig. 1 and 4 compatible with the determined Tafel slopes and reaction orders (the latter two in Fig. 4)? What values of the Tafel slope and reaction order is expected for the proposed rate-limiting steps and starting state? I am confused about the values of the slope in Fig. 4a. the reaction order with respect to pH is defined as d[logi]/dpH, which is the indicated slope in the figure. It should have values between 0 and 1 on the RHE scale (e.g. https://www.sciencedirect.com/science/article/abs/pii/S0920586115006227?via=ihub and application in https://chemistry-europe.onlinelibrary.wiley.com/doi/full/10.1002/cssc.201701582)

F4. Please show and discuss the enhancement effect due to day light or laboratory light. While a 300 W Xenon lamp is a good approach for controlled demonstration, the activation mechanism would be more interesting if daylight or stray light from common building lighting is sufficient.

F5. The Ni valence can be determined by XAS but the assignment of a spin state is mostly speculative. Surely, the spreading of p states may affect the Ni-K edge shape. To support this argument, please state what spreading of the p-states is expected and how it compares to the core hole lifetime of a Ni 1s hole. Can the expected change be resolved by the used conventional XAS or does one need HERFD-XAS? The proposed structural change may also lead to a broadening of the edge. Alternatively, are measurements of the unpaired spins possible? If so, they could better support the assignment of spin states.

F6. Please discuss what average coordination is expected for the as synthesized NR-NiOOH and the activated NR-NiOOH. Does it agree with the coordination number from EXAFS, which in not six but 5.1+/-0.5. As there are some 4-coordinated sites on the edges, I would expect a coordination number lower than six.

F7. Is it possible to measure the proposed square planar Ni oxide structure during light irradiation by XRD? Are there any other reports of square planar Ni oxides? Additional data would better support this unusual assignment. Likewise, what is the proof of square planar coordination of NiFe LDH after light irradiation?

F8. Are labelling studies of the material or electrolyte possible to support the evolution of lattice oxygen by mass spectroscopy? What is the direct experimental evidence for oxygen redox? Without direct experimental proof of either, the assignment is speculative.

F9 The proton transfer must occur on octahedral Ni. This means that the reaction must be started in darkness or at least at a time where not all Ni have been converted to square planar if that happens (see also F6). Please comment on it.

F10. The synthesis procedure involves sulfurization. Is there sulfur in “NR-NiOOH”?

G. References

The references are overall appropriate for the results and their discussion. However, I missed discussion of a previous report of Ni oxide activation by light (https://www.degruyter.com/document/doi/10.1515/zpch-2019-1431/html) and whether light-induced transformation from octahedral to square planar geometry has been reported before for Ni oxide or any other oxide (e.g. https://www.nature.com/articles/srep38514)

H. Clarity and context

The abstract is an appropriately written and concise summary of the main results and the authors’ interpretation as well as the potential impact on the electrocatalysis community. The introduction introduces the current state of knowledge on OER mechanisms well. I just missed some additional

aspects (see G. References). The presentation of the conclusions is also appropriate.

Referee #2 (Remarks to the Author):

I think that the work by Wang et al is comprehensive and some experimental aspects of it are appealing, but I am not convinced that Nature is the journal where it should be published. A more specialized catalysis journal would be more appropriate.
First, the text is too long, too technical and the quality of the writing, and hence the clarity of the article, goes down in several parts.
Second, the partaking of metal and oxygen sites in the same pathway is not new (Energy Environ. Sci., 2017,10, 2626-2637; Phys. Chem. Chem. Phys., 2014,16, 13682-13688) and the same can be said of oxygen-only lateral steps aside from the main pathway (Nature Communications volume 10, 4993 (2019)), different activities of Ni sites in octahedral and square-planar configurations (J. Power Sources 404, 2018, 56-63), or the interchange of high spin and low spin configurations to increase OER activities (Nature Energy 4, 519–525 (2019); Phys. Chem. Chem. Phys., 2017, 19, 20451-20456).
Third, in my opinion the electrocatalysis models are neither well-crafted, well-described, nor illustrative. In those, the authors mistake rate determining step for potential limiting step. The authors claim that O-O coupling has a smaller barrier than OOH formation. This claim is made based on diagrams at 0 V vs RHE not at OER relevant potentials. Because OOH formation is electrochemical, the potential will make its barrier accessible at potentials close to 1.4 V vs RHE. Besides, the authors claim that the conversion from octahedral to square planar is related to the OER enhancement but that is never shown with DFT. The COM pathway is not evaluated either with DFT, whereas the LOM and the AEM are.
Besides, the kinetic barriers for the transformation from octahedral geometry to square planar were not evaluated.
To close my report, I annotate that no tabulated data are provided (DFT electronic energies, zero-point energies, entropy corrections, solvation corrections), the method descriptions are incomplete and no coordinates are given.

Author Rebuttals to Initial Comments:

Referee #1 (Remarks to the Author):

Wang et al. report the light-induced activation of Ni oxide for the oxygen evolution reaction.
A. The key results are
R1 NR-NiOOH and also the well known NiFe LDH activate over the course of hours (on carbon cloth) or about a minute (ITO) under simulated sunlight irradiation (at 300 W).
R2 The active state differs when exposed to light as Ni valence and oxygen coordination are reduced under simulated sunlight irradiation (at 300 W).
R3. The mechanism differs when exposed to light as the Tafel slope becomes susceptible to an O2 scavenger probe in light and the reaction order with respect to pH differs in light and dark conditions.
R4. Metal bands are close to the Fermi level in octahedral coordination and oxygen bands in square planar coordination as calculated by DFT
The results are clearly visible in the data or calculations. However, I disagree with some interpretations as detailed below. The mechanistic concept to take electrons from different sites during the mechanistic sequence is exciting but I have some doubts whether this is a truly novel proposal. Nonetheless, I find the discussion is an important one for the field of electrocatalysis.

Response: Our description regarding the light source in the Supporting Information may confuse the readers. In our work, 300 W refers to the type of Xenon lamp rather than the intensity of light irradiated on the electrocatalysts. To avoid any misunderstanding, we have corrected this description in our revised Supporting Information (Page 4, highlighted in crimson): A solar simulator (NBeT Solar-500, 300 W) was used as the light source to simulate AM 1.5G. The intensity of the light irradiated on the electrocatalyst was 100 mW cm^{-2} as calibrated by a light power meter (Newport 843-R).

B. Originality and significance
Discussion about the important of orbital energy level such as this one is urgently needed to advance the understanding of electrocatalysis where often arguments are made on occupancy (e.g., of the eg orbital) alone. Catalyzing the evolution of oxygen is demanding due to the need to transfer four electrons (and protons/hydroxide). This work provides an attractive concept where two electrons come from a metal side and two electrons come from oxygen sites. A clear increase of the current is demonstrated under the conditions where the new mechanism can operate.
A light induced trigger is certainly of highest interest to the academic community for model studies, e.g., of the mechanism such as this one. Could the authors comment on whether they see any commercial relevance of the light activation of Ni oxide? I have hard times imagining a complete redesign of electrolyzer stacks and sun roof in the facilities where they are housed.

Response: We agree with the reviewer that it is difficult to realize light-induced COM in the conventional electrolyzer stacks. As shown in Figure R1a, the typical electrolyzer comprises of opaque cover materials that do not allow light to penetrate through and eventually reach the catalyst. As illustrated in Figure R1b, other than the need for light to penetrate through the cover material, it is also necessary to penetrate through the current collector and catalyst. Thus, while these cover materials can simply be replaced with glass or other transparent materials, it remains technically challenging to make the catalyst and the current collector transparent. As such, this limitation can ultimately reduce the effective utilization of light by the catalyst in conventional electrolyzer stack design. Hence, based on these considerations, it is difficult to trigger light-induced COM in conventional electrolyzer stacks due to the limited penetration of light.

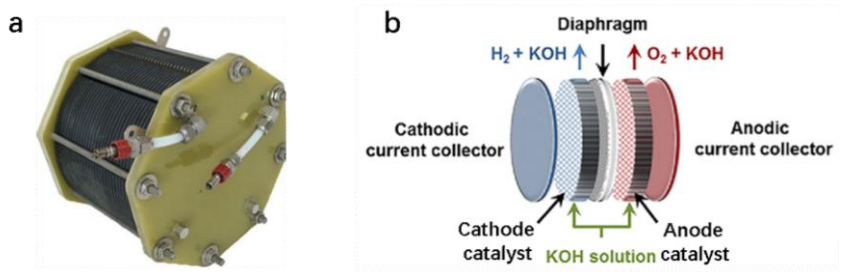

Figure R1. Schematic diagram of conventional electrolyzer stack. (a) Digital photograph of conventional electrolyzer stack device (image retrieved from Fuel Cell Store). (b) The components of a conventional electrolyzer stack (ref: *ACS Sustainable Chem. Eng. 2018, 6, 4829-4837*).

Even though it is unlikely to realize light-induced COM in a conventional electrolyzer stack, our coauthor, Prof. Wang Qing, had developed a redox decoupled water splitting device (*J. Am. Chem. Soc.* 2021, 143, 223-231) which can facilitate this mechanism. The design of this device is shown in Figure R2 (ref: *J. Am. Chem. Soc.* 2021, 143, 223-231). It enables the decoupling of HER and OER from the electrodes to spatially separated catalyst bed reactions *via* a pair of redox mediators. In contrast to the conventional electrolyzer stacks, oxygen evolution for this redox decoupled water splitting device occurs at the oxygen evolution tank, which can be made of transparent material. This option of choosing transparent material for the construction of the oxygen evolution tank implies the possibility of actualizing our proposed COM in this redox decoupled water splitting device. Furthermore, the electrocatalyst powders can be directly dispersed in the electrolyte without the need to coat on a substrate. This can then enable the effective utilization of light by the catalyst, and the photon can then be used to effectively trigger COM. Thus, based on these considerations, our proposed COM can be actualized in this redox coupled water-splitting technology. Motivated by this concept, we are currently studying the utilization of our proposed COM in this redox decoupled water-splitting device.

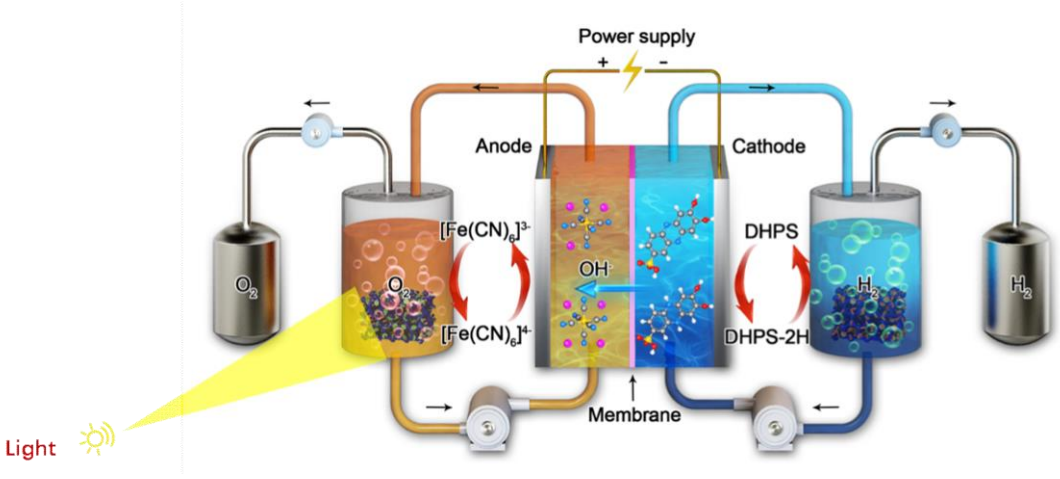

Figure R2. Illustration of our proposed COM in decoupled redox water-splitting devices. (ref: *J. Am. Chem. Soc.* 2021, 143, 223-231)

Yet, the property of light activation may be an advantage for artificial photosynthesis devices. However, these operate at near neutral conditions (e.g in phosphate buffer at pH 7). Does the catalyst show the same behavior under these conditions?

Artificial photosynthesis is a technology used to convert photonic energy (from solar irradiation) to chemical energy (such as hydrogen, carbohydrate, *etc*.). It should be noted that artificial photosynthesis in our discussion refers to the solar-driven water-splitting process. Currently, OER electrocatalysts are widely used in Photoanode

and tandem configurations, which are often comprised of Ni and Co-based compositions (Figure R3, Figure 33 a and b in our revised Supporting Information). Based on our current study, the proposed COM can be extended to both Ni and Co-based compositions (Fig. S31 and 32 in our revised Supporting Information), and therefore this provides an opportunity for the actualization of our proposed COM in these artificial photosynthesis devices. As the catalyst is subjected to light irradiation, its OER mechanism changes from AEM to COM with enhanced OER activity. Thus, when employing our COM in artificial photosynthesis, we expect that there will be a significant enhancement in the performance.

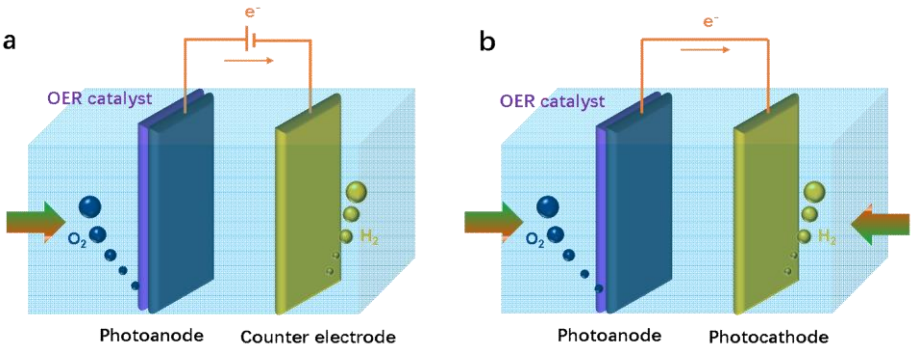

Figure R3. Schematic illustrations of artificial photosynthesis devices. (a) and (b) show the schematic illustrations of photoanode, and tandem configurations, respectively. (Figure S33 a and b in our revised Supporting Information)

As mentioned by the referee, these artificial photosynthesis devices are usually operated under neutral conditions. To determine the feasibility of COM actualization under neutral conditions, photon response measurements of NR-NiOOH and NiFe LDH were conducted in phosphate buffer solution (0.1 M, pH = 7), and the result is shown in Figure R4 (Figure S33 c to f in our revised Supporting Information). The experiment results obtained under neutral conditions exhibited the same behavior as that in alkaline conditions, whereby there was an obvious increase in current density under light irradiation and a decrease in current density under dark conditions. As such, based on this result, COM can still be triggered by light irradiation under neutral conditions. Thus, it is believed that our proposed COM can benefit the development of artificial photosynthesis devices.

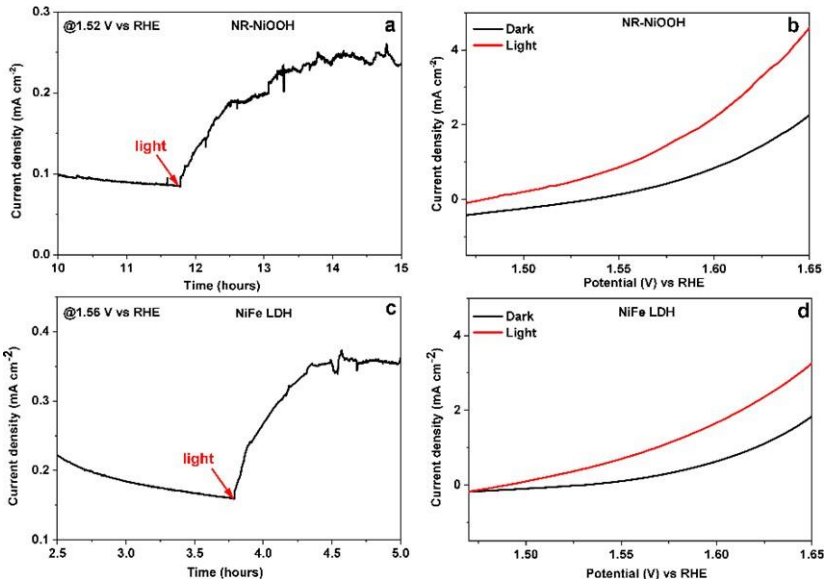

Figure R4. OER activities of NR-NiOOH and NiFe LDH in neutral conditions, with and without light irradiation. (a) and (c) light response test of NR-NiOOH and NiFe LDH using chronoamperometry measurement at the potential of 1.52 V and 1.56 V vs. reversible hydrogen electrode (RHE), respectively. (b) and (d) OER polarization curves of NR-NiOOH and NiFe LDH recorded under a scan rate of 0.1 mV/s with and without light irradiation. (Figure S33 c to f in our revised Supporting Information)

According to the reviewer's suggestion, we have added the following sentences in our revised manuscript (Page 16, highlighted in crimson):

We believe that the as-proposed COM can offer the possibility to enhance the performances of redox coupled water-splitting technology (*39*) (detailed discussion in Supplementary Text) and artificial photosynthesis devices (Fig. S33). As such, this work presents new insights into the electron transfer mechanism during OER process, which is potentially universal and extendable to other applications.

Figure R3 and R4 has been added in our revised Supporting Information (Fig. S33, highlighted in crimson).

The following discussion was added in our revised Supporting Information (Page 17 in our revised Supporting Information, highlighted in crimson):

Discussions on COM in the electrolyzer stacks

In typical electrolyzer stacks, it is difficult to trigger light-induced COM due to the limited penetration of light. Recently, Zhang *et. al*. developed a redox decoupled water splitting device which can facilitate the COM mechanism in electrolyzer stacks (*8*). It enables the decoupling of HER and OER from the electrodes to spatially separated catalyst bed reactions *via* a pair of redox mediators. Oxygen evolution for this redox decoupled water splitting device occurs at the oxygen evolution tank, which can be made of transparent material. This option of choosing transparent material for the construction of the oxygen evolution tank implies the possibility of actualizing our proposed COM in this redox decoupled water splitting device. Furthermore, the electrocatalyst powders can be directly dispersed in the electrolyte without the need to coat on a substrate. This can then enable the effective utilization of light by the catalyst, and the photon can then be used to effectively trigger COM. Thus, based on these considerations, the proposed COM can be actualized in this redox coupled water-splitting technology.

The activation of a Ni-containing oxide has been reported recently: https://www.degruyter.com/document/doi/10.1515/zpch-2019-1431/html
It should be cited and clearly stated how this work goes beyond the previous report.

Response: For the work reported by Olga *et al*., the as-prepared NiFeCr oxide catalyst exhibited enhanced current densities under light irradiation, as shown in Figure R5a (Figure 6a in the work of Olga *et al*.). This phenomenon is similar to that observed in our experimental results. In their work, the observed enhanced current density was attributed to two key factors: 1) Fe within the as-prepared catalyst was conceptualized in the form of γ -Fe_2O_3, and this could generate photocurrent under light irradiation, as shown in the inset of Figure R5b (Figure 6b in this reference). 2) The growth of crystallite during the surface reconstruction process when being irradiated with light. This allowed the larger crystallite (as facilitated by the light irradiation) to achieve more intimate contacts among the neighboring crystallites, which eventually resulted in enhanced conductivity and lower resistivity of the film. However, there was no further evidence and explanation in their report on how light led to the growth of the crystallite.

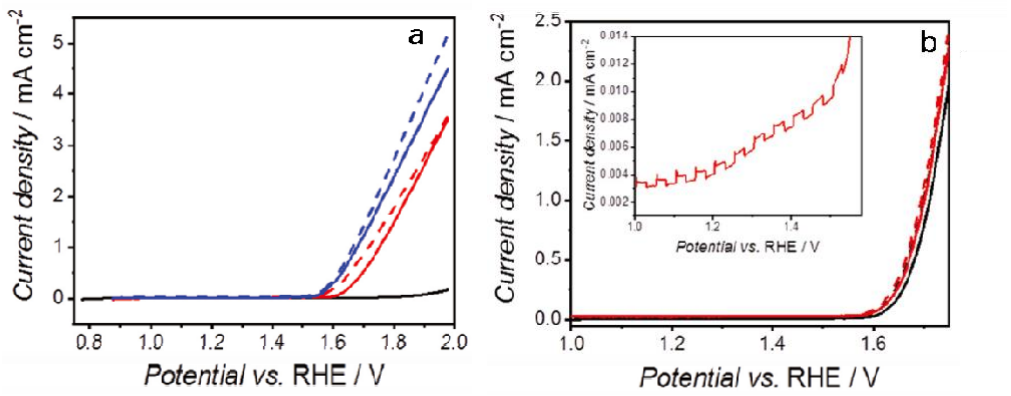

Figure R5. (a) Current density-potential plots for FTO electrode (black) and NiFeCr oxides coated on FTO in the dark (red) and under light irradiation (blue). Dashed lines represent plots recorded after applying a potential of 1.7 V vs. RHE for 60 min to the electrode. (b) Current density-potential plots for FeCr oxides coated on FTO in the dark (black) and under light irradiation (red, light on/off every 5s). The insets present an expanded region of the plots for potentials lower than the OER, showing light sensitivity for samples containing iron oxide. Dashed lines represent plots recorded after applying a potential of 1.7 V vs. RHE for 60 min to the electrode. Figure 6 in the reference *Z. Phys. Chem.* 2020, 234, 633-643.

In our work, we have also observed the increase in current densities under light irradiation for NR-NiOOH (Fig. 2 in our revised manuscript). In contrast to the work reported by Olga *et al.*, a repeated light on/off experiment under pro-longed operation was demonstrated in our work. Such a repeatable light-induced behavior observed in our work is unlikely to be due to crystal growth, since crystal growth is regarded as an irreversible process (Fig. S4b in our revised Supporting Information). Furthermore, this reversible light-induced behavior was not due to the photocurrent, as shown in our photocatalytic measurement (Fig. S4 d in our revised Supporting information). Thus, based on these analyses, the light-induced behavior observed in our work is different from that reported by Olga *et al.* in terms of its underlying mechanism and reversibility. To summarize the novelty of our work, we have presented the key idea flow of our work in Figure R6 (Fig. S7 in our revised Supporting Information), whereby a new OER mechanism involving switchable metal and oxygen redox activities under light irradiation was demonstrated.

To elucidate the underlying mechanism of the light-triggered OER performance enhancement in our work, the structural geometry under light irradiation was investigated by *operando* XAFS (Fig. 3a in our revised manuscript). This was identified from the pre-edge and white line in XAFS, and FT-EXAFS (Fig. S9 to 12 in our revised Supporting Information). According to our experimental result, there was a significant reduction in the Ni valence state, which is different from conventional OER process. Further analyses indicated that this reduction in Ni valence state was caused by the reversible geometrical conversion from octahedron to square planar under light irradiation, as identified according to the pre-edge and white line in XAFS and FT-EXAFS (Fig. S10 to 12). To the best of our knowledge, this is a new finding in OER electrocatalyst research which has yet to be reported. In addition, TMA^+ probe combining XAFS, ^{18}O isotope measurement, and simulation results all showed that as NiOOH converted to square planar geometry, there was a change in the redox center from metal to oxygen (Fig. 3c and d in our revised manuscript, Fig. S17 to 19 in our revised Supporting Information). Thus, based on these collective results, a new OER mechanism-coupled oxygen mechanism that proceeds *via* an optimized energy pathway was proposed in this work (Fig. 4 in our revised manuscript). In this optimized energy pathway, the deprotonation occurred at the metal bands, while the O-O coupling process occurred at the oxygen states. To further explore the underlying science of COM, the electronic structures of NR-NiOOH and bulk NiOOH were analyzed (Fig. S13 and S25 in our revised Supporting Information). It was demonstrated that only when there was a non-overlapping region arising from the partial overlapping of d_{z^2} orbitals with a_{1g}* bands, electron could then be transferred from (M-O) to d_{z^2} orbitals to complete the as-proposed COM (Fig. 5a in our revised manuscript). Interestingly, we found that COM can also be extended to other materials such as NiFeOOH, NiCrOOH, NiMnOOH, NiVOOH, NiCoOOH, NiCuOOH, *etc.*, and Co-based oxyhydroxide, *i.e.*, CoMnOOH and CoVOOH (Fig. S30 to 32 in our revised Supporting Information).

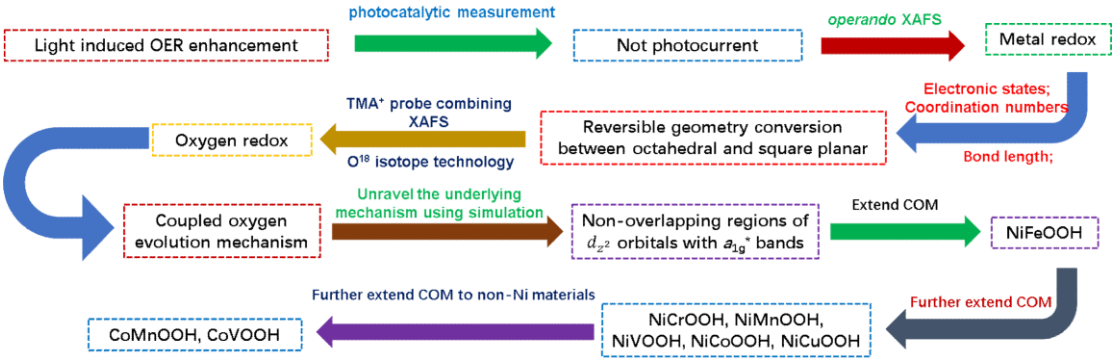

Figure R6. The organization flow of our work. (Fig. S7 in our revised Supporting Information).

According to the reviewer's suggestion, we have added this reference in our revised manuscript (ref 19, highlighted in crimson): Based on our experiment results, the improvement in the OER performance as demonstrated by NR-NiOOH under light irradiation is unlikely to be a result of reduced ohmic resistance, light-induced crystal growth or generation of holes (Fig. S4 and Supplementary Text) (*18, 19*). (Page 8 in our revised manuscript).

The Figure R6 has been added in our revised Supporting information (Fig. S7, Page 29, highlighted in crimson).

The following discussion on possible reasons for light enhanced OER activity has been added in the Supplementary Discussions in our revised Supporting Information (Page 9, highlighted in crimson):

Discussion on possible reasons for the enhanced OER activity triggered by light

There are several possible reasons for this unique phenomenon, *i. e.* (1) the influx of photon helps to decrease the ohmic resistance, (2) the generation of holes by light that become available for OER, and (3) light induced conversion of OER routes. To investigate the feasibility of the first possibility, electrochemical impedance spectroscopy (EIS) test was conducted for both samples subjected to and without light irradiation. According to Fig. S4c, the resistances of these two samples were nearly identical, which excludes the likelihood of lower catalyst resistance due to photon influx. To investigate the feasibility of second possibility, OER photocatalytic behavior of NR-NiOOH was analyzed by determining the potential of the light-induced holes. Generally, the requirements of the overall water-splitting photocatalysts are stringent, and no response can be obtained if the conditions of either oxygen evolution or hydrogen evolution reaction are not met. Performing trial oxygen evolution reaction in the presence of sacrificial electron acceptors is one way to assess the suitability of the band position of a specific composition to act as an OER photocatalyst. The potential of the holes was examined using gas chromatography with $K_2S_2O_8$ as the electron acceptor, and no oxygen was detected within 2.5 hours of operation (Fig. S4d). This result indicates that the enhanced OER activity in NR-NiOOH is not attributed to the generation of light-induced holes. At the same time, a repeated light on/off experiment under pro-longed operation was demonstrated in our work (Fig. S4b). Interestingly, we found that the light-induced behavior, *i.e.*, the enhancement in the current densities under light irradiation and reduction in the current densities once the light was switched off, is highly repeatable. Such a repeatable light-induced behavior observed in our work is unlikely to be due to crystal growth, since crystal growth is regarded to be an irreversible process. To summarize the novelty of our work, we have presented the key idea flow of our work in Fig. S7 and 8, whereby we have demonstrated a new OER mechanism involving switchable metal and oxygen redox activities under light irradiation.

To elucidate the underlying mechanism of the light-triggered OER performance enhancement in our work, the structural geometry under light irradiation was investigated by *operando* XAFS (Fig. 3a and b). According to our experimental result, there was a significant reduction in the Ni valence state, which is different from conventional OER process. Further analyses indicated that this reduction in Ni valence state was caused by the reversible geometrical conversion from octahedron to square planar under light irradiation, as identified according to the pre-edge and white line in XAFS and FT-EXAFS (Fig. S10 to 12). To the best of our knowledge, this is a new finding in OER electrocatalyst research which has yet to be reported. In addition, based on the collective results obtained from TMA^+ probe combining XAFS, ^{18}O isotope measurement, and calculations, as NiOOH converted to square planar geometry, there was a change in the redox center from metal to oxygen (Fig. 3c to d and Fig. S14 to 19). As such, a new OER mechanism-coupled oxygen mechanism that proceeds *via* an optimized energy pathway was proposed in this work (Fig. 4). In this optimized energy pathway, deprotonation occurred at the metal bands, while O-O coupling process occurred at the oxygen states. To further explore the underlying science of COM, the electronic structures of NR-NiOOH and bulk NiOOH were analyzed (Fig. S13 and 25). It was demonstrated that only when there was a non-overlapping region arising from the partial overlapping of d_{z^2} orbitals with a_{1g}^* bands, electron could then be transferred from (M-O) to d_{z^2} orbitals to complete the as-proposed COM (Fig. 5a). Interestingly, we found that COM can also be extended to other materials such as NiFeOOH, NiCrOOH, NiMnOOH, NiVOOH, NiCoOOH, NiCuOOH, *etc.*, and Co-based oxyhydroxide, *i.e.*, CoMnOOH and CoVOOH (Fig. S30 to 32).

A new type of mechanism (COM) is proposed as involving both metal and oxygen redox. There is not much discussion of it in ref. 10 but the “LOM”-type mechanisms in this paper also include metal redox (“It is postulated here that the rate-limiting step in the concerted mechanism (Fig. 4c,e)—deprotonation of hydroxyl groups $O–M^{n+}–OH + OH^- \rightarrow O–M(n-1)+–O + H2O$ (highlighted in green)—has become non-concerted and decoupled from subsequent electron transfer during the evolution of molecular oxygen, $O–M^{(n-1)+}–OO \rightarrow O–M^{n+}–□ + O_2 + e^-$ (highlighted in yellow).”). The distinction from previous LOM proposals must be improved.

Response: Currently, it is widely known that LOM occurring on perovskite is a type of oxygen redox reaction. For the study of $SrCoO_3$ reported in ref. 10, AEM-based electron transfer process ($O–M^{(n-1)+}–OO \rightarrow O–M^{n+}–□ + O_2 + e^-$, Figure R7a) was used to explain the electron transfer in their proposed LOM ($□–M–OO \rightarrow □–M–□ + O_2 + e^-$, Figure R7b). However, no experimental evidence was provided in their work to prove the existence of metal redox in their proposed LOM.

The sole oxygen redox activities within LOM in perovskite were verified by another group, using *operando* oxygen *K*-edge and metal *L*-edge X-ray absorption spectra “As a result, the electron–holes are located on states of predominantly O2*p* character, leading to a transition from a $3d^5$ to a $3d^5$L configuration where L denotes a ligand hole. Moreover, our results indicate that the Fe^{3+}/Fe^{4+}state (changing from d^5 to d^4) is too far from the Fermi level to be accessed even when electrochemically oxidizing the material with large anodic overpotentials.” (*Nature Communications* 6, 6097, 2015).

Subsequently, the main author from ref. 10 later published a review on perovskite, and they proposed that LOM proposal was a type of oxygen redox reaction “Hence, the charge transfer gap becomes zero for compounds such as $SrFeO_3$ and even negative for $SrCoO_3$, a so-called negative charge-transfer material. As mentioned earlier, for these materials the oxygen is expected to be redox active.” (Catalysts *2017*, 7, 149). At the same time, in their review, they also pointed out the difficulty in realizing a co-existence of metal and oxygen redox in perovskite structure during oxygen evolution catalytic reaction. “Interestingly, an intermediate case exists when $\Delta = U/2$, i.e., when both MO* and the O *p* states lie at the Fermi level, and for which the redox reaction can be described as a mixture of anionic and cationic redox reaction. In this case, the electron removal upon oxidation would imply that the Fermi level entered into a degenerated state for which MO* and O *p* states participated in the oxidation. Such a case is obviously unstable and charge reorganization is expected by reversing electrons from one band to the other, inducing the modification of the local structure through bond reorganization.” (Catalysts *2017*, 7, 149).

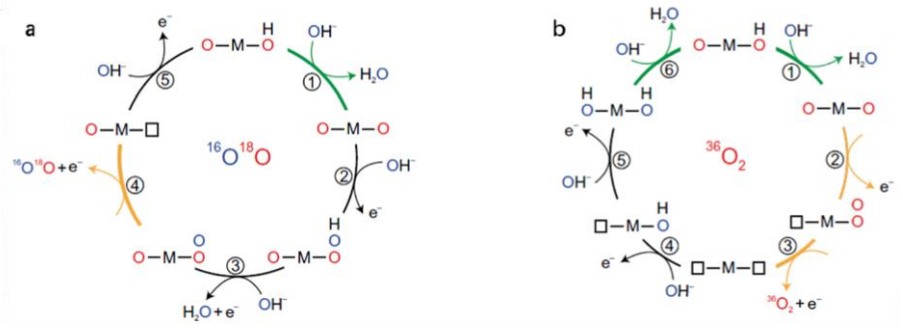

Figure R7. Possible non-concerted proton–electron transfer OER mechanisms that evolved $^{34}O_2$ (a) and $^{36}O_2$ (b). (Corresponding to Figure 4g and h in ref. 10, respectively). Ref: *Nat. Chem.* ***9,*** 457-465, (2017)

The redox activities in LOM can be analyzed based on the electron transfer process (Figure R8 to R10). There are two types of electron transfer pathways in LOM: a) Electron transfer from non-bonding OH^- states to the external circuit during the deprotonation step, and b) electron transfer from (O-O) coupling band to the external circuit during the oxygen evolution step. Then, the electron transfer during the deprotonation step is analyzed. During the deprotonation step, hydrogen-oxygen chemical bond is firstly broken, and then one proton is removed from the adsorbed OH^- group. Concurrently, the adsorbed OH^- will change into O^{2-}. In the following electron transfer process, O^{2-} will be transformed into O^- for the subsequent O-O coupling. It is well known O-O coupling step is a chemical process that proceeds by hybridizing the non-bonding oxygen states in the neighboring O^-. As a result, the electronic configuration of O^- is less than 8 which is a type of oxidized oxygen state (Figure R9). Consequently, as O^{2-} is converted to O^-, one electron is transferred from the oxygen orbitals of O^{2-} into the external circuit, which indicates that oxygen is the redox center (Figure R8).

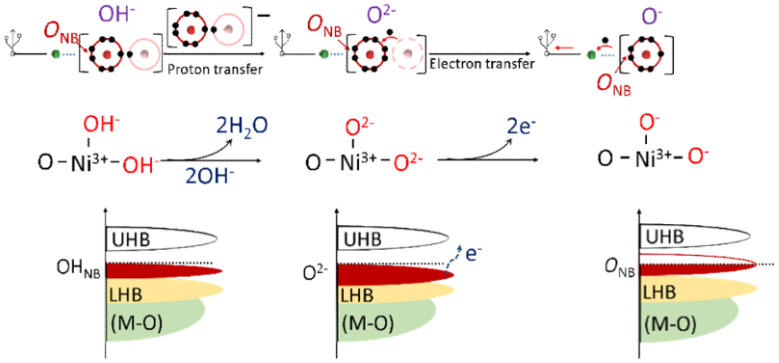

Figure R8. Proton and electron transfer process during the deprotonation step of LOM.

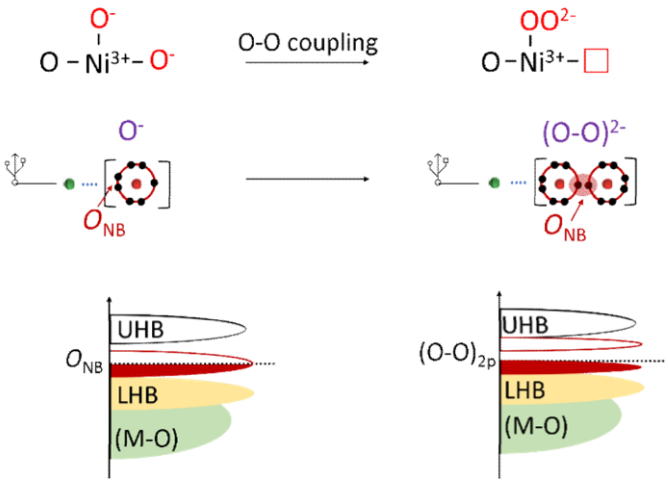

Figure R9. Electron transfer during O-O coupling process

According to Figure R10, during the oxygen evolution step, two electrons must be removed from the oxygen orbitals of $(O\text{-}O)^{2-}$ to achieve the electronic structure of O_2. Consequently, oxygen has to act as the redox center during this process. As such, according to our analyses, a two-electron transfer from oxygen orbitals occurs during the deprotonation step while the other two-electron transfer from oxygen orbitals occurs during the generation of O_2. These processes sum up to the four-electron transfer process during OER. Thus, based on our discussion, LOM is a type of oxygen redox reaction.

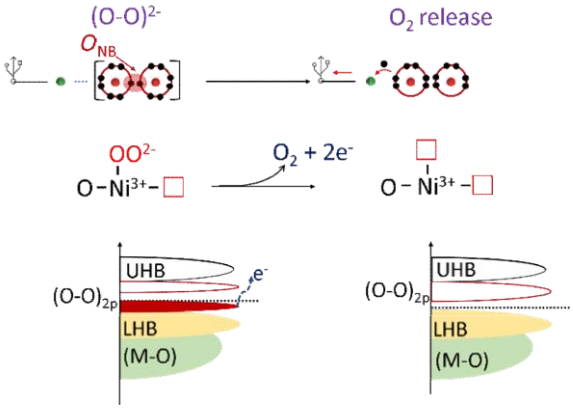

Figure R10. Electron transfer process in the oxygen evolution step of LOM.

For our proposed COM, three electron transfer processes are involved: (1) Light-induced electron transfer from (M-O) to d_{z^2} orbital, (2) electron transfer from (O-O) coupling bands to the external circuit, and (3) electron transfer from d_{z^2} orbital to the external circuit (Figure R11, Fig. 4 in our revised manuscript). The electron transfer from (O-O) coupling bands to the external circuit is an oxygen redox reaction, while electron transfer from d_{z^2} orbital to the external circuit is a metal redox reaction. As a result, our proposed COM involves switchable metal and oxygen redox chemistries. Such a redox transformation from metal to oxygen redox chemistry is realized by the geometry conversion of NR-NiOOH from octahedron to square planar when triggered by light. At the same time, the band diagram shows that the electronic states around the Fermi level exhibit alternative metal/oxygen characters throughout the entire COM process, which further shows the involvement of switchable metal and oxygen redox chemistries in COM.

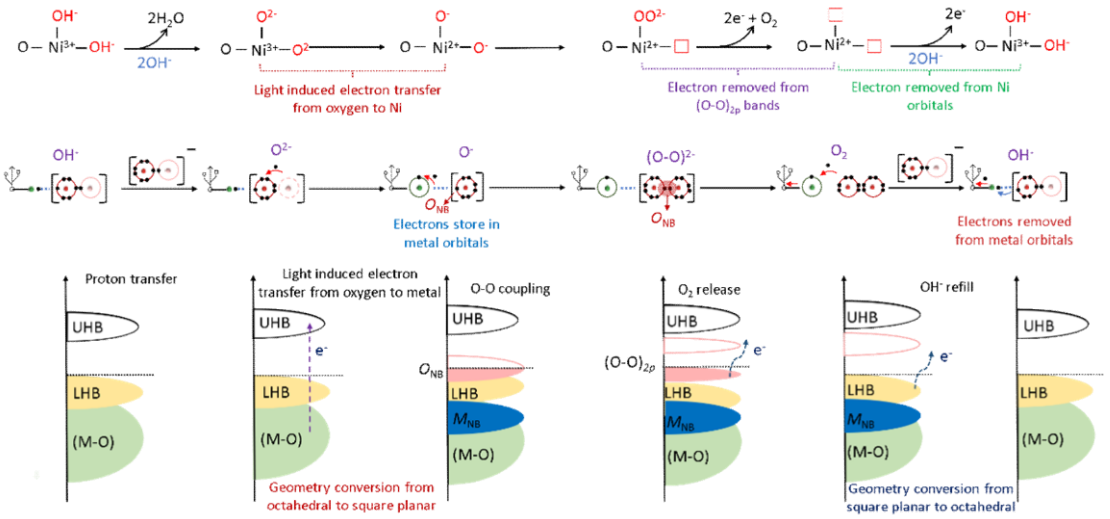

Figure R11. Electron transfer process of our proposed COM. Fig. 4 in our revised manuscript.

According to the reviewer's suggestion, we have added the discussions on the redox activities of conventional AEM and LOM in our revised supporting information (Page 8, highlighted in crimson):

Discussion on the redox activities in conventional AEM and LOM

The conventional AEM follows the pathway of OH*, O*, OOH*, and O_2. The redox activities in this proposed OER mechanism were analyzed by deciphering the electron transfer process, as shown in Fig. 1a. In the deprotonation step (from OH^- to O^{2-}), the cleavage of oxygen-hydrogen bond is accompanied by one electron and proton transfer. The electron transfer from metal orbitals to the external circuit leads to an increase in metal valence. In the OOH^- formation process, the adsorption of OH^- from the electrolyte leads to the transfer of one electron and proton. To fulfill the 8-electron configuration of oxygen, two inner electrons must be transferred from oxygen to metal, and this decreases the metal valence. In the subsequent deprotonation step (from OOH^- to OO^{2-}), the cleavage of oxygen-hydrogen chemical bond leads to a concerted electron and proton transfer. In this process, the electron is transferred from the metal orbitals to the external circuit, whereby the valence of Ni increases. In the oxygen evolution step, two types of electron transfer can occur: Removal of one electron from the metal orbitals to the external circuit, and the removal of two inner electrons from oxygen orbitals to the metal orbitals. Hence, during this step, the valence of the metal decreases. Consequently, it can be understood that metal acts solely as the redox center during the entire OER process.

On the other hand, conventional LOM process involves deprotonation, O-O coupling, and O_2 release (as shown in Fig. 1b). During the deprotonation step, hydrogen-oxygen chemical bond is firstly broken, and then one proton is removed from the adsorbed OH^- group. Concurrently, the adsorbed OH^- will change into O^{2-}. In the subsequent electron transfer process, O^{2-} will transform into O^-, to realize O-O coupling. It is well known the O-O coupling step is a chemical process that proceeds by hybridizing the non-bonding oxygen states in the neighboring O^-. As a result, the electron configuration of O^- is less than 8 which is a type of oxidized oxygen state. Consequently, as O^{2-} is converted to O^-, one electron is transferred from the oxygen orbitals of O^{2-} into the external circuit, whereby oxygen acts as the redox center. During the oxygen evolution step, two electrons have to be removed from the oxygen orbitals of $(O\text{-}O)^{2-}$ to achieve the electronic structure of O_2. Consequently, oxygen acts as the redox center during this process. As such, according to our analyses, a two-electron transfer from oxygen orbitals occurs during the deprotonation step, while the other two-electron transfer from oxygen orbitals occurs during the generation of O_2, which sums up to the four-electron transfer process during OER. Thus, based on this discussion, LOM is a type of oxygen redox reaction.

Finally, I am wondering, if the described effect can be observed in many oxides or just NR-NiOOH and the

related NiFe LDH. Please comment on how general the concept is, ideally with a Table of other selected non-Ni materials that also have suitable electronic structure.

Response: To realize COM route in Ni-based electrocatalysts, non-overlapping region must emerge from the partial overlapping of d_{z^2} orbitals with a_{1g}* bands so as to satisfy the light-induced electron transfer from (M-O) to d_{z^2} orbitals. (Figure R12a, Fig. 5 in our revised manuscript; Figure R13, Fig. S30 in our revised Supporting Information). This proposed hypothesis has been preliminarily verified by analyzing the electronic structures of NiOOH, NR-NiOOH, and NiFe LDH in this work. To examine the universality of this proposed hypothesis, the electronic states of NiCrOOH, NiMnOOH, NiVOOH, NiCoOOH, and NiCuOOH were also examined, and the results are shown in Figure R12b. According to the simulation results, non-overlapping regions were observed in all materials due to the partial overlapping of d_{z^2} orbitals with a_{1g}* bands (Figure R13, Fig. S30 in our revised Supporting Information). At the same time, it can be observed from Figure R12b that the broadness of the non-overlapping region increases with the increase in energy differences between $d_{x^2-y^2}$ and d_{z^2} orbitals. This result implies that COM route can be actualized in these structures. Subsequently, photon response measurement was performed for all materials, and it is shown that COM can be successfully triggered in NiCrOOH, NiMnOOH, NiVOOH, NiCoOOH, and NiCuOOH. Such a result clearly demonstrates the universality of our proposed COM in various electrocatalysts (Figure R14) (Fig. S31 in our revised Supporting Information).

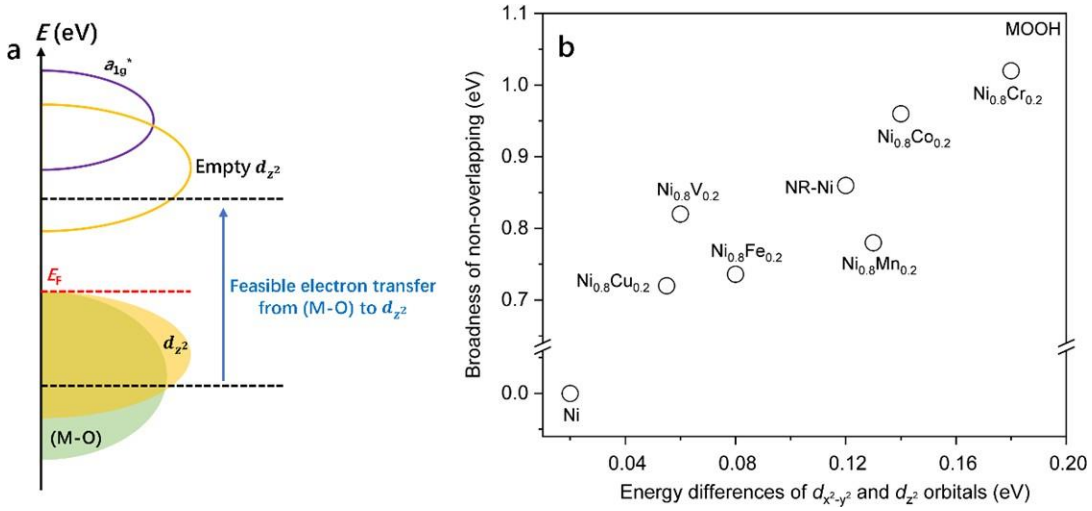

Figure R12. (a) Feasible electron transfer from (M-O) to d_{z^2} orbitals. (b) Broadness of the non-overlapping regions versus energy difference of $d_{x^2-y^2}$ and d_{z^2} orbitals in Ni-based oxyhydroxide compositions. Here, the energy difference between $d_{x^2-y^2}$ and d_{z^2} orbitals is associated with the degree of asymmetry in the NiO_6 octahedral configuration. Fig. 5 in our revised manuscript.

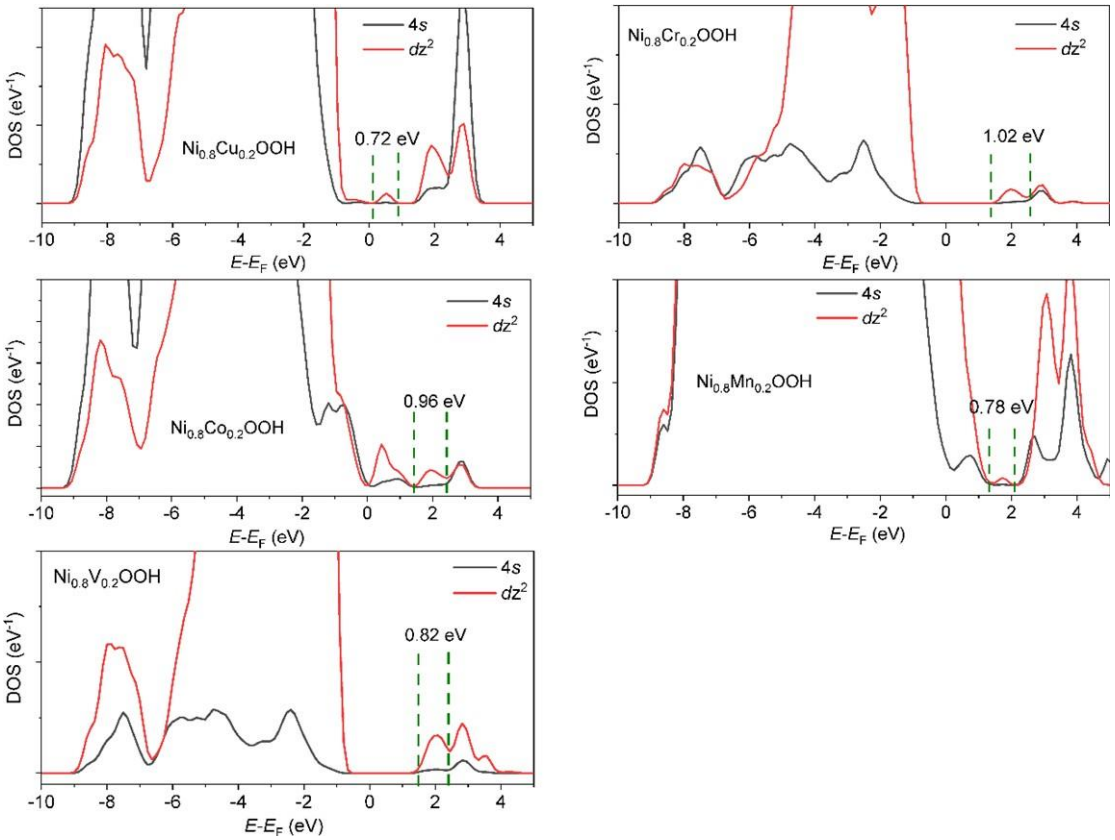

Figure R13. The PDOS of $Ni_{0.8}Cu_{0.2}OOH$, $Ni_{0.8}Cr_{0.2}OOH$, $Ni_{0.8}Co_{0.2}OOH$, $Ni_{0.8}Mn_{0.2}OOH$, and $Ni_{0.8}V_{0.2}OOH$. Here, the PDOS of 4*s* orbital above Fermi level shows the electronic states of a_{1g}^* bands. According to the simulation results, non-overlapping regions were observed in all materials due to the partial overlapping of d_{z^2} orbitals with a_{1g}^* bands. Fig. S30 in our revised Supporting Information.

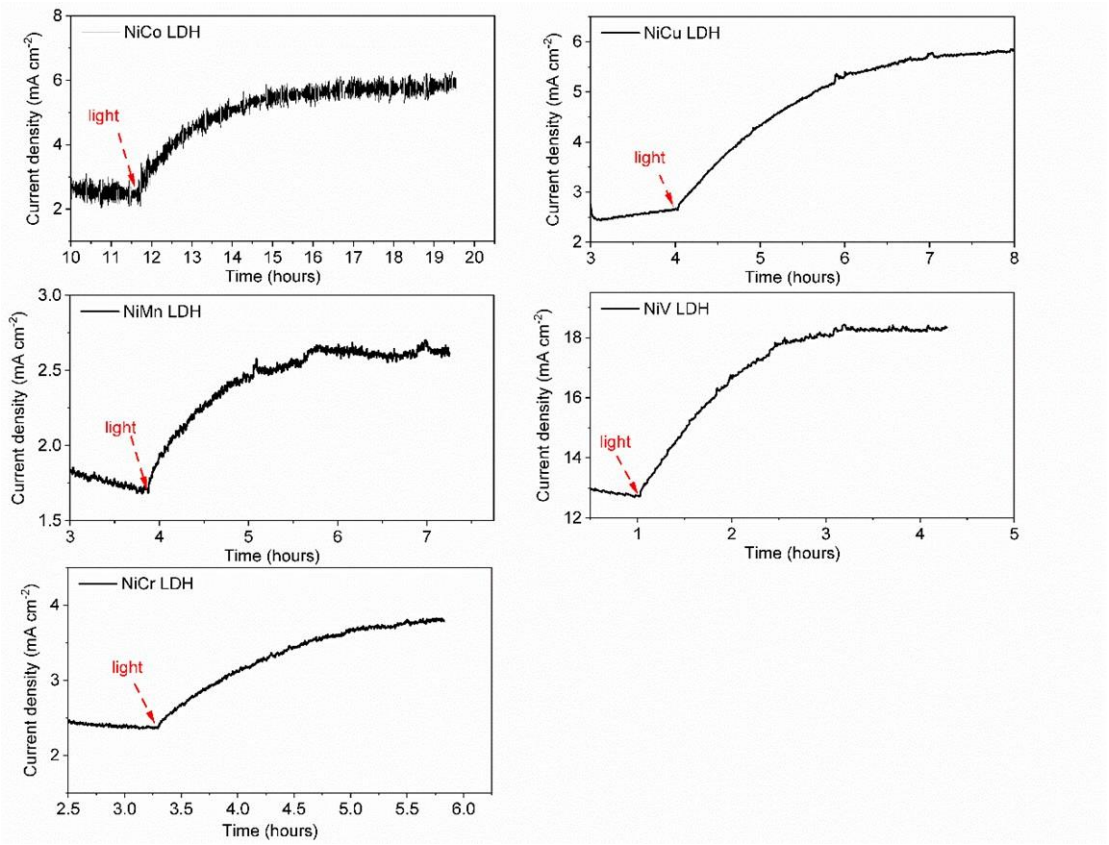

Figure R14. Photon response measurements in NiCrOOH, NiMnOOH, NiVOOH, NiCoOOH, and NiCuOOH measured at the potential of 1.50 V vs RHE. It is shown that COM can be successfully triggered in NiCrOOH, NiMnOOH, NiVOOH, NiCoOOH, and NiCuOOH. Such a result clearly demonstrates the universality of our proposed COM in various electrocatalysts. Fig. S31 in our revised Supporting Information.

According to our work, the key in triggering COM route is to realize the geometry conversion from octahedron to square planar (Figure R15, Fig. S32 in our revised Supporting Information). This means that COM may be triggered when such a geometry conversion is fulfilled in non-Ni-based compositions. When compared to Ni electronic configuration, *i.e.*, [Ar]3*d*84*s*2, Co follows the configuration of [Ar]3*d*74*s*2, which has one less electron. As a result, Co^{1+} may also possess a low spin d^8 electronic configuration while exhibiting the square planar geometry, which is similar to that of the low spin Ni^{2+}. More importantly, both Co^{2+} and Co^{3+} follow the octahedral configuration. Interestingly, we also found similar light triggered OER performance enhancement in Co-base compositions, *i.e.*, CoMn LDH and CoV LDH, as shown in Figure R15 c. These results implies that Co-based compositions may be able to exhibit photon-induced COM. To fully understand the feasibility of photon-induced COM in Co-based composition, detailed mechanism has to be further studied.

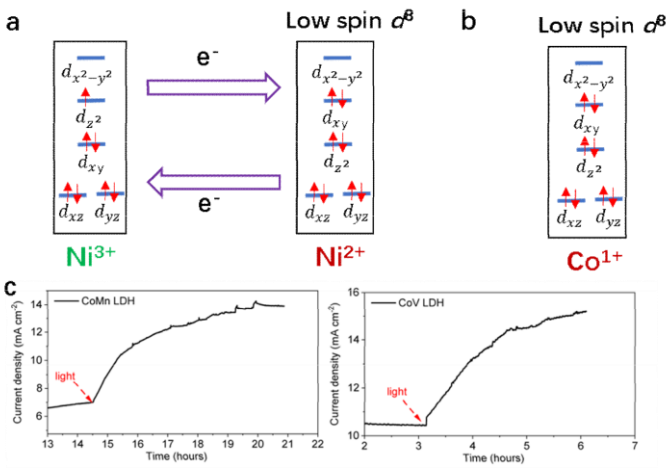

Figure R15. (a) Electronic configurations of Ni^{3+} and low spin Ni^{2+}. (b) Possible electronic configuration of low spin Co^{1+}. (c) Photon response measurements in CoMn and CoV LDH. Fig. S32 in our revised Supporting Information.

According to the reviewer's suggestion, we have added the following sentences in our revised manuscript (Page 15, highlighted in crimson):

To further examine the universality of this proposed hypothesis, the electronic states of NiCrOOH, NiMnOOH, NiVOOH, NiCoOOH, and NiCuOOH were also examined (Fig. 5b and Fig. 30). According to the calculations, all structures possessed a larger orbital energy difference value (0.05 ~ 0.18 eV) than the traditional NiOOH, and non-overlapping region (broadness: 0.72 to 1.02 eV) was observed for all materials due to the partial overlapping of d_{z^2} orbitals with a_{1g}^* bands. Subsequently, photon response measurement was conducted, and it is shown that COM was successfully triggered in NiCrOOH, NiMnOOH, NiVOOH, NiCoOOH, and NiCuOOH (Fig. S31). At the same time, it can be observed that the broadness of the non-overlapping region increased with the increase in orbital energy difference, and this further indicates that COM could be realized by introducing a certain extent of distortion to the crystal structure of NiOOH. Interestingly, similar light triggered OER performance enhancement in Co-based compositions was also observed (Fig. S32). Thus, based on these results, our proposed COM can be further applied in various OER electrocatalysts, which hint its universality.

Figure R12 has been added in the revised manuscript (Fig. 5); Figure R13-15 has been added in the revised Supporting Information (Fig. S30-32).

C. Data and methodology

The data clearly shows the ascribed effects and is of high quality. The data and concepts are very well presented. I like the cartoons of the band diagram to support the author's arguments. In a few cases, I would prefer more explanation and motivation of the experiments for non-experts, perhaps as supporting discussion.

Response: We have added the following supplementary discussions (Page 10, highlighted in crimson) and flow chart (Figure R16, Fig. S8, Page 30 in our revised Supplementary Information):

Discussion on the experiments in the revelation of COM

Two types of redox activities, *i.e.*, metal redox activities with electron removal from metal electronic states and oxygen redox activities with electron removal from non-bonding oxygen states, are possible during the oxygen evolution catalytic reaction. Generally, the removal of electrons from the metal orbitals is accompanied by the variations in the metal valence, which can be effectively identified using *operando* metal *K*-edge XAFS, *etc*. As the electrons are removed from the oxygen orbitals, oxygen will be oxidized, and this can be subsequently stabilized *via* the chemical oxygen-oxygen coupling. Since the oxygen-oxygen coupling bond is formed through the hybridization of non-bonding oxygen states in the neighboring oxygen atoms, this process requires the participation of lattice oxygen atoms. Thus, the emergence of oxidized oxygen states and participation of lattice oxygen atoms are the characteristic features of oxygen redox activities.

The flow chart depicting our experimental approach is shown in Fig. S8. To determine the involvement of metal redox activities in our new mechanism, we firstly conducted *operando* Ni *K*-edge XANES. According to our experimental results, there was a significant reduction in the Ni valence state under light irradiation (Fig. 3a). As the current stabilized, a Ni valence of about 2.2 was recorded, which indicates the co-existence of Ni^{2+} and Ni^{3+} (Fig. 3b). This is greatly different from the traditional OER process, whereby a co-existence of Ni^{3+} and Ni^{4+} is usually observed during the catalytic reaction. Meanwhile, based on the pre-edge and white line in XANES and FT-EXAFS, the variation in Ni valence state was caused by the reversible geometrical conversion from octahedron to square planar under light irradiation (Fig. S10 to 12). According to the molecular orbital diagram, such a geometry conversion is realized by the transfer of electron from (M-O) to d_{z^2} orbital induced by light (Fig. S12c). Then, the geometry of square planar was studied. Based on the calculations, as the sample converted to the square planar structure, its electronic states around the Fermi level will change to the oxygen orbital, and this implies the existence of oxygen redox activity during the OER process (Fig. S14 to 15). Next, the oxidized oxygen states were confirmed by using TMA^+ probe combined with XAFS, while oxygen-oxygen coupling was identified using isotope technology (Fig. 3c and d). Thus, according to the collective results, oxygen evolution step is based on oxygen redox activities, and this process involves a two-electron transfer mechanism.

To achieve the oxidized oxygen states, electron must transfer from oxygen orbitals to the external circuit (oxygen redox) or metal orbitals during the deprotonation step. Since metal redox activities were also identified in this OER process, this type of electron transfer is unlikely to be due to oxygen redox. Hence, the oxidized oxygen is realized through electron transfer from oxygen to metal orbitals, which is intrinsically the light-induced electron transfer from (M-O) to d_{z^2} orbital. To further analyze the deprotonation step, pH dependence was employed (Fig. S20). Based on the experimental results, deprotonation is a non-concerted proton-electron transfer process, which involves a proton transfer and a subsequent electron transfer from (M-O) to d_{z^2} orbital. Since the deprotonation step involves the light-induced geometry conversion from octahedron to square planar, the geometric conversion back to octahedron from square planar must be satisfied during the OH^- refilling process. To achieve the geometric conversion back to octahedron from square planar, electrons that are stored in the d_{z^2} orbital must be released into the external circuit where metal acts as the redox center. Moreover, since two OH^- ions that are participating in the O_2 generation process are within the neighboring square planar unit cells, these two square planar unit cells can be converted into octahedral unit cells per O_2 generated. Such a step involves a two-electron transfer.

According to the collective results, the proposed light-induced OER process with switchable metal and oxygen redox centers is illustrated in Fig. 4. In our OER route, three electron transfer processes are involved: (1) light-induced electron transfer from (M-O) to d_{z^2} orbital, (2) electron transfer from (O-O) coupling bands to the external circuit (oxygen redox), and (3) electron transfer from the d_{z^2} orbital to the external circuit (metal redox). Thus, our OER route involves both oxygen and metal redox reactions, which is termed as coupled oxygen evolution mechanism (COM). Our OER process can be summarized with these sequential steps: (1) Proton transfer occurring in octahedral NiO_6. (2) Under light irradiation, there is a geometric conversion of octahedral NiO_6 to square planar NiO_4 induced by the photon. (3) The hybridization of the formed ONB leads to oxygen-oxygen coupling to form an oxygen band. (4) Release of oxygen resulting in OH^- vacancy sites. (5) Refilling of these vacancy sites with OH^-. (6) As a result of the OH^- refilling process, there is a concomitant geometric conversion of the square planar NiO_4 to octahedral NiO_6 configuration.

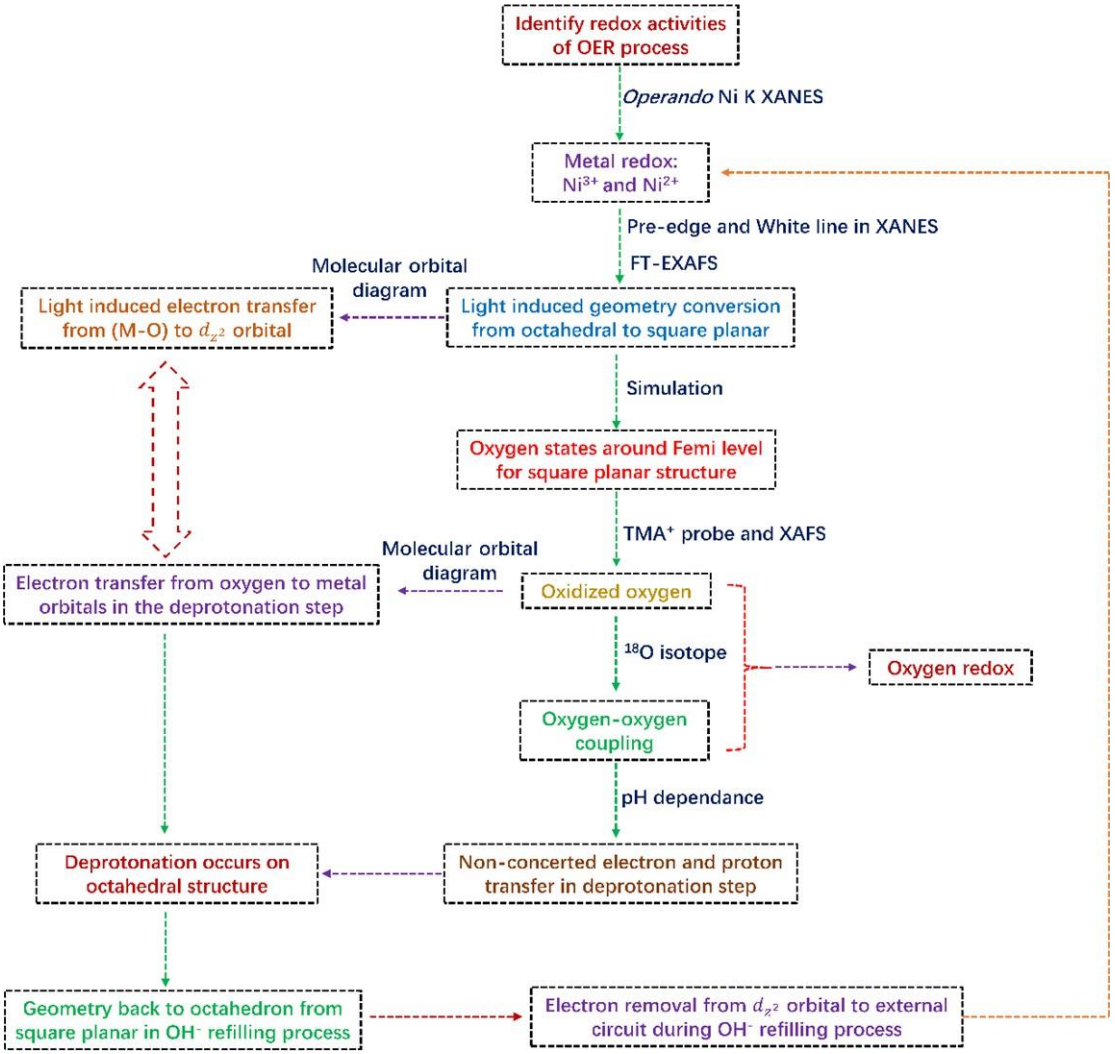

Figure R16. Idea flow of our experimental approach. Fig. S8 in our revised Supplementary Information

C1. Please give the details of the FT of the EXAFS data. What energy range was used? What window function and which parameters? The fitting parameters are also not documented? How (method) was the fit performed? In R or k-space or filtered space? What E/k/R range was used? What software was used? What model or sample was used to obtain phase functions? What was the amplitude reduction factor, S02, and energy shift E0? What energy value was used to convert to k-space? Without these experimental details, the EXAFS analysis is not reproducible by others.

Response: We sincerely appreciate this insightful suggestion. The details of the FT of the EXAFS are provided below:

Details of the FT of the EXAFS:

- Energy range: 30-450 eV above absorption edge.
- Window function: Hanning
- K range: 3-11 $Å^{-1}$.
- K-weight: 3

Fitting parameters:

- Method: least-squares
- Space: R
- K range: 3-11 $Å^{-1}$
- R rang: 1-3 Å
- Software: Artemis
- Initial structure: standard β-$Ni(OH)_2$.
- Theoretical scattering path calculation code: FEFF6

$S0^2$: 0.7, obtained from EXAFS fitting of standard Ni Foil.
E_0 used to convert from E space to K space: 8344.9 eV for NR-NiOOH dark; 8343.5 eV for NR-NiOOH light-c NR-NiOOH sample.
K weight during EXAFS fitting: 1,2,3
K weight used in plot: 3

According to the referees' advice, we have added these parameters in the revised Supporting Information (Page 5, highlighted in crimson).

C2. Please give more details on the experiment in Fig. S4e? What was the pre-treatment? What were the conditions during the experiment? Please add a sentence about the connection between hole scavenger and oxygen evolution for non-experts.

Response: The pre-treatment and conditions of photocatalytic measurement is shown below:

10 mg NR-NiOOH powder was suspended in 20 mL phosphate buffer solution (0.1 M, pH =7) containing 0.1 M $K_2S_2O_8$. Prior to the photocatalytic experiment, the suspension was bubbled with nitrogen gas (10.0 mL/min) for 10 hours in an air-tight tube to remove all dissolved O_2 in the solution. When all traces of oxygen were removed, the suspension was illuminated with a light source, supplied by a 300 W Xenon lamp equipped with AM 1.5 filter (NBeT, Solar-500, Beijing). The intensity of the light was 100 mW cm^{-2} calibrated by a light power meter (Newport 843-R). It is worth noting that the suspension was stirred at a rate of 800 r/min under illumination. Then, the gas product was manually collected and subsequently analyzed by gas chromatography. The description of our photocatalytic measurement was also included in our revised Supporting Information (Page 4, highlighted in crimson).

We have added the following paragraphs in our revised Supporting Information (Page 9, highlighted in crimson) to explain the role of sacrificial electron acceptors during the photocatalytic measurement:

Discussion on the possible reasons for the enhanced OER activity triggered by light

.... Generally, the requirements of the overall water-splitting photocatalysts are stringent, and no response can be obtained if the conditions of either oxygen evolution or hydrogen evolution reaction are not met. Performing trial oxygen evolution reaction in the presence of sacrificial electron acceptors is one way to assess the suitability of the band position of a specific composition to act as an OER photocatalyst. The potential of the holes was examined using gas chromatography with $K_2S_2O_8$ as the electron acceptor, and no oxygen was detected within 2.5 hours of operation (Fig. S4d). This result indicates that the enhanced OER activity in NR-NiOOH is not attributed to the generation of light-induced holes.

One sentence has been added in Fig. S4 to state the role of sacrificial electron acceptor in the OER photocatalyst measurement (Page 23, highlighted in crimson):

Performing a trial OER measurement in the presence of a sacrificial electron acceptor is one way to assess the suitability the band position of a specific composition as an OER photocatalyst.

C3. Fig. S4c. Please plot with equal scaling on the x and y-axis (as per EIS convention). Which resistance is indicated in the figure? Ru (uncompensated resistance of the electrolyte and material)?

Response: In the electrochemical measurement, it is assumed that the potential drop across the interfacial region at the working electrode is the same as the potential applied between the reference and working electrode.

However, this is not the real case, as there is a certain potential drop between these two electrodes due to the resistance of electrolyte and material. This potential drop is defined as iR drop, and it can be eliminated by employing iR correction/compensation. The resistance of the system can be estimated using the following simplified model of the electrochemical behavior in the electrochemical cell, as shown in Figure R17 (Fig. S4c in our revised Supporting Information). R_u is related to the electrolyte resistance, while R_s and C are related to the electrode materials. When a high-frequency current passes through the entire circuit, the current will pass through C rather than R_s. In this case, the entire resistance of the system is only R_u. However, when a low frequency passes through the circuit, the current will pass through R_s. In this case, the entire resistance of the system is R_s+R_u. In our work, we used the entire resistance for *iR* correction.

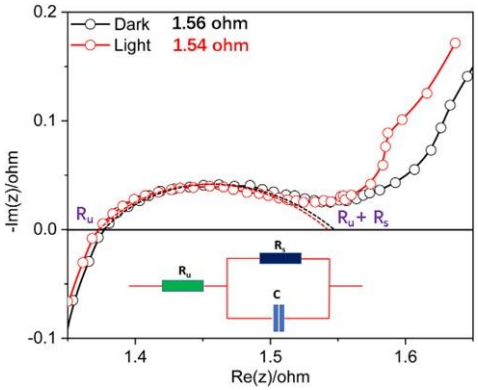

Figure R17. Electrochemical impedance spectroscopy data for NR-NiOOH with and without light. (Fig. S4c in our revised Supporting Information).

According to the reviewer's suggestion, we have revised Fig. S4c with Figure R17 (plotted with the same scaling), and its corresponding discussion is included in our revised Supporting Information (as shown below, Page 23 in our revised Supporting Information, highlighted in crimson):

…It was measured using a three-electrode configuration in 1 M KOH solution. R_u is the resistance of the catalytic material and R_s is the resistance of the electrolyte. In our work, we used the entire resistance (R_u + R_s) for *iR* correction. After fitting the result, it is found that the resistances (R_u + R_s) of NR-NiOOH under dark and in the light were relatively similar.…

C4. How can the analysis in Fig. 3b be done with only one experimental reference (b-Ni(OH2))? One needs at least two points or a point and slope for the calibration.

Response: We are very thankful for this insightful suggestion. We have added more calibration samples, *i.e.*, NiO (Ni^{2+}) and $K_2Ni(H_2IO_6)_2$ (Ni^{4+}) in our revised Supporting information as shown in Figure R18 (Fig. S9a in our revised Supporting Information).

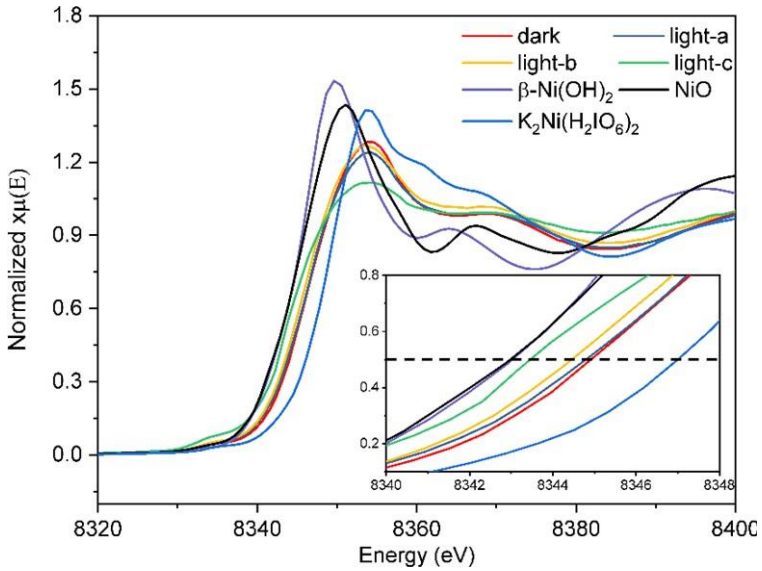

Figure R18. Ni *K*-edge XANES spectra of NR-NiOOH without and subjected to light irradiation using standard β-$Ni(OH)_2$ (Ni^{2+}), NiO (Ni^{2+}) and $K_2Ni(H_2IO_6)_2$ (Ni^{4+}) as the reference (inset showing the absorption edge of these samples). To estimate the 3*d* orbital occupancy, we track the oxidation state of each sample with XANES (absorption edge). (Fig. S9a in our revised Supporting Information, Page 31)

D. Statistics

No statistic analysis of the results is performed. The manuscript could be significantly improved if the (photo)electrochemical experiments were repeated to calculate standard deviations. It is unclear if the experiments were repeated by the authors and if the given electrochemical values are representative.

Response: Four additional NR-NiOOH samples were evaluated under light irradiation, and their overpotentials recorded at 10 mA cm^{-2} ranged between 145 mV to 155 mV (Figure R19, Fig. S5b in our revised Supporting Information). The standard deviation value of the dataset, *i.e.*, 145, 146, 155, 150, and 147 (Figure 2c), is 3.6, which indicates that the electrochemical experiments are highly repeatable.

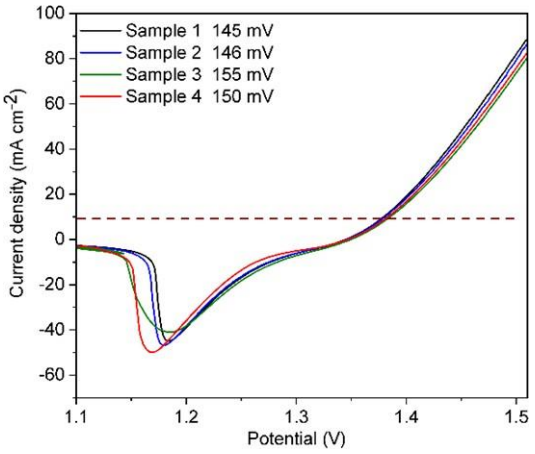

Figure R19. OER polarization curves of four additional NR-NiOOH samples recorded at a scan rate of 0.1 mV/s under light irradiation. Fig. S5b in our revised Supporting Information.

According to the reviewer's suggestion, we have added Figure R19 in our revised Supporting information as Fig. S5b, Page 25 and the following sentences in our revised manuscript (Page 6): To ensure the reliability of the OER activity measurements, four more samples were evaluated under light irradiation with recorded overpotentials ranging between 145 mV to 155 mV at 10 mA cm^{-2} (Fig. S5b).

E. Conclusions
The main conclusions
(1) light activation enables a mechanism with both metal and oxygen redox whereby the rate-liming steps with a single type of redox are improved upon
(2) superior oxygen evolution activity compared to previously reported electrocatalysts
Could be further supported by additional data and more direction measurements (see points F below).
Conclusion 1 is speculative as only metal redox is supported directly by measurements. Furthermore, no statement can be made about the activity of the electrocatalyst with the used metric. I expect that this can be easily improved by revision.

Response: We have revised our manuscript and Supporting Information according to the referee's advice (detailed revision is shown in Section E and F).

There are some statements and interpretations that I disagree with or that need to be clarified
E1 The lifetime of photoexcited holes not of the order of hours as claimed. They are typically ~<10s in other oxides: https://pubs.acs.org/doi/10.1021/ja412058x. Clearly there is a structural change which is a much more straightforward explanation for the observations than an excited state that lasts hours.

Response: According to the referee's advice, we have removed the figures of photoexcited holes and added the following in Fig. S5 in our revised Supporting Information (Page 25, highlighted in crimson):

…More importantly, our *operando* XAFS data show a geometry conversion from octahedral to square planar under light irradiation, which indicates that this type of photon-induced electron transfer is not a photocatalytic behavior (Fig. S10 to 12).

The reference https://pubs.acs.org/doi/10.1021/ja412058x. is added in our revised manuscript (ref 18, highlighted in crimson): Based on our experimental results, the improvement in the OER performance as demonstrated by NR-NiOOH under light irradiation is unlikely to be a result of reduced ohmic resistance, light-induced crystal growth, or generation of holes (Fig. S4 and Supplementary Text) (*18, 19*). (Page 8 in our revised manuscript).

E2. The coordination number of Ni-O

(Table S2) in the dark (5.1±0.5) and in light (4.2±0.9) are identical within the fit error. This contradicts the statement on P9 that "the Ni-O coordination number in NR-NiOOH is greatly reduced when subjected to light".

Response: According to the referee's advice, the result for NR-NiOOH under light irradiation was refitted, as shown in Figure R20 and Table R1. The new result indicates that the Ni-O coordination numbers in NR-NiOOH when subjected to light reduced from 5.1±0.5 to 3.8±0.6.

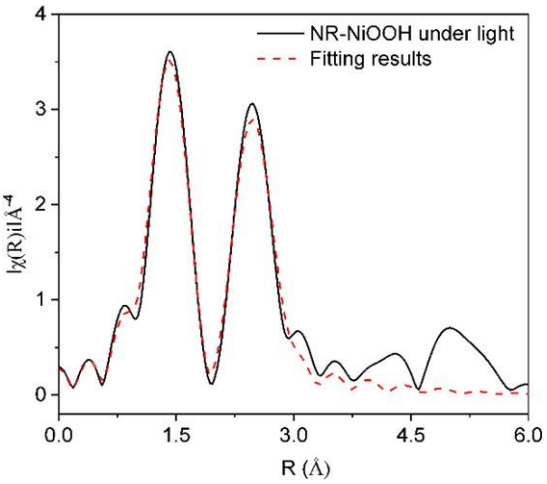

Figure. R20. Fitting result for NR-NiOOH under light irradiation.

Table R1. FT-EXAFS fitting results of NR-NiOOH under dark conditions and NR-NiOOH under light irradiation (light-c in Fig. 3a), where CN is the coordination number, R is the bond length, and σ^2 is the Debye-Waller factor.

Sample	Bond species	CN	R (Å)	σ^2 (Å^2)	R factor
NR-NiOOH under dark	Ni-O	5.1±0.5	1.85±0.01	0.0056±0.0006	0.0050
NR-NiOOH under light	Ni-O	3.8±0.6	1.87±0.01	0.0074±0.0029	0.0110

According to the referee's advice, the new fitting results are shown in Table S5 in our revised Supporting information (Page 65, highlighted in crimson).

3. P16. "which results in the COM route during the OER process. These calculations agree well with the experimental results (Fig. 2a)." It is unclear how exactly the COM route is visible in Fig 2a. I ask below to discuss the values of the Tafel slope and reaction order to support such a statement.

F3. Are the mechanisms in Fig. 1 and 4 compatible with the determined Tafel slopes and reaction orders (the latter two in Fig. 4)? What values of the Tafel slope and reaction order is expected for the proposed rate-limiting steps and starting state? I am confused about the values of the slope in Fig. 4a. the reaction order with respect to pH is defined as d[logi]/dpH, which is the indicated slope in the figure. It should have values between 0 and 1 on the RHE scale (e.g.https://www.sciencedirect.com/science/article/abs/pii/S0926586115006227?via=ihub and application in https://chemistry-europe.onlinelibrary.wiley.com/doi/full/10.1002/cssc.201701582)

Response: Since both E3 and F3 focus on the discussion of Tafel slope and reaction order, these two answers are combined. Based on the calculations, deprotonation step has become the rate-determining step in our proposed COM. Since the electron transfer during deprotonation is triggered by light, proton transfer should be considered intrinsically as the rate-determining step. Next, the Tafel slope and reaction order of the proposed COM are discussed.

Tafel slope

This theoretical Tafel slope can be calculated using the formula derived by Fletcher (*J. Solid State Electrochem*. 13, 537-549, 2009):

$$\frac{2.303RT}{\alpha F}$$

In this equation, $\alpha = n_p + n_q \beta_f$, where n_p is defined as the number of electrons transferred prior to the rate-determining step, n_q is the number of electrons transferred during the rate-determining step, and β_f is the fundamental term describing the rate-determining step of a single electron transfer reaction. Here, OH^* adsorption step was used as the starting step. In our proposed COM, a two-electron transfer from the d_{z^2} orbital to the external circuit occurs during the OH^* adsorption step, and another two-electron transfer from (O-O) coupling bands to the external circuit during the oxygen evolution step. Hence, n_p is 2 and n_p is 0. As a result, the calculated Tafel slope value is 29.5.

In our work, the theoretical value agrees well with the measured Tafel slope value under light irradiation, *i.e.*, 31 (Figure R21, Fig. S5d in our revised Supporting Information). At the same time, according to our calculation results based on the AEM route, OOH* is regarded as the rate-determining step. A previous report showed that the calculated Tafel slope in the case of high O* surface coverage was 60 mV dec^{-1} when OOH* was the rate-determining step (*Sci. Rep.* 5, 13801, 2015). This value agrees well with the Tafel slope value obtained for the sample under dark conditions, *i.e.*, 63 (Figure R21, Fig. S5d in our revised Supporting Information). These results clearly indicate that the rate-determining step changes from OOH* formation to proton transfer under light irradiation, which is highly consistent with our proposed light-induced OER mechanism conversion from AEM to COM. The variations of rate determining step under light could be further identified through TMAOH measurement. TMA^+ ions would block the formation of (O-O) coupling, further inhibiting the COM process (detailed mechanism discussion is shown in response to F8). It shows that after adding TMAOH, the Tafel slope of NR-NiOOH under light irradiation decreased from 31 mV dec^{-1} to 60 mV dec^{-1}, which agrees well with the OER mechanism from COM to AEM after the addition of TMAOH (Figure R22, Fig. S18 in our revised Supporting Information).

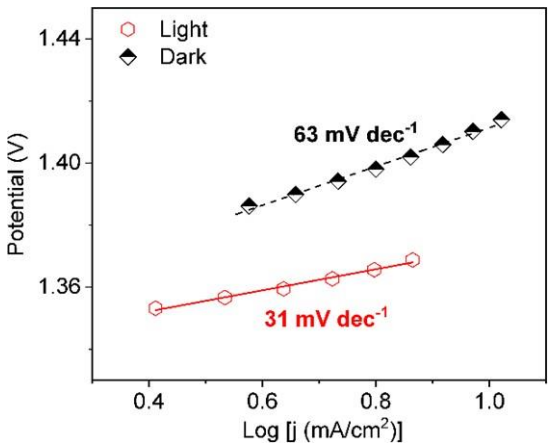

Figure R21. Tafel slope of NR-NiOOH under AM 1.5G and dark. To achieve a better linear fitting, the current range value was selected between 0.4 and 0.9 for the sample under light irradiation, and between 0.5 and 1.0 for the sample under dark conditions. Fig. S5d in our revised Supporting Information.

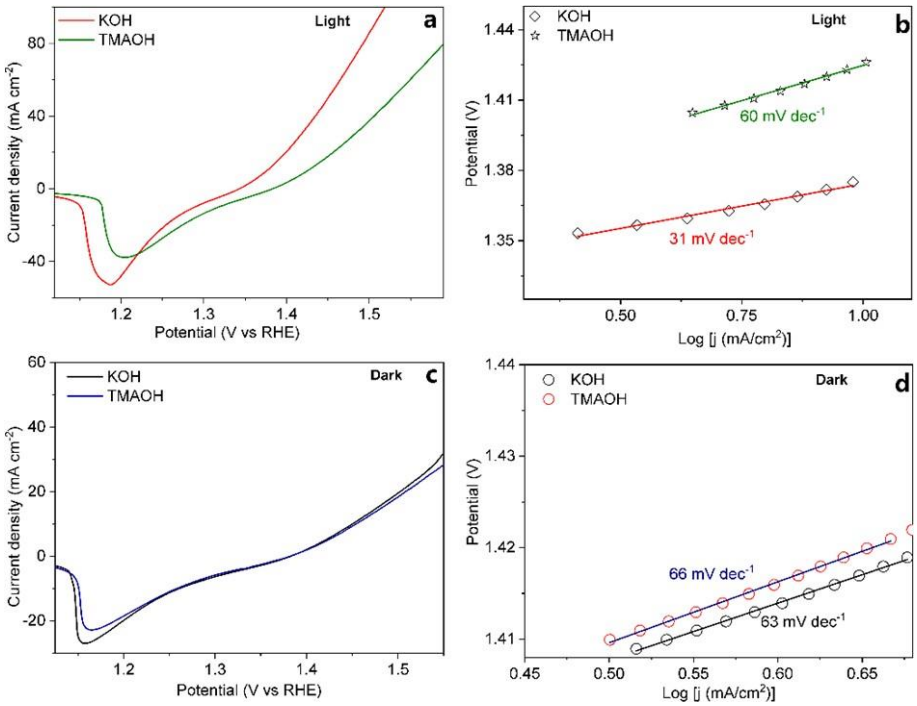

Figure R22. LSV and Tafel slopes of NiFe LDH in the dark (a) and (c), and light (b) and (d) in KOH and TMAOH electrolyte. Fig. S18 in our revised Supporting Information.

Reaction order. Identification of the pH dependence of OER activity can provide insights into the reaction path, *i.e.*, a zero-order reaction indicates a concerted electron and proton transfer, while a first-order reaction indicates a non-concerted electron and proton transfer. In the conventional AEM route, proton and electron transfer is a concerted process. In contrast, for our proposed COM route, the deprotonation step becomes a non-concerted process, whereby it involves (1) proton transfer on the octahedron, and (2) subsequent light-induced electron transfer from (M-O) to d_{z^2} orbital. According to these discussions, when compared to NR-NiOOH under dark conditions, NR-NiOOH under light irradiation is expected to exhibit OER activity that is significantly dependent on the pH value. To verify this, OER performances of the samples under and without light irradiation were recorded under various pH values (Figure R23, Fig. 20 in our revised Supporting Information). The experiment results show that the reaction order of NR-NiOOH subjected to light irradiation is 0.36, which is three times larger than that under dark (0.12). The significant increase in the reaction order indicates the presence of non-concerted proton and electron transfer during the OER process for the sample under light irradiation.

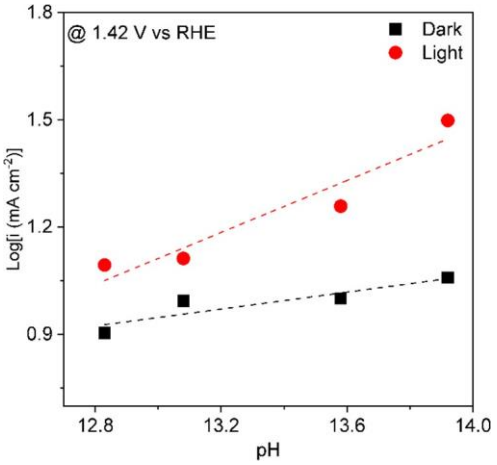

Figure R23. pH dependence of OER activities of NR-NiOOH exposed to light and in dark conditions. Fig. S20 in our revised Supporting Information

According to the reviewer's suggestion, we have conducted the following changes:

1) The discussion on Tafel slope and reaction order has been added in the revised manuscript and Supplementary Information:

a) In the revised manuscript (Page 13, highlighted in crimson):

Based on the calculations, the rate determining step in our proposed COM route is the proton transfer step, which is consistent with the results obtained from the Tafel slope and reaction orders (Fig. S5d, S20 to 21 and Supplementary Text) (*34-35*).

b) In the revised Supplementary Information (Paragraph 3, Page 14, highlighted in crimson):

Discussion on the Tafel slope

Theoretical Tafel slope can also be calculated based on the formula derived by Fletcher (*2*):

$$\frac{2.303RT}{\alpha F}$$

In this equation $\alpha = n_p + n_q\beta_f$, where n_p is defined as the number of electrons transferred prior to the rate-determining step, n_q is the number of electrons transferred during the rate-determining step, and β_f is the fundamental term describing the rate-determining step of a single electron transfer reaction. Here, we used OH^* adsorption step as the starting step. In our proposed COM, a two-electron transfer from d_{z^2} orbital to the external circuit occurs during the OH^* adsorption step, and another two-electron transfer from the (O-O) coupling bands are transferred to the external circuit during oxygen evolution step. Hence, n_p is 2 and n_p is 0. Based on these conditions, the Tafel slope value is 29.5.

In our work, the theoretical value agrees well with the measured Tafel slope value obtained from the sample under light irradiation, *i.e.*, 31 (Fig. S5d). At the same time, based on our calculations of the AEM route, OOH* is regarded as the rate-determining step. Previous report has shown that the calculated Tafel slope in the case of high O^* surface coverage was 60 mV dec^{-1} when OOH^* is the rate-determining step (*3*). This value is in good agreement with the Tafel slope value obtained from the sample in dark condition, *i.e.*, 63 (Fig. S5d). These results clearly indicate that the rate determining step changes from the typical OOH^* formation to proton transfer when being subjected to light. This phenomenon is highly consistent with our proposed light induced OER mechanism as it switches from AEM to COM under light irradiation. The variations in the rate determining step under light can be further identified *via* TMAOH measurement. TMA^+ can block the formation of (O-O) coupling, which further inhibits the COM process. It shows that the Tafel slope of NR-NiOOH under light irradiation decreased from 31 mV dec^{-1} to 60 mV dec^{-1} after adding TMAOH, which indicates the reverting of the OER mechanism from COM back to AEM (Figure S18).

Discussion on the reaction order

Identification of the pH dependence of OER activity can provide insights into the reaction path, *i.e.*, a zero-order reaction shows a concerted electron and proton transfer, and a first-order reaction indicates a non-concerted electron and proton transfer. In conventional AEM route, proton and electron transfer is a concerted process, while in our proposed COM route, deprotonation step becomes a non-concerted process. The deprotonation step involves (1) the occurrence of proton transfer at the octahedron, and (2) subsequent light-induced electron transfer from (M-O) to d_{z^2} orbital. According to these discussions, as compared to NR-NiOOH under dark conditions, NR-NiOOH under light irradiation is expected to exhibit an OER activity with significant pH dependence. To verify this, OER performances of the samples under and without light irradiation were recorded at various pH values (Figure S20). The experiment results shows that the reaction order of NR-NiOOH subjected to light irradiation is 0.36, which is three times larger than that under dark conditions, *i.e.*, 0.12. The significant

increase in the reaction order indicates the presence of non-concerted proton and electron transfer during OER process for the sample under light irradiation.

2) In our original manuscript, the current range value for the sample under light irradiation was between 0.4 and 1.1, while the current range value for the sample under dark conditions was selected between 0.55 and 1.05. (Fig. S9 in our original Supplementary Information). To achieve a better linear fit for the Tafel slope, the current range value for the sample under light irradiation was selected between 0.4 and 0.9, while the current range value for the sample under dark conditions was selected between 0.5 and 1.0 (Fig. S5d in revised Supplementary Information, Page 25).

3) The current density i in Figure 4a of our original manuscript is changed to Log[i] in Fig. S20 in our revised Supplementary Information (Page 44).

4) The experiment results regarding D_2O are removed in our revised manuscript

5) The discussion on OER performance after the addition of TMAOH is combined with XAFS (detailed in the response to F8 and oxygen redox discussion in our revised manuscript and Supplementary information).

6) The references of https://www.sciencedirect.com/science/article/abs/pii/S0926586115006227?via=ihub and https://chemistry-europe.onlinelibrary.wiley.com/doi/full/10.1002/cssc.201701582 are added in our revised manuscript (as ref 34 and 35, respectively. Highlighted in crimson): Based on the calculations, the rate determining step in our proposed COM route is the proton transfer step, which is consistent with the results obtained from the Tafel slope and reaction orders (Fig. S5d, S20 to 21 and Supplementary Text) (*34-35*). (Page 13 in our revised manuscript).

F. Suggested improvements

F1. The “catalyst activity” is given as overpotential at 10 mA/cm2 by normalization of the electrode area. This metric measures the activity of a composite electrode, not solely of the catalyst material, refer to e.g.https://onlinelibrary.wiley.com/doi/abs/10.1002/adma.201806296. This reference also provides state-of-the art intrinsic activities of electrocatalyst materials.

Please normalize by a catalyst property such as loading or surface area of the catalyst or the turnover frequency and compare those to literature.

Response: According to the referee’s advice, we have added the results of the current normalization to electrochemically active surface areas/loading mass and turnover frequency, as shown in Figure R23 (Fig. S7 in our revised Supporting Information). Electrochemically active surface areas (ECSAs) of the samples were evaluated based on the C_{dl} (double layer capacitance) measurement, and the current densities were normalized to ECSAs (Figure R24 a and b). The loading mass of NR-NiOOH was 0.42 mg cm^{-2}, which was calculated based on the Inductive Coupled Plasma (ICP) analysis. The turnover frequency (TOF) was calculated using the following equation; $TOF=\frac{I}{4*F*m}$ (where I: current in amperes; F: Faraday constant; m: number of moles of the active catalyst). Note that all catalysts were assumed to be active in this work.

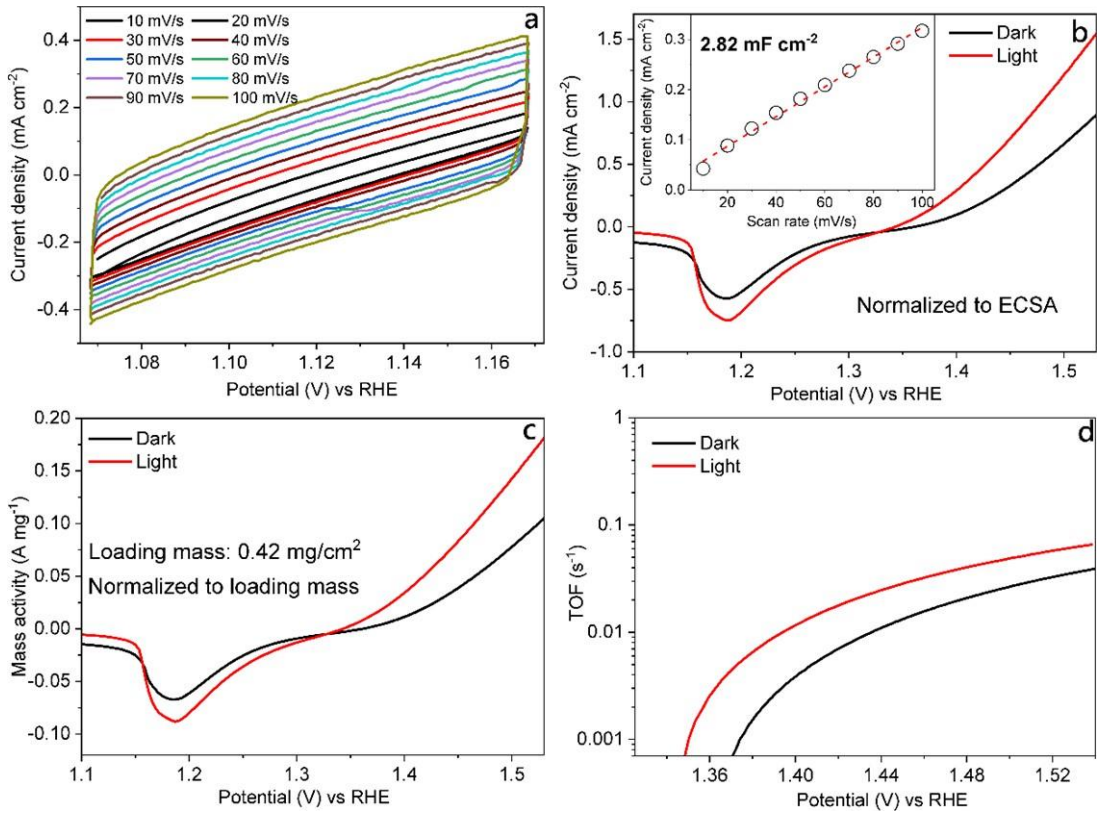

Figure R24. (a) Electrochemical surface area (ECSA) of NR-NiOOH sample; (b) current density normalized to ECSA; (c) current density normalized to loading mass; (d) turnover frequency of NR-NiOOH sample under dark conditions and light irradiation. (Fig. S6 in our revised Supporting Information)

The comparisons of the current normalized to ECSA for our work and the previous reports are provided in Table R2 in the revised Supporting Information as shown below:

Table R2. Comparison of the current normalized to ECSA of NR-NiOOH under light irradiation and selected previously reported OER catalysts. Table S2 in our revised Supporting Information.

Catalyst	Electrolytes	j (mA $cm^{-2}_{specific}$) at potential 1.50 V vs RHE	Ref
IrO_2 NP	0.1 M $HClO_4$	0.010	*J. Phys. Chem. Lett.* **3,** 399, 2012
RuO_2 NP	0.1 M $HClO_4$	0.020	
$Ru_{0.7}Ni_{0.3}O_{2-y}$	0.1 M $HClO_4$	0.080	*J. Solid State Electrochem.* **13,** 959, 2009
La_2LiIrO_6	0.05 M H_2SO_4	0.600	*Nat. Energy* **2,** 16189, 2016
Sputter RuO_2	0.05 M H_2SO_4	1.050	*ChemElectroChem* **1,** 2075, 2014
$IrO_x/SrIrO_3$	0.5 M H_2SO_4	7.300	*Science* **353,** 1011, 2016,

		0.32 (1.45 V)	
$LaCoO_3$	0.1M KOH	0.009	*Nat. Chem.* **9,** 457, 2017
$La_{0.5}Sr_{0.5}CoO_{3-\delta}$	0.1M KOH	0.017	
$SrCoO_{3-\delta}$	0.1M KOH	0.300	
$CaCu_3Fe_4O_{12}$	0.1M KOH	0.045	*Nat. Commun.* **6,** 8249, 2015
NR-NiOOH under light irradiation	1 M KOH	1.230 0.730 (1.45V)	**Our work**

Comparisons of the current normalized to loading mass for our work and the previous reports are provided in Table R3 in the revised Supporting Information as shown below:

Table R3. Comparison of the current normalized to loading mass of NR-NiOOH under light irradiation and selected previously reported OER catalysts. Table S3 in our revised Supporting Information.

Catalyst	Electrolyte	j (A mg^{-1}) at potential 1.50 V vs RHE	Ref
IrO_2 NP	0.1 M $HClO_4$	0.007	*J. Phys. Chem. Lett.* **3,** 399, 2012
RuO_2 NP	0.1 M $HClO_4$	0.030	
$IrNi_{3.3}$ NP	0.05 M H_2SO_4	0.180	*Chem. Sci.* **5,** 2955, 2014
$2.9*10^6$ u Ru NP	0.05 M H_2SO_4	0.040 (1.40 V)	*Chem. Sci.* **6,** 190, 2015
BCFSn-721	0.1 M KOH	0.081 (1.68 V)	*Adv. Sci.* **3,** 1500187, 2016
Co-Fe-O frames	1 M KOH	0.170 (1.53 V)	*Chem* **4,** 1967-1982, 2018
$LaCo_{0.8}Fe_{0.2}O_3$	0.1M KOH	0.004 (1.52 V)	*Energy Environ. Sci.* **11,** *2945-2953, 2018*
SrCoO0.85- δ Fe0.15	1M KOH	0.093 (1.65 V)	*J. Mater. Chem. A* **7,** 12538-12546, 2019
NR-NiOOH under light irradiation	1 M KOH	0.036 (1.40 V) 0.140 (150 V)	**Our work**

The comparisons of TOF for our work and the previous reports are provided in Table R4 in the revised Supporting Information as shown below:

Table R4. Comparison of turnover frequency (TOF) of NR-NiOOH under light irradiation and selected previously reported OER catalysts. Table S4 in our revise Supporting Information.

Catalyst	Electrolytes	turnover frequency (s^{-1})	Ref
Co_3O_4	1 M KOH	0.09 (1.62 V) 0.02 (1.56 V)	*J. Phys. Chem. Lett.* **113,** 33, 2009
CoO	1 M KOH	0.040 (1.74 V)	*ChemSusChem.* **4,** 1566-1569, 2011
RuO_2	0.5 M H_2SO_4	0.005 (1.46 V)	*Nat. Commun.* **10,** 162, 2019
$Cr_{0.6}Ru_{0.4}O_2$	0.5 M H_2SO_4	0.080 (1.46 V)	
Graphene-NiFe	1 M KOH	0.030 (1.53 V)	*Sci. Adv.* **4,** eaap7970, 2018
IrO2-RuO_2	0.5 M H_2SO_4	0.003 (1.55 V)	*J. Mater. Chem. A* **5,** 17221-17229, 2017
NR-NiOOH under light irradiation	1 M KOH	0.030 (1.45 V) 0.050 (150 V)	**Our work**

Based on Table R2 to R4, by normalizing to the electrochemical surface area, NR-NiOOH under light irradiation was able to maintain superior activities especially in the low potential range, *i.e.*, <1.45 V *vs.* RHE, as compared to other OER electrocatalysts. However, when this is normalized to loading mass or when considering the turnover frequency, the merits of NR-NiOOH under light irradiation are not outstanding. Such an observation can be easily understood. In the case of the normalization of current to loading mass and turnover frequency, all catalysts are assumed to be active. However, this is not the real case, since most catalysts are buried within, which remain to be inactive during the OER process. The loading mass of our NR-NiOOH was 0.42 mg/cm^2, while for most of the cited works, the loading mass on the glassy carbon was usually in the range of 0.03 to 0.2 mg/cm^2. Hence, for our NR-NiOOH, the ratio of active catalysts to all catalysts is much lower than that of the one coated on the glassy carbon.

According to the reviewer's suggestion, we have done the following changes:

1) We have added the following sentence in our revised manuscript (Page 7, highlighted with crimson color): The intrinsic activity, *i.e.*, current normalized to electrochemical surface area/loading mass and turnover frequency, of NR-NiOOH was compared with those in the previous reports as shown in Fig. S6 and Table S2 to S4 (*17*).

2) The results of the current normalized to electrochemically active surface areas/loading mass and turnover frequency have been added in the revised Supporting Information (Fig. S6, Page 27, highlighted with crimson color)

3) Table R2 to R4 have been added in the revised Supporting Information (Table S2 to S4, Page 62, highlighted with crimson color)

3) https://onlinelibrary.wiley.com/doi/abs/10.1002/adma.201806296 has been cited in our manuscript as ref 17 (highlighted in crimson): The intrinsic activity, *i.e.*, current normalized to electrochemical surface area/loading

mass and turnover frequency, of NR-NiOOH was compared with those in the previous reports as shown in Fig. S6 and Table S2 to S4 (*17*). (Page 7, highlighted with crimson color)

Table S1 contains few entries. More active NiFe LDH electrodes are known: https://onlinelibrary.wiley.com/doi/10.1002/aenm.201600621

Response: According to the reviewer's suggestion, we have included more examples of active NiFe LDH electrode in Table R5 (Table S1 in our revised Supporting Information, highlighted with crimson color):

Catalyst	Electrolytes	Overpotential (mV) at 10 mA cm^{-2}	Tafel slope	Ref
G-FeCoW	1 M KOH	191	-	*Science* **352,** 333-337, 2016
$NixFe_{1-x}Se_2$-DO	1M KOH	195	28	*Nat. Commun.* **7,** 12324, 2016
Ni_3N COF	1M KOH	230	79	*Adv. Energy. Mater.* **6,** 1601189, 2016
Co_3O_4/N-rmGO	1 M KOH	310	67	*Nat. Mater.* **10,** 780-786, 2011
CoZnOOH	1M KOH	285	35	*Nat. Ener.* **4,** 329-338, 2019
PBSCF-III	0.1M KOH	358	52	*Nat. Commun.* **8,** 14586, 2017
$Ba_{0.5}Sr_{0.5}Co_{0.8}Fe_{0.2}O_3$	0.1M KOH	370	-	*Science* **334,** 1383-1385, 2011
$CaFeO_3$	0.1M KOH	390	47	*Nat. Commun.* **6,** 8249, 2015
NiCo-UMOFENs	1 M KOH	189	65	*Nat. Ener.* **1,** 16184, 2016
IrO_2	1M KOH	325	54	*J. Am. Chem. Soc.* **135,** 16977-16987, 2013
NiFe/NF	1M KOH	215	28	*Nat. Commun.* **6,** 6616, 2015
FeNi-rGO LDH	1M KOH	206	39	*Angew. Chem. Int. Ed.* **53,** 7584, 2014
NR-NiOOH under light irradiation	1 M KOH	135	31	Our work

https://onlinelibrary.wiley.com/doi/10.1002/aenm.201600621 has been cited in our manuscript as ref 16 (highlighted in crimson): This result, to the best of our knowledge, is the best OER performance reported so far (Table. S1) (*16*). (Page 7 in our revised manuscript).

Please also show the iR corrected data that is mentioned on P6.

Response: According to the reviewer's suggestion, the iR corrected LSV is provided in our revised Supporting Information, as shown in Figure R25 (Fig. S5c in our revised Supporting information). It shows that the overpotential of NR-NiOOH sample under light irradiation at 10 mA cm^{-2} was 135 mV after applying 90% *iR* correction (R= 1.5 ohm), which is approximately similar to the value mentioned in our manuscript, *i.e.*, 133 mV (Line 9, Page 6 in our original manuscript).

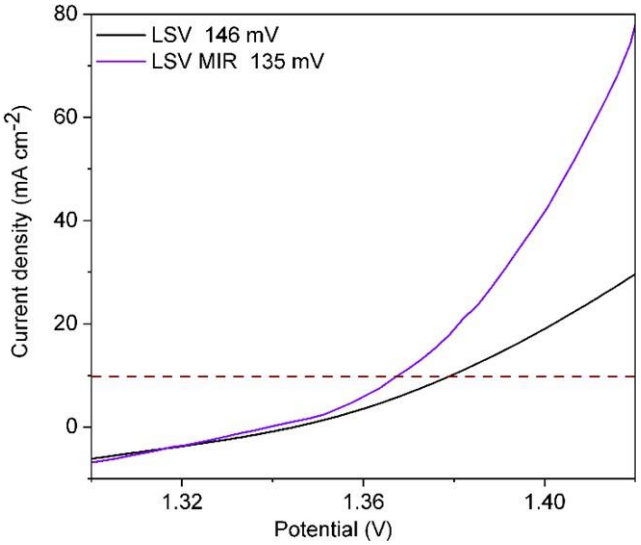

Figure R25. OER polarization curves at a scan rate of 0.1 mV s^{-1} and 90% *iR* correction. Fig. S5c in our revised Supporting Information.

According to the reviewer's suggestion, Figure R25 has been added in our revised Supporting Information (Fig. S5c, Page 25).

One sentence was added in our revised manuscript: Simultaneously, with 90% *iR* correction, NR-NiOOH under light irradiation exhibited an extremely low overpotential of 135 mV at 10 mA cm^{-2} (Fig. S5c). (Page 6 in our revised manuscript).

F2. LOM in Fig 1b is based on ref 11 but in ref 10, the authors propose both metal and oxygen redox. A more comprehensive discussion of previous LOM proposals would improve the manuscript and help to highlight the novelty of this work.

Response: In the previous response, we have shown that LOM is a type of oxygen redox reaction. To give a comprehensive understanding of LOM, we have added the following discussion on the oxygen redox activities of LOM in our revised supporting information (Page 8):

Conventional LOM process involves deprotonation, O-O coupling, and O_2 release (as shown in Fig. 1b). During the deprotonation step, hydrogen-oxygen chemical bond is firstly broken, and then one proton is removed from the adsorbed OH^- group. Concurrently, the adsorbed OH^- will change into O^{2-}. In the subsequent electron transfer process, O^{2-} will transform into O^-, to realize O-O coupling. It is well known the O-O coupling step is a chemical process that proceeds by hybridizing the non-bonding oxygen states in the neighboring O^-. As a result, the

electron configuration of O^- is less than 8 which is a type of oxidized oxygen state. Consequently, as O^{2-} is converted to O^-, one electron is transferred from the oxygen orbitals of O^{2-} into the external circuit, whereby oxygen acts as the redox center. During the oxygen evolution step, two electrons have to be removed from the oxygen orbitals of $(O\text{-}O)^{2-}$ to achieve the electronic structure of O_2. Consequently, oxygen acts as the redox center during this process. As such, according to our analyses, a two-electron transfer from oxygen orbitals occurs during the deprotonation step, while the other two-electron transfer from oxygen orbitals occurs during the generation of O_2, which sums up to the four-electron transfer process during OER. Thus, based on this discussion, LOM is a type of oxygen redox reaction.

F4. Please show and discuss the enhancement effect due to day light or laboratory light. While a 300 W Xenon lamp is a good approach for controlled demonstration, the activation mechanism would be more interesting if daylight or stray light from common building lighting is sufficient.

Response: We are very thankful for this insightful suggestion. Our description regarding the light source in Supporting Information may confuse the readers. In our work, 300 W refers to the type of Xenon lamp rather than the intensity of light irradiated on the electrocatalysts. To avoid any misunderstanding, we have corrected the description in our revised Supporting Information (Page 4, highlighted in crimson): A solar simulator (NBeT Solar-500, 300 W) was used as the light source to simulate AM 1.5G. The intensity of light irradiated on the electrocatalyst was 100 mW cm^{-2} as calibrated by a light power meter (Newport 843-R).

According to the referee's advice, the LSV curves of NR-NiOOH under laboratory light (12.3 mW cm^{-2}) is also provided in Figure R26 (Fig. 5a in our revised Supporting Information). The experiment shows that when the sample is subjected to laboratory light irradiation, an overpotential of 167 mV is required to reach a current density of 10 mA cm^{-2}. This measured overpotential is 6 mV lower than that of NR-NiOOH in the dark, which implies the positive effects of laboratory light irradiation on enhancing OER performance of NR-NiOOH. However, this enhancement is incomparable to that under AM 1.5G. The reason for such a difference is related to the step whereby electron from (M-O) is transferred to d_{z^2} orbital when induced by light. In our proposed COM, the electron transfer from oxygen to metal orbital is triggered by light, while the electron transfer from metal orbital to external circuit and oxygen orbital to external circuit is fueled by electricity. It means that the reaction rate of COM depends on both potential and light irradiation. As compared to the light in the laboratory, the intensity of photon in AM 1.5G is significantly higher. It can result in the transfer of more electrons from (M-O) to d_{z^2} orbital, which in turn improves the OER activities further.

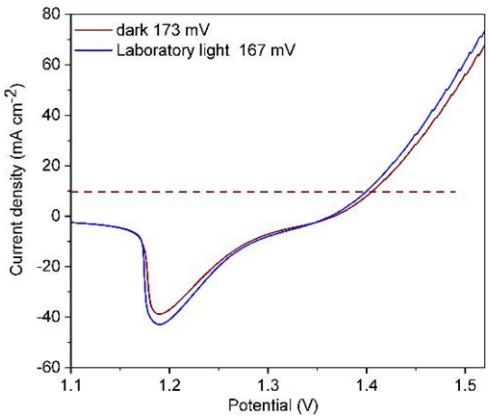

Figure R26. OER polarization curves of NR-NiOOH recorded at a scan rate of 0.1 mV/s under dark conditions and light (in laboratory situation). Fig. S5a in our revised Supporting Information

"Interestingly, even when the sample is subjected to laboratory light irradiation (12.3 mW cm^{-2}), the measured overpotential is 6 mV lower than that of NR-NiOOH in the dark (Fig. S5a)." was added in our revised manuscript (Page 6).

F5. The Ni valence can be determined by XAS but the assignment of a spin state is mostly speculative. Surely, the spreading of p states may affect the Ni-K edge shape. To support this argument, please state what spreading of the p-states is expected and how it compares to the core hole lifetime of a Ni 1s hole. Can the expected change be resolved by the used conventional XAS or does one need HERFD-XAS? The proposed structural change may also lead to a broadening of the edge. Alternatively, are measurements of the unpaired spins possible? If so, they could better support the assignment of spin states.

F7. Is it possible to measure the proposed square planar Ni oxide structure during light irradiation by XRD? Are there any other reports of square planar Ni oxides? Additional data would better support this unusual assignment. Likewise, what is the proof of square planar coordination of NiFe LDH after light irradiation?

Response: F5 focuses on the identification of square planar electronic states using XAFS. F7 focuses on other evidence to support the identification of square planar. Since F5 and F7 are both related to the evidence of square planar, *i.e.*, low spin Ni^{2+}, the answers to these two questions are combined.

To identify the spreading of 4*p* states in square planar geometry, a material with known low spin Ni^{2+} electronic configuration, *i.e.*, $[Ni(CN)_4]^{2-}$ ion, was measured with HR-XAFS (High-resolution X-ray absorption fine structure) in our revised version (Figure R27b, Fig. S10b in our revised Supporting Information). The white line (8340 to 8360 eV) is split into two peaks, which corresponds to p_z and p_x, p_y orbitals, respectively. Concurrently, the difference between these two peaks is 7.2 eV, which is significantly larger than that of Ni 1s core hole lifetime (1.62 eV). Given that Ni-O and Ni-CN exhibit approximately similar bond strength, the effect of Ni 1s core hole lifetime could be ignored in XAFS measurement. As a result, the splitting of white line in HR-XAFS spectra is one of the features of low spin Ni^{2+} electronic configuration in NR-NiOOH sample. At the same time, the variations of pre-edge under light irradiation are further studied through *operando* XAFS and HR-XAFS in our revised version showing the increased intensity, which indicates the appearance of low spin Ni^{2+} (detailed discussion is shown in the following section of electronic states discussion).

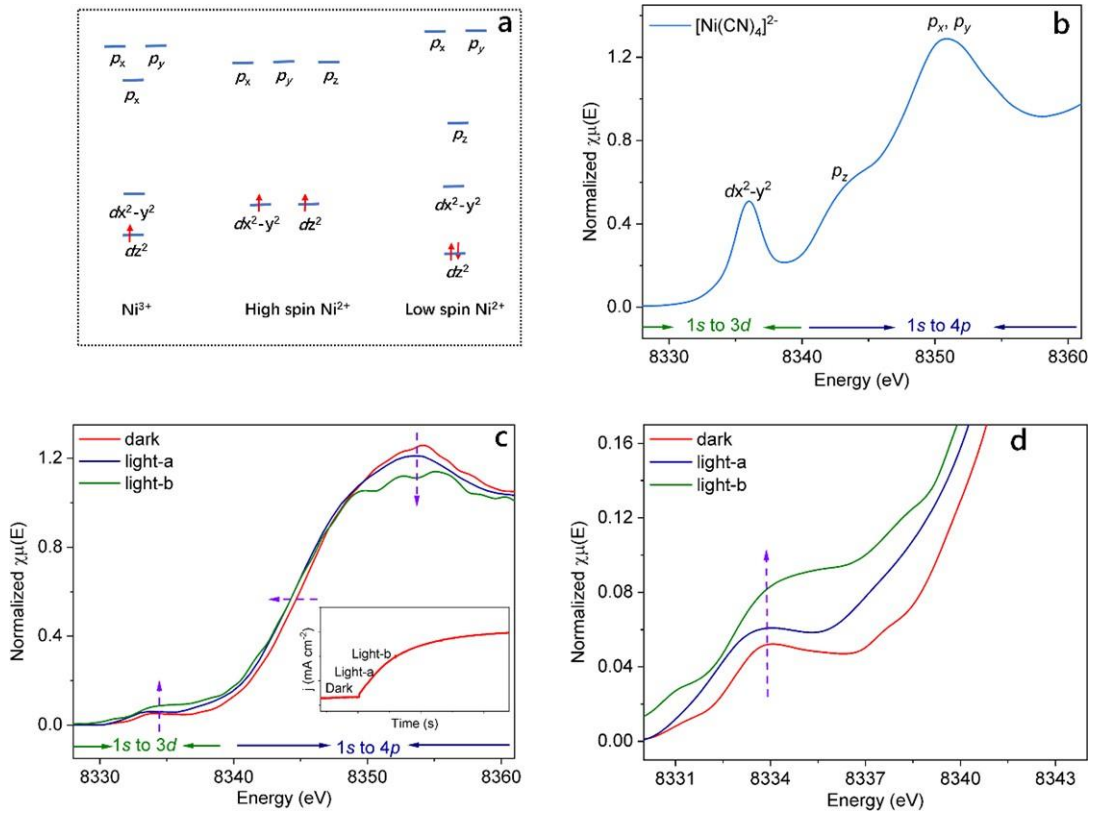

Figure R27. (a) Orbital diagram of Ni^{3+}, high spin Ni^{2+}, and low spin Ni^{2+}. (b) HR-XAFS spectra of $[Ni(CN)_4]^{2-}$ ion.

(c) *Operando* HR-XAFS spectra of NR-NiOOH subjected to light irradiation (inset showing the electrochemical curves accompanying the *operando* HR-XAFS). It should be noted that due to the longer collection time required for HR-XAFS measurement, it is difficult to capture the spectra at the high current regions, *i.e.* stabilized current state in the inset of Figure R27c. (d) Pre-edge in HR-XAFS spectra of NR-NiOOH subjected to light irradiation. Fig. S10 in our revised Supporting Information.

Since low spin Ni^{2+} can only be formed under the conditions of light irradiation and at OER potentials, it is challenging to analyze the spin states using conventional measurements, *i.e.*, EPR. Concurrently, as our NR-NiOOH possessed a two-dimensional nanoribbon structure, with a length of 10-20 nm and a width of 2-5 nm, it is challenging to analyze this nanostructure with XRD, or even synchrotron-XRD. In our previous work, synchrotron-XRD was used to analyze this structure. However, only two broad peaks were observed in our result (Figure 1k in our previous work, *Energy Environ. Sci.*, **13,** 229-237, 2020). According to the referees' advice, we have provided more evidence to identify the existence of square planar geometry under light irradiation. In our revised version, the square planar geometry was verified based on the electronic states, Ni-O coordination numbers, and Ni-O bond length (as discussed in detail as below).

1) Electronic states

As shown in the orbital diagram (Figure R27a, Fig. S10a in our revised Supporting Information), when the electronic state of Ni^{3+} changes into low spin Ni^{2+}, d_{z^2} orbital will be fully occupied, while $d_{x^2-y^2}$ orbital will be empty, which subsequently becomes a localized state. At the same time, the 4*p* orbitals will undergo higher degree of splitting. In our original manuscript, low spin Ni^{2+} was identified by the variations in the white line (8340 to 8360 eV in XANES spectra, corresponding to the Ni 4*p* orbitals). As shown in Figure R28b (Fig. 3d in our original manuscript, Fig. S11a in our revised Supporting Information), the white line of NR-NiOOH under light irradiation becomes broader with lower intensity as compared to that of NR-NiOOH in the dark conditions. This result suggests that there is greater degree of splitting of the Ni 4*p* orbitals in NR-NiOOH under light irradiation as compared to that under dark conditions. According to the referee's advice, we have further studied the localized $d_{x^2-y^2}$ orbital and splitting of 4*p* orbitals using HR-XAFS in our revised version.

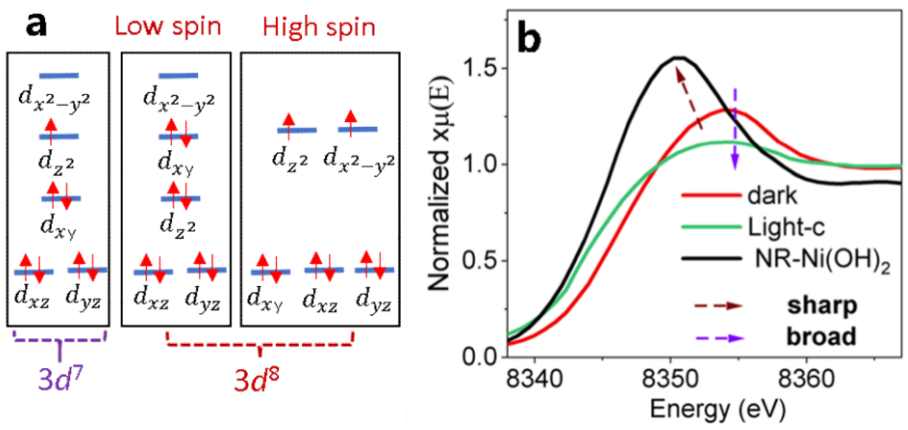

Figure R28. (a) Electron configuration of Ni^{3+}, high spin Ni^{2+}, and low spin Ni^{2+}. (b) White line (corresponding to electronic states of 4*p*) of NR-NiOOH subjected to light irradiation and NR-$Ni(OH)_2$. Figure R28a and b are presented in our original manuscript as Figure 3c and d, respectively, Fig. S11a in our revised Supporting Information.

To identify the features of low spin Ni^{2+} in HR-XAFS spectra, a material with known low spin Ni^{2+} electronic configuration, *i.e.*, $[Ni(CN)_4]^{2-}$ ion, was investigated with HR-XAFS (Figure R27b, Fig. S10b in our revised Supporting Information). A sharp peak is observed in the pre-edge range (8330 to 8340 eV), which corresponds to the localized $d_{x^2-y^2}$ orbital of the low spin Ni^{2+}. At the same time, the white line (8340 to 8360 eV) is split into

two peaks, which corresponds to p_z and p_x, p_y orbitals, respectively. The HR-XAFS experiment results agree well with the orbital diagram of low spin Ni^{2+} (Figure R27a, Fig. S10a in our revised Supporting Information). Hence, the increased intensity of the pre-edge peak or splitting of the white line in HR-XAFS spectra are two characteristics of low spin Ni^{2+} electronic configuration. Next, *operando* HR-XAFS was used to analyze the light activation process. The corresponding electrochemical curve is shown in the inset of Figure R27c. The pre-edge peak intensity of NR-NiOOH sample under light irradiation increases significantly as compared to that of NR-NiOOH in the dark condition (Figure R27d, Fig. S10d in our revised Supporting Information). The increased intensity of pre-edge peak is also observed through the *operando* XAFS (Figure R29, Fig. 3a in our original and revised manuscript). These results clearly indicate that the localization of $d_{x^2-y^2}$ orbital, which implies the formation of low spin Ni^{2+}. Concurrently, the white line of NR-NiOOH under light irradiation becomes broader with lower intensity as compared to that of NR-NiOOH in the dark conditions (purple arrows in Figure R27c, Fig. S10c in our revised Supporting Information), which suggests the increased degree of splitting of the white line. In our work, the complete splitting of p_z and p_x, p_y orbitals were not observed in both conventional XAFS and HR-XAFS. This phenomenon is mainly due to the co-existence of Ni^{2+} and Ni^{3+} in the light sample, which implies that the real electronic state of the sample under light irradiation is between Ni^{3+} and low spin Ni^{2+}. These *operando* XAFS and HR-XAFS results clearly indicate that Ni^{2+} in NR-NiOOH possessed a low spin Ni^{2+} configuration when subjected to light irradiation.

b) Coordination numbers

It is well known that Ni-O coordination numbers will reduce from six to four when the geometry of NiO_6 changes from octahedron to square planar. Hence, the variation in the coordination number is a very powerful evidence to identify the square planar geometry. To estimate the average Ni coordination number of the sample under light irradiation (light-c in Figure R29a, Fig. 3a in our original and revised manuscript), it is necessary to determine the ratios of Ni^{2+}/Ni^{3+} in the sample by analyzing the Ni valence. Here, the valence of NR-NiOOH is around 3+ (dark in Figure R29b, Fig. 3b in our revised manuscript) and the valence of low spin Ni^{2+} is set as 2+. Given that the measured Ni valence of the sample under light irradiation is about 2.2, the ratio of Ni^{2+}/Ni^{3+} in the sample is estimated to be 8:2 (Figure R29b, Fig. 3b in our revised manuscript). If the Ni^{2+} in NR-NiOOH is in low spin Ni^{2+} configuration, the average Ni coordination number of the sample under light irradiation can be calculated as such; 0.8*5.1+0.2*4 = 4.22 (the average Ni coordination number of NR-NiOOH under dark conditions is 5.1 in Table R1). This value is within the range of the experiment value, *i.e.*, 3.8±0.6 (Table R1). This result clearly indicates that the Ni^{2+} in NR-NiOOH possessed a low spin Ni^{2+} configuration when subjected to light irradiation.

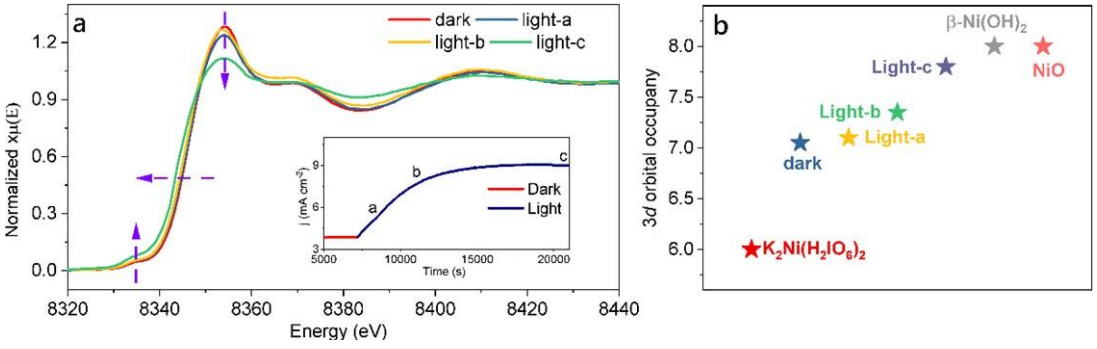

Figure R29. (a) *Operando* Ni *K*-edge XANES spectra of NR-NiOOH subjected to light irradiation (inset showing the electrochemical curves accompanying the *operando*-XAFS); (b) 3*d* orbital occupancy of NR-NiOOH subjected to light being benchmarked with β-$Ni(OH)_2$, NiO and $K_2Ni(H_2IO_6)_2$. Fig. 3a and b in our revised manuscript.

Table R1. FT-EXAFS fitting results of NR-NiOOH under dark conditions and NR-NiOOH under light irradiation (light-c in Fig. 3a), where CN is the coordination number, R is the bond length, and σ^2 is the Debye-Waller factor. Table S5 in our revised Supporting Information.

Sample	Bond species	CN	R (Å)	σ^2 (Å^2)	R factor
NR-NiOOH under dark	Ni-O	5.1±0.5	1.85±0.01	0.0056±0.0006	0.0050
NR-NiOOH under light	Ni-O	3.8±0.6	1.87±0.01	0.0074±0.0029	0.0110

3) Ni-O bond length

In our work, the bond length variations in our NR-NiOOH were studied with calculations and FT-EXAFS measurements as the geometry of NiO_6 changes from octahedral to square planar. Based on the calculations, O-O coupling state is the most stable square planar geometry model, which is used to analyze the variations in the bond length (Figure R30b, Fig. S11d in our revised Supporting Information). Figure R30 (Fig. S11c and d in our revised Supporting Information) shows that the bond length of the square planar unit cell is slightly small than that of the octahedral unit cell, while the O-O coupling adjacent Ni-O bond length (2.22 Å, 2.24 Å) in square planar unit cell is much larger than the Ni-O bond length in octahedron (1.90 Å, 2.01 Å). The slight decrease in the bond length of the unit cell is due to the increased Ni-O bonding energy. Based on the ligand field theory, when the geometry is converted from octahedral to square planar, the crystal field splitting energy increases significantly, which results in a stronger Ni-O bonding. The significant increase in the bond length is related to the hybridization of non-bonding oxygen states, which results in the extension of Ni-O bond length for the subsequent O-O coupling. Next, the average bond length of octahedral and square planar NR-NiOOH models were calculated. According to the results, the calculated average bond length of square planar is 1.95 Å, which is 0.02 Å larger than that of the octahedron (1.93 Å). At the same time, the *operando* FT-EXAFS results show that Ni-O bond length becomes larger when the sample is subjected to light irradiation (Figure R31, Fig. S11b in our revised Supporting Information). The consistent variations in the bond length obtained from the calculation and the experimental results clearly indicate the Ni^{2+} in NR-NiOOH possessed a low spin Ni^{2+} configuration when subjected to light irradiation.

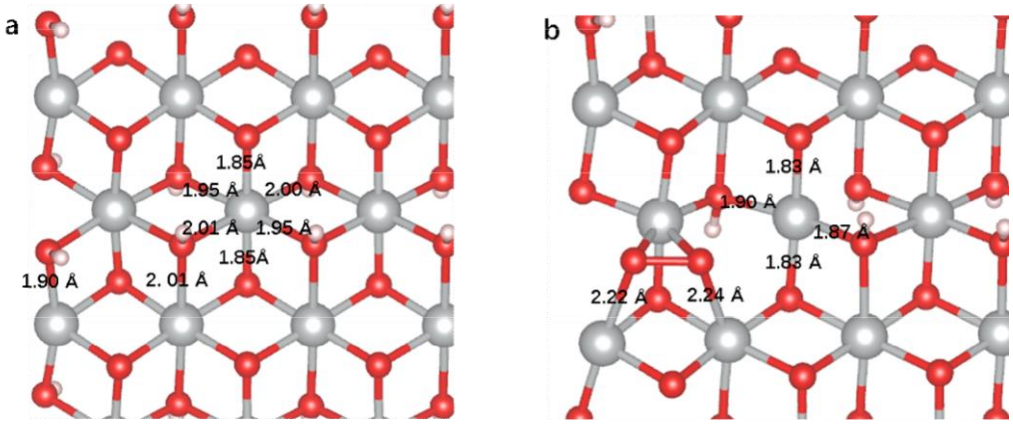

Figure R30. Octahedral (a) and square planar (b) NR-NiOOH models. Fig. S11 c and d in our revised Supporting Information.

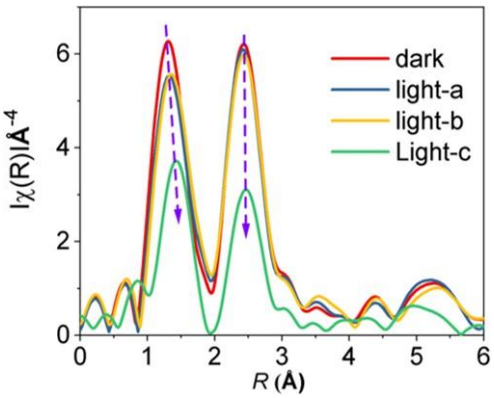

Figure R31. FT-EXAFS spectra of NR-NiOOH subjected to light irradiation. Fig. S11b in our revised Supporting Information.

The square planar geometry in NiFe LDH under light irradiation can also be identified with *operando* XAFS. According to the results, *operando* XAFS of the sample under light irradiation reveals a red-shift in its absorption edge by ~ 0.5 eV, with a slight broadening of white line, as compared with NiFe LDH sample under dark (Figure R32, Fig. 5h in our original version and Fig. S27e in our revised Supporting Information).

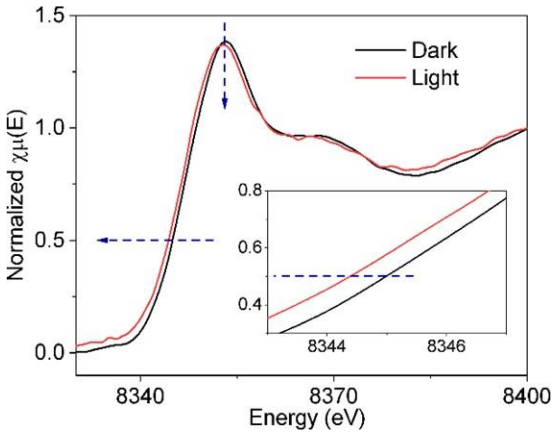

Figure R32. *Operando* Ni *K*-edge XANES spectra of NiFe LDH subjected to light irradiation, as compared with NiFe LDH sample under dark. Fig. 5h in our original version and Fig. S27e in our revised Supporting Information.

According to the reviewer's advice, we have done the following changes in our revised version:

1 *Operando* HR-XAFS data is added in our revised Supporting Information (Fig. S10, Page 32);

2 Figure R29 is added in our revised Supporting Information (Fig. S11 c and d, Page 33).

3 The discussion on the geometry conversion from octahedral to square planar is added in our revised manuscript (Page 8, highlighted in crimson):

Using the standard β-$Ni(OH)_2$, NiO, and $K_2Ni(H_2IO_6)_2$ as references, it was estimated that Ni in NR-NiOOH under light irradiation obeyed a $3d^{8-x}$ electronic configuration (where *x* is in the range of 0.2 ~ 0.85) (Fig. 3b and Fig. S9a) (*21*, *22*). As the current stabilized (light-c sample), a Ni valence of about 2.2 was recorded, which shows the co-existence of Ni^{2+} and Ni^{3+} during the OER process. This result is significantly different from the traditional OER process, whereby a co-existence of Ni^{3+} and Ni^{4+} is usually observed during the catalytic reaction (*23*). Thus, this shows that the OER performance enhancement observed from NR-NiOOH under light irradiation is associated with the formation of Ni^{2+} triggered by light. Ni^{2+} ($3d^8$ orbital occupancy) in NR-NiOOH under light irradiation may exhibit two possible electronic configurations, *i.e.*, (1) low spin Ni^{2+} configuration, with fully occupied d_{z^2} orbital and empty $d_{x^2-y^2}$ orbital or (2) high spin Ni^{2+} configuration, with one spin-up electron each in the d_{z^2} orbital and $d_{x^2-y^2}$ orbital (Fig. S10a). As compared with the high spin Ni^{2+} configuration, low spin Ni^{2+} configuration has a localized $d_{x^2-y^2}$ orbital. When compared with the sample under dark condition, the pre-edge peak (8330 to 8340 eV, corresponding to the localized $d_{x^2-y^2}$ orbital in HR-XANES and XANES spectra) of the sample under light condition increased significantly, which implies that a low spin Ni^{2+} configuration was formed under light irradiation (Fig. 3a and Fig. S10d).

The low spin Ni^{2+} configuration in NR-NiOOH under light irradiation was further identified with respects to the structural geometry of the unit cell. The low spin Ni^{2+} electronic configuration follows a square planar geometry due to its high crystal field splitting energy between d_{z^2} and $d_{x^2-y^2}$ orbitals, where its 4*p* orbitals *i.e.*, p_x, p_y and p_z, exhibit greater extent of splitting when compared to that of Ni^{3+} (Fig. S10a) (*24, 25*). Simultaneously, when the octahedral geometry is converted to square planar, it will result in the concomitant change in the Ni coordination number from six to four. *Operando* XANES and HR-XANES results show that the white line (8340 to 8360 eV, corresponding to the Ni 4*p* orbitals) of NR-NiOOH under light irradiation became broader with lower intensity when compared to that of NR-NiOOH in the dark conditions (Fig. S10c and 11a). Such a result suggests that the Ni 4*p* orbitals of NR-NiOOH exhibited greater extent of splitting. *Operando* Fourier transformed extended X-ray near fine structure (FT-EXAFS) results indicate that the Ni-O coordination number in NR-NiOOH was greatly reduced after being subjected to light (Fig. S11b and Table S5). Concurrently, the consistent variation of bond length in experimental and calculation results can also serve as an evidence to verify the low spin Ni^{2+} configuration in NR-NiOOH under light irradiation (Fig. S11b to d and Table S5). Detailed discussions on the low spin Ni^{2+} in NR-NiOOH sample under light irradiation are shown in the Supplementary Text.

4, The detailed discussion on the geometry conversion from octahedral to square planar is added in our revised Supporting Information (Page 12, highlighted in crimson):

Discussion on experiment to identify square planar

In our work, the square planar geometry is verified in view of electronic states, Ni-O coordination numbers, and Ni-O bond length.

1), Electronic states

As shown in orbital diagram (Fig. S10a), when the electronic state of Ni^{3+} changes into low spin Ni^{2+}, d_{z^2} orbital will be fully occupied while $d_{x^2-y^2}$ orbital will be empty, which subsequently becomes a localized state. To investigate Ni^{2+} in NR-NiOOH under light irradiation, *operando* XANES (X-ray absorption fine structure) and HR-XANES (high-resolution X-ray absorption fine structure) were employed (Fig 3a and Fig. S10d). The pre-edge peak intensity (8330 to 8340 eV, corresponding to the localized $d_{x^2-y^2}$ orbital) of the sample under light condition significantly increases, as compared to that of NR-NiOOH in the dark condition. This result indicates that the localization of $d_{x^2-y^2}$ orbital, which implies the formation of low spin Ni^{2+}. At the same time, the low spin Ni^{2+} electronic configuration follows a square planar geometry due to its high crystal field splitting energy between d_{z^2} and $d_{x^2-y^2}$ orbitals, where its 4*p* orbitals *i.e.*, p_x, p_y and p_z, become more splitting as compared with that of Ni^{3+} (Fig. S10a). *Operando* XANES and HR-XANES results show that the white line (8340 to 8360 eV, corresponding to the Ni 4*p* orbitals) of NR-NiOOH under light irradiation becomes broader with lower intensity as compared to that of NR-NiOOH in the dark condition, which suggests the increased splitting of Ni 4*p* orbitals (Fig.

S10 and 11). These results clearly indicates that Ni^{2+} in NR-NiOOH possessed a low spin Ni^{2+} configuration when subjected to light irradiation.

2) Coordination numbers

It is well known that Ni-O coordination numbers will be reduced from six to four when the geometry of NiO_6 changes from octahedron to square planar. Hence, the variation of coordination numbers is a very powerful evidence to identify the square planar geometry. To estimate the average Ni coordination numbers of light sample (light-c in Fig. 3a), it is necessary to determine the ratios of Ni^{2+}/Ni^{3+} in the sample by analyzing the Ni valence. Here, the valence of NR-NiOOH is around 3+ (dark in Fig. 3a) and the valence of low spin Ni^{2+} is set as 2+. Given that the measured Ni valence of light sample is about 2.2, the ratio of Ni^{2+}/Ni^{3+} in the light sample is estimated to be 8:2. If the Ni^{2+} in NR-NiOOH is in low spin Ni^{2+} configuration, the average Ni coordination numbers of light sample could be calculated as following: 0.8*5.1+0.2*4 = 4.22 (the average Ni coordination numbers of NR-NiOOH under dark is 5.1 in Table S5). This value is in the range of the experiment value 3.8±0.6 (Table S5). This clearly indicates that Ni^{2+} in NR-NiOOH possessed a low spin Ni^{2+} configuration when subjected to light irradiation.

3) Ni-O bond length

In our work, the bond length variations of NR-NiOOH sample were studied using calculations and FT-EXAFS measurement as the geometry changes from octahedron to square planar. Based on the calculations, O-O coupling state is the most stable square planar geometry model, which was used to analyze the variations of bond length (Fig. S11d). It shows that the bond length of square planar unit cell is slightly small than that of octahedral unit cell, while the Ni-O bond length adjacent to O-O coupling becomes much larger than that of octahedral unit cell. The slight decrease in the bond length of the square planar unit cell is due to the increased Ni-O bonding energy. Based on ligand field theory, when the geometry is converted from octahedral to square planar, the crystal field splitting energy would greatly increase, resulting in a stronger Ni-O bonding. The significant increase of bond length is related to the hybridization of non-bonding oxygen states, which would result in the extension of Ni-O bond length for the subsequent O-O coupling. Next, the average of bond length in octahedral and square planar NR-NiOOH models are calculated. It shows that the calculated value of square planar is 1.95 Å, which is 0.02 Å lager than that of octahedral (1.93 Å). At the same time, the *operando* FT-EXAFS results show that under light irradiation the Ni-O bond length becomes larger (Fig. S11b). The consistent variations of bond length in calculation and experiment results clearly indicates that Ni^{2+} in NR-NiOOH possessed a low spin Ni^{2+} configuration when subjected to light irradiation.

F6. Please discuss what average coordination is expected for the as synthesized NR-NiOOH and the activated NR-NiOOH. Does it agree with the coordination number from EXAFS, which in not six but 5.1+/-0.5. As there are some 4-coordinated sites on the edges, I would expect a coordination number lower than six.

Response: According to our previous results (*Energy Environ. Sci.*, **13,** 229-237, 2020), the edge of NR-NiOOH consists of alternating four-and six-coordinated Ni atoms in a periodic manner (Figure R33). The four-coordinated Ni atom possesses 2 three-coordinated OH and 2 two-coordinated OH, leaving two dangling bonds available, while the six-coordinated Ni atoms has 4 three-coordinated OH and 2 two-coordinated OH. The average Ni coordination number of NR-NiOOH could be estimated using the model of Figure R33, showing this value is 5.6 which is within the range of the experiment value, *i.e.*, 5.1±0.5. Concurrently, the average coordination number of NR-NiOOH under light can be calculated as such; 0.8*5.1+0.2*4 = 4.22 (the ratio of Ni^{2+}/Ni^{3+} in the sample is estimated to be 8:2 through *operando* XAFS and the average Ni coordination number of NR-NiOOH under dark conditions is 5.1 in Table R1). This value is also within the range of the experiment value, *i.e.*, 3.8±0.6 (Table R1).

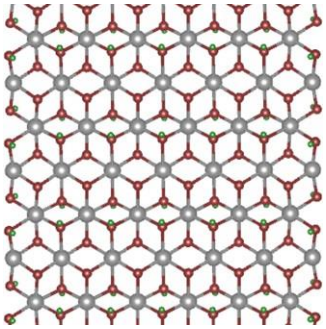

Figure R33. Simulated NR-NiOOH structure.

Table R1. FT-EXAFS fitting results of NR-NiOOH under dark conditions and NR-NiOOH under light irradiation (light-c in Fig. 3a), where CN is the coordination number, R is the bond length, and σ^2 is the Debye-Waller factor. Table S5 in our revised Supporting Information.

Sample	Bond species	CN	R (Å)	σ^2 (Å^2)	R factor
NR-NiOOH under dark	Ni-O	5.1±0.5	1.85±0.01	0.0056±0.0006	0.0050
NR-NiOOH under light	Ni-O	3.8±0.6	1.87±0.01	0.0074±0.0029	0.0110

As a result, the average NI-O coordination numbers of NR-NiOOH is lower than six, which agrees well with the EXAFS results.

According to the reviewer's advice, we have added the discussions on the Ni-O coordination numbers in our revised Supporting Information (Page 14, highlighted in crimson):

2) Coordination numbers

It is well known that Ni-O coordination numbers will be reduced from six to four when the geometry of NiO_6 changes from octahedron to square planar. Hence, the variation of coordination numbers is a very powerful evidence to identify the square planar geometry. To estimate the average Ni coordination numbers of light sample (light-c in Fig. 3a), it is necessary to determine the ratios of Ni^{2+}/Ni^{3+} in the sample by analyzing the Ni valence. Here, the valence of NR-NiOOH is around 3+ (dark in Fig. 3a) and the valence of low spin Ni^{2+} is set as 2+. Given that the measured Ni valence of light sample is about 2.2, the ratio of Ni^{2+}/Ni^{3+} in the light sample is estimated to be 8:2. If the Ni^{2+} in NR-NiOOH is in low spin Ni^{2+} configuration, the average Ni coordination numbers of light sample could be calculated as following: 0.8*5.1+0.2*4 = 4.22 (the average Ni coordination numbers of NR-NiOOH under dark is 5.1 in Table S5). This value is in the range of the experiment value 3.8±0.6 (Table S5). This clearly indicates that Ni^{2+} in NR-NiOOH possessed a low spin Ni^{2+} configuration when subjected to light irradiation.

F8. Are labelling studies of the material or electrolyte possible to support the evolution of lattice oxygen by mass spectroscopy? What is the direct experimental evidence for oxygen redox? Without direct experimental proof of either, the assignment is speculative.

Response: We have added the experiment involving ^{18}O isotope technology according to the referee's advice to identify the participation of lattice oxygen atoms in oxygen evolution in our revised manuscript. Also, TMA^+ probe measurement is combined with XAFS to verify the emergence of the oxidized oxygen states. The detailed discussions are shown below.

1) ^{18}O isotope technology

The process of ^{18}O isotope technology is summarized as two sections, *e.g.,* ^{18}O labelling electrocatalyst and gas product analysis using mass spectrometry. In the ^{18}O labelling section, NiS_2 precursor was oxidized in 97% $H_2{}^{18}O$ KOH electrolyte for 10 hours under a current density of 10 mA cm^{-2}. Our NR-$Ni^{18}O^{18}OH$ sample was prepared using this method. After which, the sample was washed using distilled water and then it was placed in a $H_2{}^{16}O$ contained gastight electrochemical cell that was connected to a gas carrier and mass spectrometer (Figure R34a, Fig. S19 in our revised Supporting Information). In this work, a 5 mL glass tube was used as the electrochemical cell to achieve the effective utilization of light by the catalyst. To decrease the effect of the remanent gas product (in the electrochemical cell and tube) on the GC-MS (as chromatography-mass spectrometry) analysis, the average ratio of $^{36}O_2$ to $^{32}O_2$ in 120s was used. The experimental result show that, when the sample is subjected to light irradiation, there is a significant increase in the ratio of $^{36}O_2$ to $^{32}O_2$, whereby it reaches the maximum within six to eight minutes (Figure R34b, Fig. 3d in our revised manuscript). Interestingly, other than this peak, two more small peaks in the range of 12 to 14 minutes and 22 to 24 minutes remain. The significant increase in the $^{36}O_2/^{32}O_2$ ratio clearly indicates the participation of lattice oxygen atoms in the oxygen evolution reaction. Two more $^{36}O_2/^{32}O_2$ ratio peaks show that more lattice oxygen atoms become active and they participate in the OER process during the oxygen catalytic reaction. This result is consistent with our *operando* XAFS results, whereby a gradual increase in the ratio of square planar to octahedron is observed (Fig. 3b in our revised manuscript).

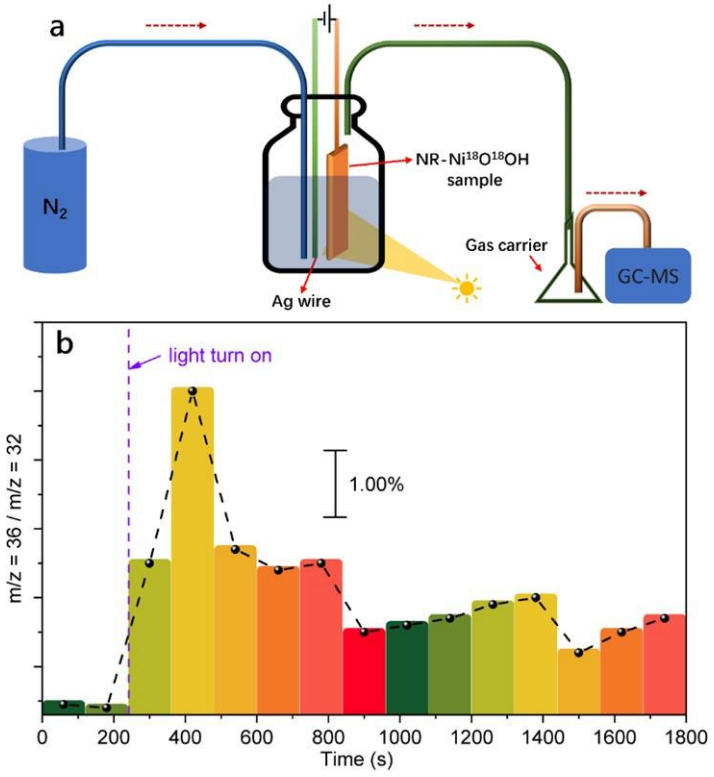

Figure R34. (a) Schematic of our isotope devices. In our work, a two-electrode configuration was used with Ag wire as the counter electrode. The flow rate of N_2 was 3mL/min. Before experiment, the electrolyte was bubbled with N_2 for 24 hours to remove the dissolved oxygen in electrolyte. The entire experiment was conducted under a constant current density of 2 mA cm^{-2}, with 0 to 4 minutes in dark and 4 to 30 minutes under light. To minimize the effect of the remanent gas product on the analysis results, the gas product was stored in a gas carrier, and then it was transferred into GC-MS after 120s. By using this method, the average ratios of $^{36}O_2$ to $^{32}O_2$ in 120s were obtained. Fig. S19 in our revised Supporting Information. (b) ^{18}O isotope labelling experiment. Fig. 3d in our revised manuscript.

2) TMA^+ probe measurement combining with XAFS

The emergence of oxidized oxygen is another powerful evidence to verify the existence of oxygen redox. According to the previous reports, TMA^+ could interact with the oxidized oxygen sites, which inhibited the formation of (O-O) coupling (*Angew. Chem.* **129,** 8778-8782, 2017; *Nat. Energy.* **4,** 329-338, 2019). In our work, TMA^+ probe measurement is combined with XAFS to study the oxidized oxygen. As shown in Figure R35 (Fig. 3c in our revised manuscript and Fig. S17 in our revised Supporting Information), when TMAOH is added in the electrolyte for the cell under light irradiation, there is an obvious decrease in the current densities, while no variations in the current are observed for the sample under dark conditions. This result clearly indicates that the addition of TMA^+ ion greatly inhibits the oxygen evolution process for the sample under light irradiation. At the same time, this TMA^+ ion addition does not affect the AEM-based OER process, *i.e.*, NR-NiOOH under dark conditions. The interaction of the oxidized oxygen atoms and TMA^+ is shown in Figure R35e (Fig. S17e in our revised Supporting Information). To satisfy the 8-outermost electron configuration of oxygen, the non-bonding oxygen states of oxidized oxygen atoms have to hybridize with TMA^+ ions by forming a chemical bond. Since the structure of TMA^+ remains unaltered after interactions (*Angew. Chem.* **129,** 8778-8782, 2017; *Nat. Energy.* **4,** 329-338, 2019), such a chemical bond has to be realized by the transfer of an inner electron from Ni metal to TMA^+, and this process can increase the valence of the metal. Then, OER measurement was terminated and Ni *K*-edge XANES was performed on NR-NiOOH samples. According to the experimental result, there is a significant increase in the Ni valence in the sample under light irradiation after the addition of TMA^+, while no variations in the Ni valence are observed for NR-NiOOH under dark conditions (Figure R35 b and d, Fig. S17 b and c in our revised Supporting Information). This result agrees well with the electron transfer shown in Figure R35e (Fig. S17e in our revised Supporting Information), which indicates that the oxidized oxygen is formed during the OER process for the sample under light irradiation.

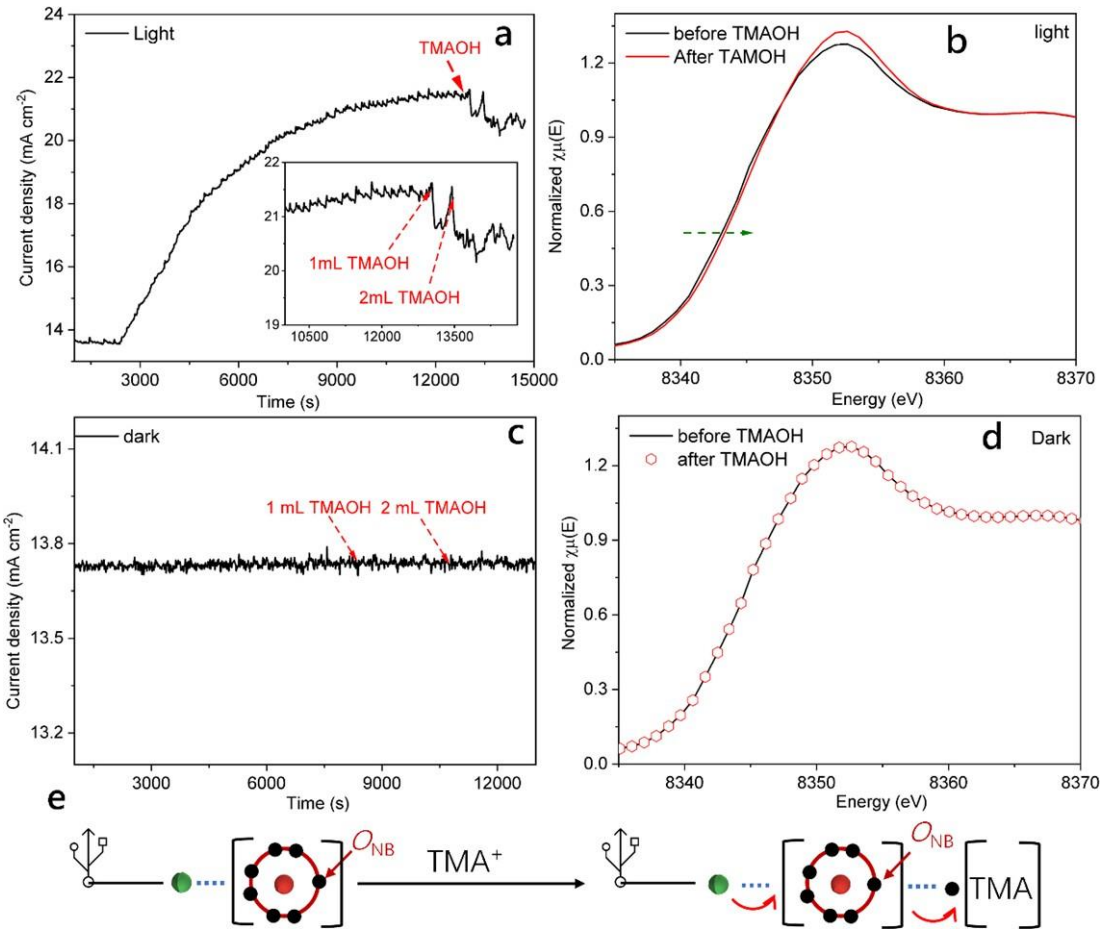

Figure R35. (a) (c) TMAOH test of NR-NiOOH using chronoamperometry measurement at a potential of 1.51 V *vs.* reversible hydrogen electrode (RHE) under light and dark conditions. (b) (d) Ni *K*-edge XANES of NR-NiOOH

sample before and after TMA^+ under light and dark conditions. (e) The electron transfer for the interaction of oxidized oxygen and TMA^+. Fig. S17 in our revised Supporting Information.

According to the reviewer's advice, we have added ^{18}O isotope technology measurement and TMA^+ probe measurement combining with XAFS in our revised version:

1. In our revised manuscript, the following discussions were added (Page 10, highlighted in crimson):

The emergence of the oxidized oxygen states and participation of lattice oxygen atoms are the features of oxygen redox activities. In our work, these features were identified with TMA^+ probe combining XAFS and ^{18}O isotope labelling measurement (Fig. 3c to d).

Given that TMA^+ can inhibit OER process by interacting with the oxidized oxygen sites to block the formation of (O-O) coupling, any modulation in the OER kinetics after the addition of TMA^+ can provide an indication of the oxygen configuration (*8*, *27*). It is worth noting that after adding TMA^+, NR-NiOOH under light irradiation exhibited a significantly reduced OER activity, while the sample in dark conditions showed negligible changes in the OER activity (inset of Fig. 3c and Fig. S17 and 18). This result indicates an interaction between the oxidized oxygen states and TMA^+ in NR-NiOOH under light irradiation, which suggests the presence of oxidized oxygen sites. Electron transfer diagram shows that such an interaction is realized through an inner electron transfer from Ni atom to TMA^+, which increases the Ni valence (Fig. S17e). According to the Ni *K*-edge XANES conducted on NR-NiOOH under light irradiation (after the addition of TMA^+), there was a significant increase in the Ni valence (Fig. S3c). Interestingly, no observable change was observed for NR-NiOOH under dark after the addition of TMA^+ (Fig. S17d). This result is consistent with the electron transfer diagram, which further indicates that oxidized oxygen was formed in NR-NiOOH under light irradiation.

Next, the participation of lattice oxygen atoms in NR-NiOOH under light irradiation was examined with ^{18}O labelling measurement (Fig. 3d). This experiment comprised of two sections, *i.e.*, ^{18}O labelling electrocatalyst and gas product analysis using mass spectrometry. The ^{18}O labelled NR-NiOOH was prepared *via* the electro-oxidation of NiS_2 precursor in 97% $H_2{}^{18}O$ KOH electrolyte under a current density of 10 mA cm^{-2} for 10 hours. The gas product analysis results show a significant increase in the ratio of $^{36}O_2$ to $^{32}O_2$ when the sample was subjected to light, and this ratio reached a maximum within 6 to 8 minutes (Fig. 3d and Fig. S19). The significant increase in the $^{36}O_2/^{32}O_2$ ratio clearly shows the participation of lattice oxygen atoms during the oxygen evolution reaction. Interestingly, after the first peak, two more small peaks were observed between 12 to 14 minutes and 22 to 24 minutes, respectively (Fig. 3d). The latter two peaks show that more lattice oxygen atoms participated in OER process as the catalytic reaction proceeded. This result agrees well with our *operando* XAFS results that a gradual increased ratio of Ni^{2+}/Ni^{3+} was observed (Fig. 3b).

2. Figure R34 is added in our revised manuscript (Fig. 3d) and Supporting Information (Fig. S19, Page 43).

3. Figure R35 is added in our revised manuscript (Fig. 3c) and Supporting Information (Fig. S17, Page 40).

F9 The proton transfer must occur on octahedral Ni. This means that the reaction must be started in darkness or at least at a time where not all Ni have been converted to square planar if that happens (see also F6). Please comment on it.

Response: In our proposed COM, proton transfer occurs on the octahedral NiO_6, while oxygen release process occurs on the square planar geometry. Hence, there is a co-existence of square planar Ni^{2+} and octahedral Ni^{3+} in our sample under light irradiation. The co-existence of square planar Ni^{2+} and octahedral Ni^{3+} can be identified by analyzing the average Ni valence and coordination numbers from Ni *K*-edge XANES, whereby a square planar/octahedral ratio of 8:2 was calculated for the light-c sample.

We have made the following changes in our revised manuscript according to the referee's advice (Page 8, highlighted in crimson):

Using the standard β-$Ni(OH)_2$, NiO, and $K_2Ni(H_2IO_6)_2$ as references, it was estimated that Ni in NR-NiOOH under light irradiation obeyed a $3d^{8-x}$ electronic configuration (where *x* is in the range of 0.2 ~ 0.85) (Fig. 3b and Fig. S9a) (*21*, *22*). As the current stabilized (light-c sample), a Ni valence of about 2.2 was recorded, which shows the co-existence of Ni^{2+} and Ni^{3+} during the OER process.

F10. The synthesis procedure involves sulfurization. Is there sulfur in "NR-NiOOH"?
Response: According to the STEM-EDS results in Figure R36, very weak S signal can be observed in the sample. This result was provided in our previous work (Fig. S31 in *Energy Environ. Sci.* **13,** 229-237, 2020).

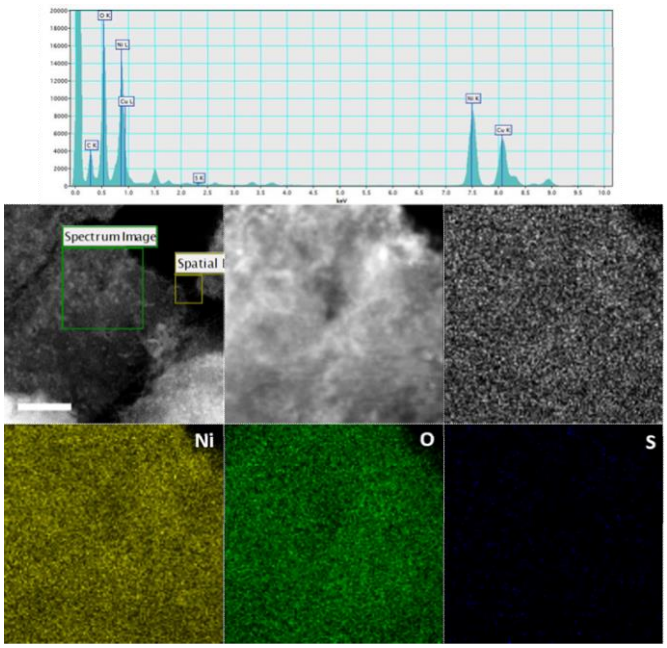

Figure R36. STEM-EDS elemental mapping of NR-$Ni(OH)_2$.

G. References
The references are overall appropriate for the results and their discussion. However, I missed discussion of a previous report of Ni oxide activation by light (https://www.degruyter.com/document/doi/10.1515/zpch-2019-1431/html) and whether light-induced transformation from octahedral to square planar geometry has been reported before for Ni oxide or any other oxide (e.g. https://www.nature.com/articles/srep38514)

Response: The first reference focuses on the light activation of Ni oxides, *i.e.*, NiFeCr, which has been answered in response to Q3 (Page 4 in this response). In this work, the as-prepared NiFeCr oxide catalyst exhibited

enhanced current densities under light irradiation. The observed enhanced current density is attributed to two key factors: 1) Fe within the as-prepared catalyst was conceptualized in the form of γ -Fe_2O_3, and this could generate photocurrent under light irradiation. 2) The attributing factor to the enhanced current density was the growth of crystallite during the surface reconstruction process when being irradiated with light. It is greatly different from our proposed COM.

The second reference focuses on the laser pulse induced phase transition, which is a widely studied physics area. After the excitation using laser pulses, the thermodynamic ground state of VO_2 will become less stable, and a metastable state M_2 will appear. It is significantly different from our work. In our work, the geometry conversion is triggered by the natural light, which participated in the oxygen evolution reaction. Our finding provides a new way to harness solar energy in the energy field.

According to the reviewer's advice, these two works have been cited in our revised manuscript (seen ref 19 and 26, highlighted in crimson):

Based on our experimental results, the improvement in the OER performance as demonstrated by NR-NiOOH under light irradiation is unlikely to be a result of reduced ohmic resistance, light-induced crystal growth, or generation of holes (Fig. S4 and Supplementary Text) (*18, 19*). (Page 8, highlighted in crimson)

This occurrence is different from the previously reported laser pulse induced phase transition in transition metal oxides (*26*). (Page 10, highlighted in crimson)

H. Clarity and context
The abstract is an appropriately written and concise summary of the main results and the authors' interpretation as well as the potential impact on the electrocatalysis community. The introduction introduces the current state of knowledge on OER mechanisms well. I just missed some additional aspects (see G. References). The presentation of the conclusions is also appropriate.

Response: We are very grateful for the positive endorsement by the referee.

Referee #2 (Remarks to the Author):

I think that the work by Wang et al is comprehensive and some experimental aspects of it are appealing, but I am not convinced that Nature is the journal where it should be published. A more specialized catalysis journal would be more appropriate.
First, the text is too long, too technical and the quality of the writing, and hence the clarity of the article, goes down in several parts.

Response: We have revised our manuscript according to the referee's advices.

Second, the partaking of metal and oxygen sites in the same pathway is not new (Energy Environ. Sci., 2017,10, 2626-2637; Phys. Chem. Chem. Phys., 2014,16, 13682-13688) and the same can be said of oxygen-only lateral steps aside from the main pathway (Nature Communications volume 10, 4993 (2019)), different activities of Ni sites in octahedral and square-planar configurations (J. Power Sources 404, 2018, 56-63), or the interchange of high spin and low spin configurations to increase OER activities (Nature Energy 4, 519–525 (2019); Phys. Chem. Chem. Phys., 2017, 19, 20451-20456).

Response: We are very thankful for the advice provided by the referee. In the oxygen evolution catalytic reaction, two types of redox activities are possible: (1) metal redox activities with the removal of electrons from the metal electronic states, and (2) oxygen redox activities with the removal of electrons from the non-bonding oxygen states. The actual proceeding of either redox activity is determined by the electronic states around the Fermi level of the catalyst. When the Fermi level is pinned to the top of the electronic states exhibiting metal character, oxygen evolution will proceed *via* the metal redox activities. On the other hand, when oxygen orbitals become accessible to the Fermi level, oxygen evolution will involve oxygen redox activities. If the electronic states near the Fermi level remain unaltered during the OER process, the catalytic reaction will be based solely on either metal or oxygen redox chemistry. The OER process that proceeds based solely on metal redox chemistry is known as the adsorbate evolution mechanism (AEM), which follows the pathway of OH*, O*, OOH*, and O_2. AEM proceeds *via* the variations of metal valence, which can be identified by using *operando* XAFS, *etc*. As the electrons are removed from the oxygen orbitals, oxygen will be oxidized whose outermost electrons are less than 8. Then, the oxidized oxygen states are stabilized *via* chemical oxygen-oxygen coupling. Since oxygen-oxygen coupling is formed through the hybridization of non-bonding oxygen states in the neighboring oxygen atoms, participation of lattice oxygen atoms is required. The emergence of the oxidized oxygen states and the participation of lattice oxygen atoms are the features of oxygen redox activities, and they can be identified by using operando XAS, ^{18}O isotope technology, *etc*. In contrast, OER process that proceeds solely on oxygen redox activity is known as lattice oxygen oxidation mechanism (LOM). In this mechanism, OER process involves OH^- adsorption, deprotonation, O-O coupling, and O_2 release. After carefully reading the works mentioned by the reviewer, we found that their **redox activities were all based solely on either metal or oxygen redox chemistry.** In the following section, the redox activities reported in these works are discussed in detail:

1) *Energy Environ. Sci.*, 2017,10, 2626-2637

The OER mechanism proposed in *Energy Environ. Sci.*, 2017,10, 2626-2637 is based solely on metal redox activity. In this work, the authors used *operando* crystal truncation rod analysis to propose their OER mechanism. In their proposed OER mechanism, unsaturated Ru sites were responsible for the efficient water adsorption, and the subsequent conversion of water to oxygen under the assistance of bridging oxygen sites. As shown in Figure R37 (Figure 4 in *Energy Environ. Sci.*, 2017,10, 2626-2637), their newly proposed OER mechanism followed the pathway of OH*, O*, OOH*, and O_2, which is the same as those in conventional AEM route. This result implies that their observed OER mechanism was based solely on metal redox, which was further supported by their work and our detailed analysis of the electron transfer mechanism. Firstly, the authors claimed the absence of oxygen redox activity in their proposed OER mechanism. According to their work, "No evidence was found to support lattice oxygen involvement reported previously for RuO_2, which is agreement with recent online electro-chemical mass spectrometry (OLEMS) measurement on oriented RuO_2 films and powders, showing no measurable oxygen exchange unlike Co-base perovskite." Next, the redox activities in their proposed OER mechanism were analyzed by deciphering the electron transfer process, as shown in Figure R38. According to the authors, water adsorption is a chemical process that occurs without electron transfer (this was stated in their work, "The vacant site was then filled by chemisorbed water (II)). From step II to III, the cleavage of oxygen-hydrogen bond was accompanied by one electron and proton transfer. To satisfy the 8-outermost electron configuration of oxygen, an inner electron transfer from metal to oxygen must occur, and this led to the increase in metal valence. From step III to IV, the cleavage of another oxygen-hydrogen chemical bond led to a concerted electron and proton transfer. In this process, an inner electron transfer from metal to oxygen was required to fulfill the 8-electron configuration of oxygen, and this increased the metal valence. In the OOH* formation process (from step IV to V), the adsorption of one water molecule led to one electron and proton transfer. To fulfill the 8-electron configuration of oxygen, the inner electron must be transferred from oxygen to metal, and this decreased the metal valence. In the subsequent oxygen evolution process (from step V to VII), the transfer of an inner electron from oxygen to metal led to the decrease in metal valence. Consequently, it could be understood that metal acted solely as the redox center during the entire OER process in their work.

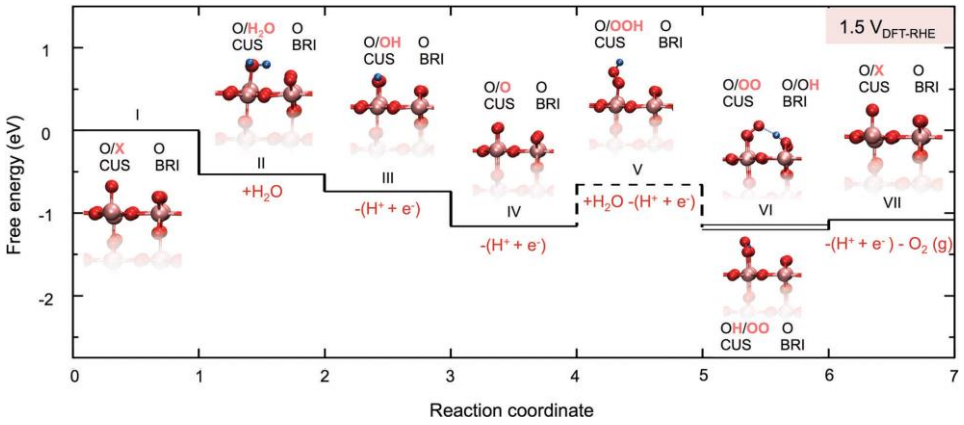

Figure R37. Free energy diagram of the OER mechanism proposed in *Energy Environ. Sci.*, 2017,10, 2626-2637 (Figure 4 in their paper).

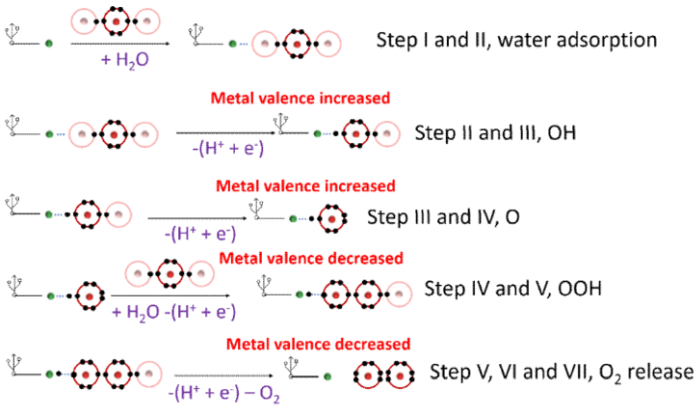

Figure R38. The electron transfer diagram based on the proposed OER mechanism in Figure R37.

2), *Phys. Chem. Chem. Phys.*, 16, 13682-13688, 2014,

The OER mechanism reported in *Phys. Chem. Chem. Phys.*, 16, 13682-13688, 2014 was based solely on metal redox activity. In this work, the authors proposed a new idea to optimize the relative bonding strength of the intermediates, *i.e.* OH*, and OOH*, on the surface of the catalyst. In their work, they incorporated Ni and Co into RuO_2, and this could activate the bridge site which subsequently acted as a proton donor-acceptor to lower OH* and OOH* energy states. Their proposed OER route was based on the pathway of OH*, O*, OOH*, and O_2. According to our discussions in Figure R38, this process proceeded *via* the variations of metal valence. At the same time, no experimental evidence was provided in their work to confirm the occurrence of oxygen redox activities during the entire oxygen evolution process.

3), *Nat. Commun.* 10, 4993, 2019

The OER mechanism reported in *Nat. Commun.* 10, 4993, 2019 was based solely on metal redox activities. In this work, the authors found that when using the conventional WNA (whose pathway is the same as those in the conventional AEM route) descriptor $\Delta G_{O^*} - \Delta G_{HO^*}$ to predict the activity of the molecular OER catalyst, its catalytic performance was underestimated. The reason for such a phenomenon was that the molecular OER catalyst would undergo a one-electron transfer before the formation of OOH*. As a result, the electron and proton transfer from O* to OOH* in molecular OER catalyst is a non-concerted process, which involves an electron transfer $O(IV)^* \rightarrow O(V)^* + e^-$ and a subsequent proton transfer $O(V)^* + H_2O \rightarrow HOO^* + H^+$

(here, O(IV)* and O(V)* represent M(IV)-oxo and M(V)-oxo spices, respectively). Hence, a new descriptor $\Delta G_{O(V)^*} - \Delta G_{O(IV)^*}$ was proposed by the authors to rationally estimate the OER activities. According to their work, this proposed new mechanism was based solely on the metal redox activity. There are few pieces of evidence to this statement. Firstly, their proposed OER mechanism followed the pathway of OH*, O*, OOH*, and O_2, and its main difference from the conventional AEM route was the transfer of electron and proton from O* to OOH* to achieve a non-concerted process. As shown in Figure R39, one electron was removed from the metal orbitals into the external circuit during the electron transfer step, which led to the increase in metal valence. This result agreed well with the transition from M(IV)-oxo to M(V)-oxo as stated by the authors. In the subsequent step, one water molecule was adsorbed together with a proton transfer. During this process, the inner electron in oxygen was transferred to the metal to fulfill the 8-electron configuration of oxygen, and this decreased the metal valence. Such a process agreed well with the transition from M(V)-oxo to M(III)-OOH (where M represented Ru, Mn, and Fe, as stated in Table S3 of *Nature Communications* 10, 4993 (2019)). Consequently, this non-concerted process proceeded *via* the variations of metal valence. Thus, their proposed OER mechanism was based solely on the metal redox activity. Secondly, no experimental evidence was provided in their work to confirm the co-occurrence of the metal and oxygen redox activities during the entire oxygen evolution process. Furthermore, the authors claimed that the OER process proceeded *via* either metal or oxygen redox depending on the condition reactions. According to their work, "Besides, when comparing the WNA and I2M mechanisms, one should bear in mind that the preference for one or the other pathway will be strongly dependent on the reaction conditions, something that can be overlooked", "Hence, the I2M mechanism is expected to have an important contribution to the observed OER activity at low to moderate potentials (or mild chemical oxidants), whereas the WNA is expected to compete at strong oxidizing conditions". Here, WNA has the same pathway as AEM, while I2M has the same pathway as LOM.

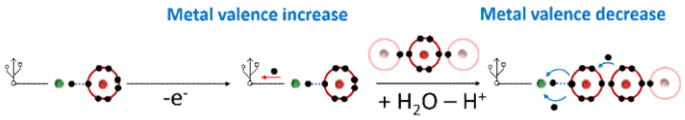

Figure R39. Electron transfer in a non-concerted process from O* to OOH* for the work, *Nat. Commun.* 10, 4993 (2019).

4) *J. Power Sources* 404, 56-63, 2018

The OER mechanism reported in *J. Power Sources* 404, 56-63, 2018 was based solely on metal redox activities. In this work, the authors found that the $BaNiO_2$ composition with Ni^{2+} in square-planar configuration was able to exhibit a higher intrinsic OER activity as compared to $BaNiO_{2.78(2)}$ whose Ni was located in octahedral configuration. According to the authors, the excellent OER activity exhibited by $BaNiO_2$ was attributed to the increased oxygen vacancies in the square planar geometry, which is beneficial for OER activity. **After carefully reading through their work, we have identified two key differences between our work and their work.** Firstly, the OER mechanism exhibited by $BaNiO_2$ followed the pathway of OH*, O*, OOH*, and O_2, which was based solely on metal redox activities (their detailed discussion is shown in Figure R38). At the same time, no experimental evidence was provided to confirm the emergence of oxygen redox activities during the entire OER process. Secondly, in their work, the OER reaction occurred solely on either the octahedral (for $BaNiO_{2.78(2)}$) or square planar sites (for $BaNiO_2$), whereby no reversible geometrical conversion within a single material was reported. Furthermore, it is worth noting that the geometrical conversion from square planar to octahedron in their work was a chemical process, and this conversion was realized by subjecting the material to thermal treatment at 600 ˚C in air for 12h. The geometrical conversion of the reported samples is shown in Figure R40 (Figure 1 in *J. Power Sources* 404, 2018, 56-63). In stark contrast to their work, the geometrical conversion of our material between octahedron and square planar was realized without the intricate heat treatment method. Instead, the geometrical conversion observed in our material is largely due to the variations of electronic configuration. When light induces electron transfer from (M-O) to d_{z^2} orbital, the Ni^{3+} (octahedron) would be transformed into low spin Ni^{2+} (square planar); when the electrons are removed from d_{z^2} orbital, the low spin Ni^{2+} (square planar) would be back to Ni^{3+} (octahedron). Such a reversible geometrical conversion between octahedron and square planar reported in our work is the basis of our proposed COM, which involves a switchable metal and oxygen redox chemistry.

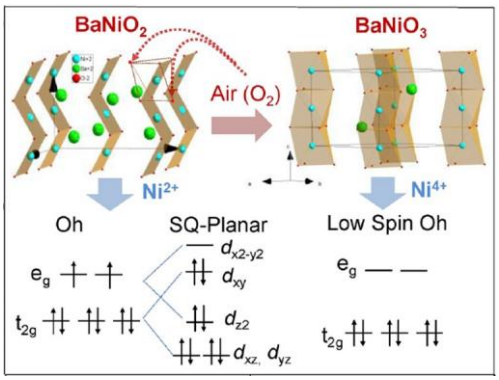

Figure R40. Crystal structure and spin configurations of $BaNiO_2$ and $BaNiO_{2.78}$, respectively. Figure 1 in *J. Power Sources* 404, 2018, 56-63

5) *Nat. Energy.* 4, 519–525, 2019

The OER mechanism reported in *Nat. Energy.* 4, 519–525, 2019 was based solely on oxygen redox activities. In this work, the authors demonstrated the positive effects of an external magnetic field on accelerating the oxygen evolution reaction for nickel and iron-based oxides. As shown in Figure R41, the magnetic field could lead to the spin orientation of two neighboring sites from antiparallel to parallel, and this is thermodynamically more favored in the OER process. However, the applied magnetic field did not alter the OER pathway, whereby it still followed the process of OH^- adsorption, deprotonation, O-O coupling, and O_2 release (Figure R41). The redox activities during this process were analyzed in terms of electron transfer (Figure R42 to R44). Since O-O coupling was formed through the hybridization of non-bonding oxygen states in the neighboring oxygen atoms, this indicated that the number of the outmost electron in oxygen was less than 8 prior to O-O coupling (an oxidized state) (Figure R42). As a result, during the deprotonation step, oxygen acted as the redox center as the electron was removed from the oxygen orbitals and into the external circuit (Figure R43). During the oxygen evolution step, two electrons must be removed from the oxygen orbitals of $(O\text{-}O)^{2-}$ to achieve the electronic structure of O_2 (Figure R44). Consequently, oxygen acted as the redox center in this process. As such, according to our analyses, a two-electron transfer from the oxygen orbitals occurred during the deprotonation step, while the other two-electron transfer from oxygen orbitals occurred during the generation of O_2, and these two processes summed up to a four-electron transfer process during OER. **Hence, based on our analyses, their proposed OER mechanism was based solely on oxygen redox chemistry.** At the same time, no experimental evidence was provided in this work to prove the emergence of metal redox activities.

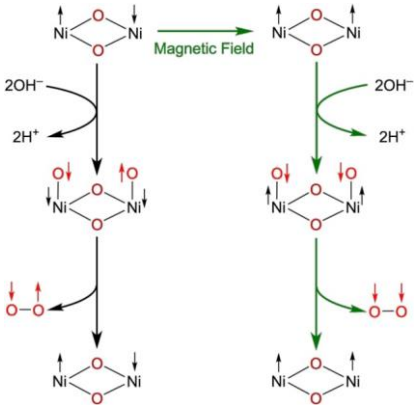

Figure R41. A simplified OER mechanism with and without magnetic field. Figure S18 in *Nature Energy* 4, 519–525 (2019)

Figure R42. Electron transfer during O-O coupling process.

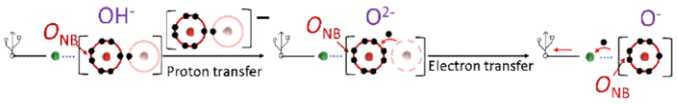

Figure R43. Proton and electron transfer process during the deprotonation step.

Figure R44. Electron transfer process in the oxygen evolution step.

6), *Phys. Chem. Chem. Phys.*, 19, 20451-20456, 2017

The OER mechanism reported in *Phys. Chem. Chem. Phys.*, 19, 20451-20456, 2017 was based solely on metal redox activities. In this work, the authors proposed that electrons had to travel *via* the conduction band to trigger the electrocatalytic reaction. The electron transfer could be significantly increased by the spin-dependent potential, which was induced under exchange interactions, spin-orbital coupling, or magneto-electric effects. In their work, the conduction band for the transfer of electron was formed *via* the hybridization of metal *d* orbitals and oxygen 2*p* orbitals (according to their work, "The overlapping of semi-occupied d-shells with the oxygen orbitals forms the conducting channels, and the reduced value of the Coulomb integrals by FM spin-potentials indicates facile e-spin transport" *Phys. Chem. Chem. Phys.*, 2017, 19, 20451-20456). The molecular orbital of the NiO_6 octahedral structure was selected as an example to analyze the electronic states of the conduction band ($EuNiO_3$ and $LaNiO_3$ in Figure 4 of *Phys. Chem. Chem. Phys.*, 2017, 19, 20451-20456)). As shown in Figure R45, e_g^*, t_{2g}^*, e_g, and t_{2g} orbitals were formed through the hybridization of Ni 3*d* and O 2*p* orbitals. Among these electronic bands, e_g, t_{2g} and t_{2g}^* were fully occupied, while e_g^* was partially occupied. As a result, the conduction band was located at e_g^* orbitals that exhibited metal character. As such, the electron transfer on the conduction band is considered a type of metal redox. Meanwhile, for the oxygen redox activities, the electron transfer process occurred on the non-bonding oxygen orbitals. However, no experimental or theoretical evidence was provided in their work to verify the location of the conduction band in the non-bonding oxygen orbitals.

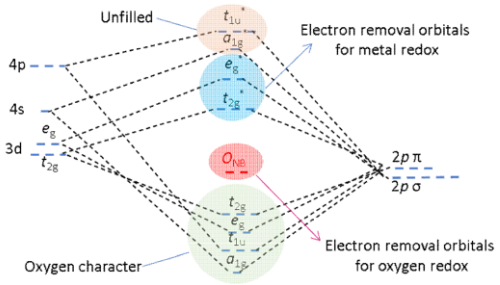

Figure R45. Molecular orbital diagram of octahedral NiO_6. The bonding bands, including a_{1g}, t_{1u}, e_g, and t_{2g}, exhibit oxygen character (denoted as M-O), while the antibonding bands $(M\text{-}O)^*$, *i.e.*, t_{2g}^*, a_{1g}^*, t_{1u}^*, and e_g^* that show metal character. The O_{NB} represents the non-bonding oxygen states.

The coupled oxygen evolution mechanism (COM) proposed in our work

Distinct from other previously reported works, we have provided a unique OER route in our work, denoted as coupled oxygen evolution mechanism (COM), which involves a switchable metal and oxygen redox chemistry. In this COM, the electron transfer process proceeds *via* the lowest available energy pathway. In our work, the metal

redox activities were identified by *operando* XAFS, while the oxygen redox activities were confirmed by TMA^+ probe combining XAFS and ^{18}O isotope measurements, as shown in Figure R46 (Fig. 4 in our revised manuscript). **To the best of our knowledge, such an OER mechanism based on switchable metal and oxygen redox chemistry has never been reported. In our work, we have provided the following insights based on our findings: a) Our proposed COM designates the electronic states around the Fermi level exhibiting alternative metal/oxygen characters, which is different from partaking of metal and oxygen sites in the same pathway. b) Our proposed COM involves a reversible conversion between metal and oxygen redox activities, which is distinct from the oxygen-only lateral steps aside from the main pathway. c) In contrast to the different activities of Ni sites in octahedral and square-planar configurations, COM is realized *via* a reversible geometric conversion of a unit cell between octahedron (NiO_6) and square planar. d) COM is triggered by electron transfer from (M-O) to d_{z^2} orbital, which is different from OER mechanisms based on exchange interactions, spin-orbital coupling, or magneto-electric effects.**

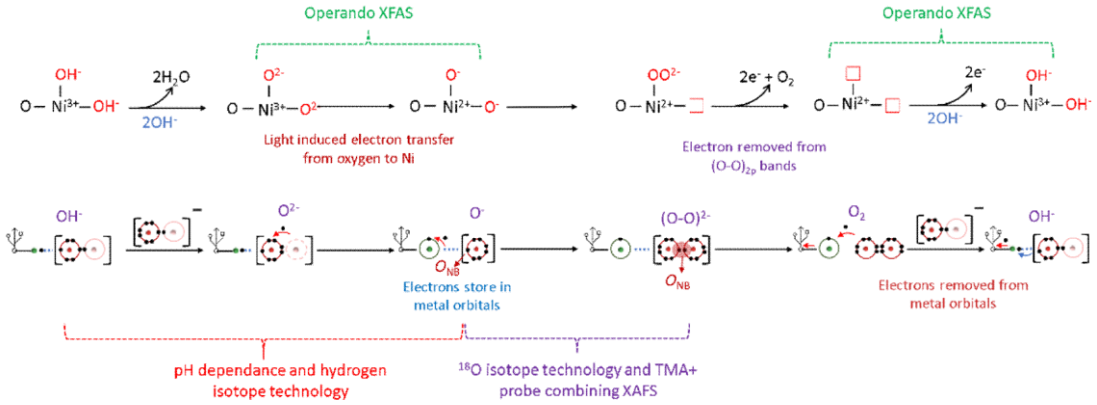

Figure R46. Electron transfer pathway of our proposed COM. Fig. 4 in our revised manuscript.

According to the referee's advice, these mentioned references have been added in our revised manuscript (seen references *28-33*, highlighted in crimson),

We have added the following sentence in our revised manuscript (Page 13): Our proposed COM is different from the OER mechanisms reported in previous studies, *i.e.*, partaking of metal and oxygen sites, OER process on square-planar configurations, interchange of high spin and low spin configurations, *etc.* (*28-33*).

Third, in my opinion the electrocatalysis models are neither well-crafted, well-described, nor illustrative. In those, the authors mistake rate determining step for potential limiting step. The authors claim that O-O coupling has a smaller barrier than OOH formation. This claim is made based on diagrams at 0 V vs RHE not at OER relevant potentials. Because OOH formation is electrochemical, the potential will make its barrier accessible at potentials close to 1.4 V vs RHE.

Response: The LOM pathway was recalculated in our revised version (the process is shown in Figure R47b, Fig. S3 d in our revised Supporting Information). As shown in Figure R47 (Fig. S3 c and d in our revised Supporting Information), the calculated relative energy of OOH^* formation based on NR-NiOOH crystal structure is 1.59 eV (1.79 eV, Solvent), and the calculated energy of forming O-O coupling is -0.50 eV (-0.57 eV, Solvent). This result indicates that the O-O coupling is a favorable energy process, while OOH* formation is an energy-demanding process, which is consistent with previous LOM reports (*Nat. Chem.* ***9,*** 457-465, 2017; *Nat. Energy.* **4,** 329-338, 2019). This highlights the merit of LOM as compared to AEM. Noted that in our LOM pathway calculation, the deprotonation of two OH* is regarded as one step. Given the large energy of deprotonation (3.87 eV, 3.87 eV

Solvent) as compared with other steps, deprotonation process is the rate-determining step in LOM route, even though this process is split into two steps.

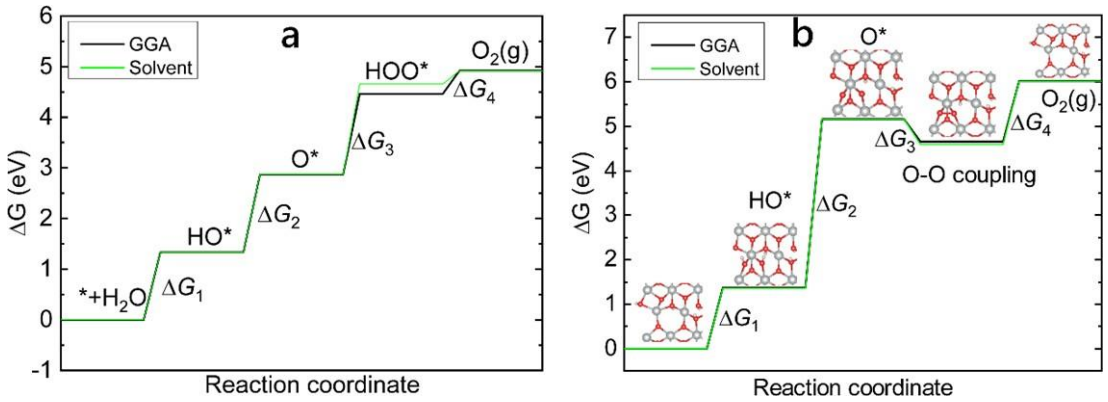

Figure R47. Calculated reaction free energy change of the AEM (a) and LOM (b) route. Fig. S3 c and d in our revised Supporting Information. AEM calculation results come from our previous work (*Energy Environ. Sci.,* **13,** 229, 2020)

According to the referee's advice, we have added the revised LOM energy landscape calculations in our revised Supporting Information (Fig. S3d in our revised Supporting Information, Page 21, highlighted in crimson).

Besides, the authors claim that the conversion from octahedral to square planar is related to the OER enhancement, but that is never shown with DFT. The COM pathway is not evaluated either with DFT, whereas the LOM and the AEM are.

Response: In our revised version, the calculated reaction-free energy change of the COM pathway is provided (Figure R48, Fig. S21a in our revised Supporting Information). It indicates the deprotonation step is the rate-determining step. Since the electron transfer during deprotonation is triggered by light, proton transfer should be considered intrinsically as the rate-determining step, which is in good agreement with the results obtained from the measured Tafel slope and reaction orders (Fig. S5d and S20, Supplementary Text in our revised Supplementary Information). From this result, we can see that electron transfer process proceeds *via* the lowest available energy pathway, in which the deprotonation occurs at the metal bands and O-O coupling occurs in the oxygen states. In comparison with the traditional AEM route, COM route involves a direct O-O coupling, and it can bypass the traditional RDS step, *i.e.*, OOH, in AEM. At the same time, deprotonation occurs at the metal bands, which invokes a smaller amount of energy (3.0 eV, 2.90 eV Solvent) as compared with that needed in the LOM route (3.87 eV, 3.87 eV Solvent). Noted that in our LOM and COM pathway calculation, the deprotonation of two OH* is regarded as one step. Hence, we compared the relative energy of deprotonation in LOM and COM. Theoretically, the deprotonation process in COM involves proton transfer that occurs at the metal bands and a subsequent light-triggered electron transfer from (M-O) to d_{z^2} orbital. This process is analogous to the proton transfer during the deprotonation in AEM and a subsequent light-triggered electron transfer. As a result, the energy required in the deprotonation step in COM is, in principle, smaller than those in AEM.

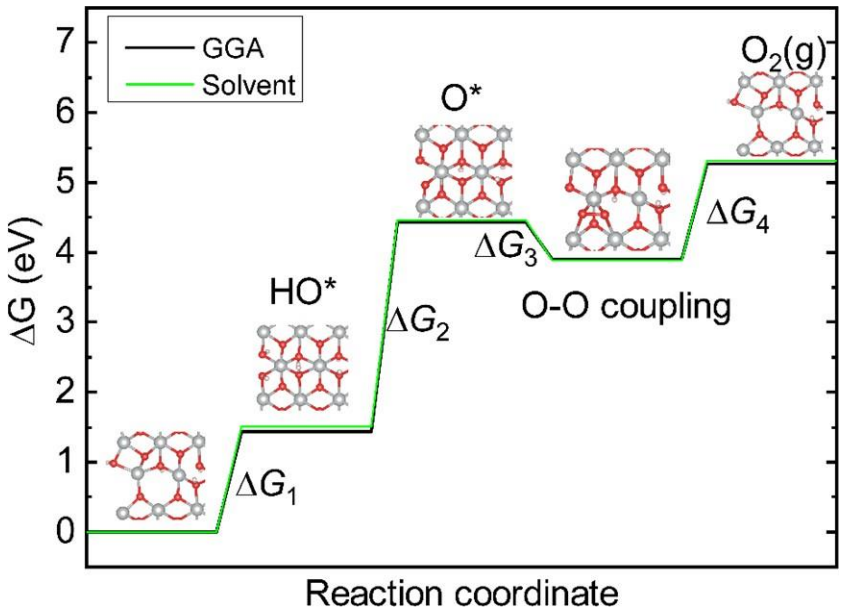

Figure R48. Calculated reaction free energy change of COM pathway. Fig. S21a in our revised Supporting Information.

According to the referee's advice, the revised COM energy landscape calculation is added in our revised Supporting Information (Fig. S21a in our revised Supporting Information, Page 45, highlighted in crimson).

Besides, the kinetic barriers for the transformation from octahedral geometry to square planar were not evaluated.

Response: In our revised version, the kinetic barrier was calculated based on the Nudged Elastic Band (NEB) method, and the result is shown in Figure R49 (Fig. S21b in our revised Supporting Information). Here, O^* in COM pathway states was selected as the starting state. O-O coupling is the most stable square planar geometry structure model, and therefore it was selected as the ending state. Based on the calculation, the energy barrier of the geometry transformation from octahedral to square planar in NR-NiOOH is 0.7928 eV.

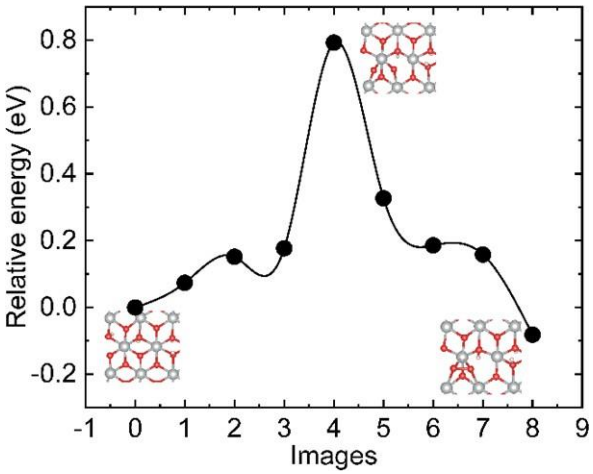

Figure R49. The energy barrier of the geometry conversion from octahedron to square planar. Fig. S21b in our revised Supporting Information.

According to the referee's advice, we have added the energy barrier of the geometry conversion from octahedron to square planar in our revised Supporting Information (Fig. S21b, Page 45, highlighted in crimson).

To close my report, I annotate that no tabulated data are provided (DFT electronic energies, zero-point energies, entropy corrections, solvation corrections), the method descriptions are incomplete, and no coordinates are given.

Response: We have included the parameters and method description of LOM and COM in our revised Supporting Information.

The first step is 2OH refilling at the lattice sites:

$\Delta G_1 = E(2OH) - E(Voo) - 2E(OH) - +(\Delta ZPE - T\Delta S)$

The second step is the deprotonation and releasing of two electrons:

$\Delta G_2 = E(O\text{-}O) - E(2OH) - E_{H_2} + (\Delta ZPE - T\Delta S)$

The third step is O-O coupling:

$\Delta G_3 = E(OO) - E(O\text{-}O) + (\Delta ZPE - T\Delta S)$

The fourth step is the evolution of oxygen:

$\Delta G_4 = E(Voo) - E(OO) - E_{O_2} + (\Delta ZPE - T\Delta S)$

COM		GGA	Solvent		GGA	GGA	Solvent	Solvent
		energy (eV)	energy (eV)	ΔZPE-TΔS (eV)	ΔG (eV)		ΔG (eV)	
1	$E(2OH)$	-515.1824	-518.8839	0.7165	1.4325	1.4325	1.5133	1.5133
2	$E(O\text{-}O)$	-504.4978	-508.2404	0.1374	2.9895	4.4220	2.9484	4.4617
3	$E(OO)$	-504.4160	-508.1241	0.1300	-0.5166	3.9054	-0.5701	3.8916
4	$E(Voo)$	-494.2696	-498.0519		1.3669	5.2723	1.4257	5.3173
LOM		GGA	Solvent		GGA		Solvent	
		Energy (eV)	Energy (eV)	ΔZPE-TΔS (eV)	ΔG (eV)		ΔG (eV))	
1	$E(2OH)$	-515.1824	-518.9766	0.6549	1.3709	1.3709	1.3590	1.3590

2	$E(O\text{-}O)$	-503.8654	-507.6530	0.0961	3.7972	5.1681	3.8038	5.1628
3	$E(OO)$	-504.4160	-508.2570	0.1300	-0.5166	4.6514	-0.5701	4.5927
4	$E(Voo)$	-494.2696	-498.0519		1.3669	6.0184	1.4257	6.0184

Here, $E(Voo)$, $E(2OH)$, $E(O\text{-}O)$, and $E(OO)$ are the energies of NR-NiOOH with two oxygen vacancies (O_2 releasing), two OH ions refilling, two deprotonations, and O-O coupling, respectively. E_{H_2} and E_{O_2} are the energies of hydrogen and oxygen molecules. The details are shown in Table R6.

Table R6. Corrections to the Gibbs free energies (in eV) for LOM and COM routes. Table S6 in our revised Supporting Information.

Note the parameters and method description of AEM are provided in our previous work (*Energy Environ. Sci.,* **13,** 229, 2020).

According to the referee's advice, Table R6 was added in our revised Supporting Information (Table S6, Page 66). The method described is added in the Calculation section in the revised Supporting Information (Page 6, highlighted in crimson).

Reviewer Reports on the First Revision:

===== Referees' comments =====

Referee #1 (Remarks to the Author):

Wang et al. have significantly revised their manuscript. New data and analyses were included that greatly strengthen the key results.

The significance of the paper is now clear and the new mechanism has a plausible use in an energy conversion device. The new mechanism is now mostly sufficiently demarcated from earlier work but I found the reply regarding LOM vs COM to me more convincing than the text change (see below). All points that I disagreed with were resolved by the revision. Yet, points raised by the other reviewer(s) need to be addressed to sufficiently strengthen the novelty of the mechanism.

I find the use of light to induce a coordination change a highly interesting and very general approach to optimize electrocatalysts by controlling the source of the electrons passed to the external circuit. I think the study would spark much fundamental (and maybe even applied) research in the field to further optimize electrocatalysts that are at a dead-end when driven only by electricity. For these reasons, I would support publication in Nature if the remaining issues regarding the calculations to support the mechanism were addressed fully.

Please address:
1) P23 in supplemental:
While it does not change the conclusions, an iR correction as the sum of Rs and Ru is not correct. The correction is done by iRu only. Further discussion in
https://pubs.rsc.org/en/content/articlelanding/2021/CP/D1CP00661D#!divAbstract
Please correct it.

2) Thanks for adding the additional normalizations by ECSA and the catalyst loading.
Please add further detail how the ECSA is calculated from the CVs in Fig. S6
What double layer capacitance (C_DL) was obtained? I like to point out that the CV is box-like but slanted. Maybe the authors find some hints how to improve the measurement of C_DL in
https://iopscience.iop.org/article/10.1088/2515-7655/abee33
I do not think it is very reliable to determine EXAFS from these CVs
What specific capacitance (C_S) was used?
Are all specific activities in Table S2 based on ECSA? Since it often differs, please add C_S to the table entries. If not, the other method, e.g., BET should be included in the table. I do not think ECSA from CV and BET normalized data are directly comparable.

3) Fig. S10. I was confused by the order of the panels. Is it possible to exchange current panels c and d, so that Ni(CN)4 can be easier compared to NR-NiOOH?

4) The reduction in bond length with irradiation in Table S5 is within the error (1.85±0.01 vs 1.87±0.01) and not “greatly reduced”. Please revise the statement in the text. Looking at the structural model and the reply, it is not surprising to me that the expected difference is not resolved by EXAFS. I find the other data already convincing.

5) Please mention in the revised manuscript that NR-NiOOH contains some sulfur.

6) “NR-NiOOH under light irradiation exhibited an extremely low overpotential of 135 mV at 10 mA cm-2 (Fig. S5c). This result, to the best of our knowledge, is the best OER performance reported so far (Table. S1)” The overpotential at 10 mA/cm2 is not meaningful without the loading as it can be changed simply by variation of the loading. Are all entries in Table S1 given for the same loading? The statement is not correct. Lower electrode overpotentials can be found, e.g. here for Ni(Fe) oxides:

https://onlinelibrary.wiley.com/doi/10.1002/aenm.201600621

7) P11 “The latter two peaks show that more lattice oxygen atoms participated in OER process as the catalytic reaction proceeded.” Could the latter two peaks be noise? Eventually, the ratio should be constant when 16O diffusion to the surface balances with lattice oxygen evolution. Why are peaks expected?

8) P9 Supplemental. Difference between LOM and COM
Rebuttal P8: The sole oxygen redox activities within LOM in perovskite were verified by another group, using operando oxygen K-edge and metal L-edge X-ray absorption spectra (Nature Communications 6, 6097, 2015).
It would be clearer to include that statement and reference in the manuscript or supplemental as it is important to define the LOM mechanism that the authors use as a reference. As you have seen by all referees’ comments, the LOM mechanism is often not considered as having only oxygen redox. Making this point explicit helps to demarcate the COM from the LOM mechanism.

9) Distinction of the COM from other mechanisms
Please address the outstanding comments regarding the DFT calculations fully. I agree that the DFT calculations of all three mechanisms should be performed at an overpotential relevant to the experiments. Since the rate-determining step is discussed, the kinetic barriers should be discussed. These calculations should rigorously support that the COM is a distinctively new mechanism, which the current state of the (DFT) analysis does not.

Referee #2 (Remarks to the Author):

The authors did a lengthy and diligent revision of the paper, mainly on the experimental part. However, I am now convinced that this paper does not warrant publication in Nature. Mainly because the DFT modelling is unclear, inconclusive, and incomplete, which prevents the authors from validating the hypothesis drawn from their experiments. I would advise a referral to Nature Communications.
- The authors did not address my comments in full. Let me be specific: I said that the authors are making claims based on plots at 0 V vs RHE, whereas the potentials of the reaction are no less than 1.23 V vs RHE (plus the usual overpotential).
- The authors say that OOH formation takes 1.59 eV, which leads to an overpotential of 0.36 eV. This low overpotential would be located at the very top of the volcano in Norskov’s pathway (AEM in the authors’ notation. See e.g. ChemCatChem 3 (7), 1159-1165, Journal of Electroanalytical Chemistry 2007, 607 (1-2), 83-89). In addition, a favorable formation energy for O-O coupling does not imply that the kinetics will be low. Such a chemical barrier (potential independent) should have been calculated and compared to the electrochemical barrier (potential dependent) for OOH formation to arrive at sound conclusions.
- Figure R49 shows that the transformation from octahedral to square planar complexes requires a

large kinetic barrier of 0.79 eV. Based on simple considerations, Chorkendorff et al (Chem. Rev. 2019, 119, 12, 7610–7672) established that the hard limit for a surmountable barrier at room temperature is 0.75 eV.

- Besides, in Figure S21 the potential limiting step takes 3.00 eV for the COM to happen. This step has to be decoupled for the pathway to be meaningful. Assuming it is fully symmetric (which would be the best-case scenario), the overpotential would be 3 eV/2e- -1.23 V = 0.27 V vs RHE. This value is not so different compared to the value of 0.36 V vs RHE obtained in Norskov's pathway, which again calls for the assessment of the barriers.
- About Figures S3d and S21a: there must be something wrong, as the total energy of the reaction is in the range of 5-6 eV, while it should be 4.92 eV. This questions the whole modelling.
- Finally, about Figure R37: it is not just a mechanism based on metal sites only, as the authors claim. The bridge sites on the rutile oxide are made of oxygen. Although the authors made long summaries of the articles I mentioned in the rebuttal letter, the discussion in the paper is too simplistic.
- Still no coordinates of the simulated slabs with and without the adsorbates were given.
- No description whatsoever to the method used to calculate the data labelled as "solvent" was provided.

Author Rebuttals to First Revision:

Referee #1 (Remarks to the Author):

Wang et al. have significantly revised their manuscript. New data and analyses were included that greatly strengthen the key results.

The significance of the paper is now clear and the new mechanism has a plausible use in an energy conversion device. The new mechanism is now mostly sufficiently demarcated from earlier work but I found the reply regarding LOM vs COM to me more convincing than the text change (see below). All points that I disagreed with were resolved by the revision. Yet, points raised by the other reviewer(s) need to be addressed to sufficiently strengthen the novelty of the mechanism.

I find the use of light to induce a coordination change a highly interesting and very general approach to optimize electrocatalysts by controlling the source of the electrons passed to the external circuit. I think the study would spark much fundamental (and maybe even applied) research in the field to further optimize electrocatalysts that are at a dead-end when driven only by electricity. For these reasons, I would support publication in Nature if the remaining issues regarding the calculations to support the mechanism were addressed fully.

Response: We sincerely appreciate the reviewer for the time and efforts in assessing our manuscript, together with very valuable comments. In our revised version, we have faithfully addressed all the reviewer's concerns.

Please address:

1) P23 in supplemental:

While it does not change the conclusions, an iR correction as the sum of Rs and Ru is not correct. The correction is done by iRu only. Further discussion in https://pubs.rsc.org/en/content/articlelanding/2021/CP/D1CP00661D#!divAbstract

Please correct it.

Response: We are very thankful for this insightful suggestion. We used Ru in the *iR* correction in our revised version, and the result is shown in Fig. R1 (Fig. S5c in our revised Supporting Information). We greatly appreciate the reference provided by the reviewer and found it very useful in our work. As such, we have included the mentioned reference in our revised manuscript (as reference 16, which was highlighted in crimson in our revised manuscript).

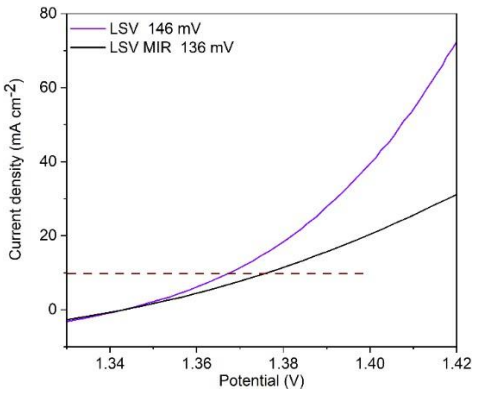

Fig. R1. OER polarization curves of NR-NiOOH under light irradiation at a scan rate of 0.1 mV s^{-1} with 90% *iR* correction. The result shows that by using 90% *iR* correction (R = 1.38 ohm, the resistance of the catalytic material), the overpotential of NR-NiOOH under light irradiation at 10 mA cm^{-2} was 136 mV. Fig. R1 is represented as Figure S5c in our revised Supporting Information.

2) Thanks for adding the additional normalizations by ECSA and the catalyst loading.

Please add further detail how the ECSA is calculated from the CVs in Fig. S6

What double layer capacitance (C_DL) was obtained? I like to point out that the CV is box-like but slanted. Maybe the authors find some hints how to improve the measurement of C_DL in https://iopscience.iop.org/article/10.1088/2515-7655/abee33

I do not think it is very reliable to determine EXAFS from these CVs

What specific capacitance (C_S) was used?

Are all specific activities in Table S2 based on ECSA? Since it often differs, please add C_S to the table entries. If not, the other method, e.g., BET should be included in the table. I do not think ECSA from CV and BET normalized data are directly comparable.

Response: We are very thankful for this insightful suggestion. We have re-conducted the ESCA measurements based on the reference provided by the reviewer. The results are shown in Fig. R2 (Fig. S6 a and b in our revised Supporting Information). The detailed procedure in conducting the ECSA measurement is described as follows: During the electrochemical surface area (ECSA) experiment, the measurement window was selected between 1.00 V to 1.15 V vs RHE, whereby neither the electrode nor the electrolyte undergoes the electrochemical process. 90% *iR* correction (R = 1.38 ohm, the resistance of the catalytic material) was used to correct the measured potentials. The scan rates used for the ECSA measurement were 10 mV/s, 20 mV/s, 30 mV/s, 40 mV/s, 50 mV/s, 60 mV/s, 70 mV/s, 80 mV/s, 90 mV/s, 100 mV/s, 200 mV/s and 300 mV/s. For each scan rate, several consecutive CVs were measured until no changes were observed, and the last CV result was used for further data analysis. The ideal capacitor model (Y = bX, where Y is the current and X is the scan rate) was used to determine the double layer capacitance (C_{DL}), whereby a fitting value of 2.47 mF cm^{-2} (R-factor ~ 0.9996) was achieved. Then, the ESCA was determined based on the equation ECSA = C_{DL}/C_s (C_s is the specific capacitance with the widely used value 0.04 mF cm^{-2}). We have included these procedures in our revised Supporting

Information (Line 17, Page 4, highlighted in crimson). The reference provided by the reviewer was also included in our revised manuscript (as reference 19, highlighted in crimson in our revised manuscript).

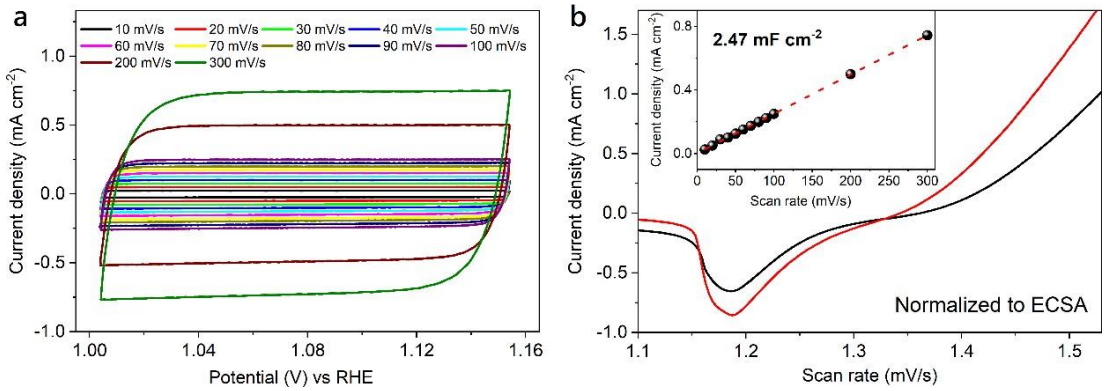

Fig. R2. (a) Electrochemical surface area (ECSA) of NR-NiOOH; (b) Current density normalized to ECSA. In our work, the specific capacitance C_s was 0.04 mF cm^{-2}. Fig. R2 is represented as Fig. S6 a and b in our revised Supporting Information.

Based on the literature review, we have summarized the methods used in the previous works in Table R1 (highlighted in crimson, Table S2 in our revised Supporting Information). From Table R1, we could see that five methods were used to estimate the actual surface area, *i.e.*, ECSA, BET, SEM, TEM and preparing well-defined epitaxial oxide thin-film (geometric surface area). We fully agreed with the reviewer that the specific activities derived from these different normalization methods cannot be compared directly. If we were to compare the performance based on the normalization to the electrochemical surface area, NR-NiOOH under light irradiation was able to achieve superior activities as compared to other OER electrocatalyst.

Table R1. Comparison of the current normalized to the actual surface area of NR-NiOOH under light irradiation and selected previously reported OER catalysts. C_s is the specific capacitance calculated from ECSA measurement; j (mA cm$^{-2}_{specific}$) is the normalized current at a potential of 1.50 V vs RHE (if not, the potential was provided). Table R1 is represented as Table S2 in our revised Supporting Information.

Catalyst	Electrolytes	Method/(C_s)	j (mA cm$^{-2}_{specific}$)	Ref
IrO_2 NP	0.1 M $HClO_4$	TEM	0.010	*J. Phys. Chem. Lett.* **3,** 399, 2012
RuO_2 NP	0.1 M $HClO_4$	TEM	0.020	
RuO_2/C	0.5 M H_2SO_4	ECSA (0.035)	0.800	*Nat. Commun.* **10,** 4849, 2019
Ru-N-C	0.5 M H_2SO_4	ECSA (0.035)	0.850	
$Cr_{0.6}RuO_2$ (550)	0.5 M H_2SO_4	ECSA (0.035)	0.04 (1.45 V)	*Nat. Commun.* **10,** 162, 2019
$Ru_{0.7}Ni_{0.3}O_{2-y}$	0.1 M $HClO_4$	SEM	0.080	*J. Solid State Electrochem.* **13,** 959, 2009
La_2LiIrO_6	0.05 M H_2SO_4	TEM	0.600	*Nat. Energy* **2,** 16189, 2016

Sputter RuO_2	0.05 M H_2SO_4	Geometric surface area	1.050	*ChemElectroChem* **1,** 2075, 2014
$IrO_x/SrIrO_3$	0.5 M H_2SO_4	Geometric surface area	7.300 0.32 (1.45 V)	*Science* **353,** 1011, 2016
$LaCoO_3$	0.1M KOH	BET	0.009	*Nat. Chem.* **9,** 457, 2017
$La_{0.5}Sr_{0.5}CoO_{3-\delta}$	0.1M KOH	BET	0.017	
$SrCoO_{3-\delta}$	0.1M KOH	BET	0.300	
$CaCu_3Fe_4O_{12}$	0.1M KOH	BET	0.045	*Nat. Commun.* **6,** 8249, 2015
Co_3O_4/CeO_2	0.5 M H_2SO_4	ECSA (0.035)	0.024 (1.68V)	*Nat. Commun.* **12,** 3036, 2021
$NaNiO_2$	1 M KOH	ECSA (0.04)	0.35 (1.58 V)	*Energy Environ. Sci.,* **10,** 121, 2021
$NaNi_{0.9}Fe_{0.1}O_2$	1 M KOH	ECSA (0.04)	1.15 (1.58 V)	
IrO_x/9R-$BaIrO_3$	0.5 M H_2SO_4	ECSA (0.035)	0.50 (1.49 V)	*J. Am. Chem. Soc.* **143,** 18001, 2021
CoO_x	1 M KOH	ECSA (0.04)	0.09 ± 0.04 (1.58 V)	*J. Am. Chem. Soc.* **135,** 16977, 2013
$CoFeO_x$	1 M KOH	ECSA (0.04)	0.4 ± 0.2 (1.58 V)	
NiO_x	1 M KOH	ECSA (0.04)	0.12 ± 0.05 (1.58 V)	
$NiCoO_x$	1 M KOH	ECSA (0.04)	0.2 ± 0.1 (1.58 V)	
NR-NiOOH under light irradiation	1 M KOH	ECSA (0.04)	1.230 0.730 (1.45V)	**Our work**

3) Fig. S10. I was confused by the order of the panels. Is it possible to exchange current panels c and d, so that Ni(CN)4 can be easier compared to NR-NiOOH?

Response: We are very thankful for this suggestion. We agree with the reviewer that the order of the panels for Fig. S10 can be optimized. We have revised Fig. S10 according to the reviewer's suggestion. The revised Fig. S10 is shown as Figure R3 (Fig. S10 in our revised Supporting Information).

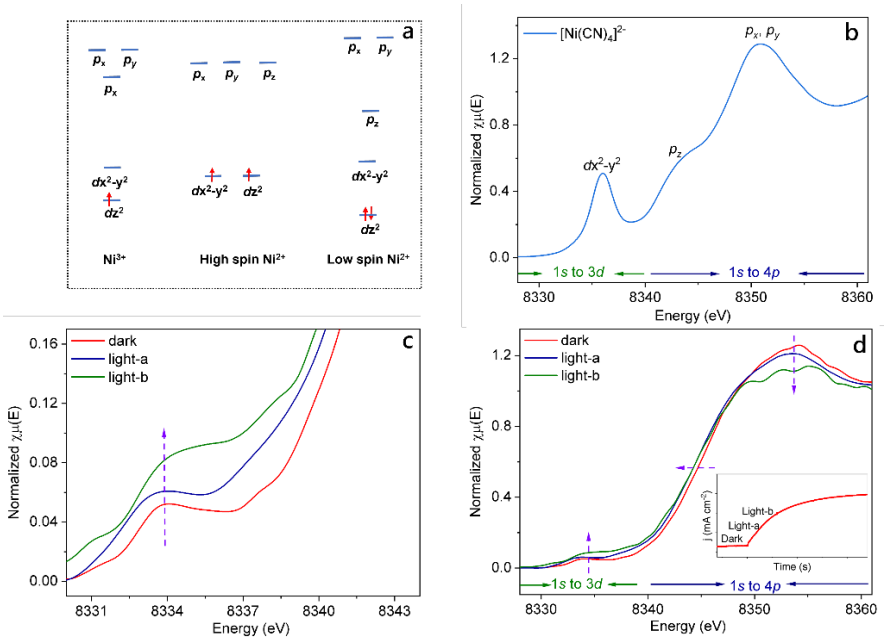

Fig. R3. (a) The orbital diagram of Ni^{3+}, high spin Ni^{2+} and low spin Ni^{2+}. (b) The HR-XAFS spectra of $[Ni(CN)_4]^{2-}$ ion. (c) The pre-edge in HR-XAFS spectra of NR-NiOOH subjected to light irradiation. (d) *Operando* HR-XAFS spectra of NR-NiOOH subjected to light irradiation (inset showing the electrochemical curves accompanying the *operando* HR-XAFS). (Figure S10 in our revised Supporting Information)

4) The reduction in bond length with irradiation in Table S5 is within the error (1.85±0.01 vs 1.87±0.01) and not "greatly reduced". Please revise the statement in the text. Looking at the structural model and the reply, it is not surprising to me that the expected difference is not resolved by EXAFS. I find the other data already convincing.

Response: We are very thankful for this insightful suggestion. We have revised this statement and changed "greatly" into "slightly" in our revised Supporting Information (Page 14, highlighted in crimson).

5) Please mention in the revised manuscript that NR-NiOOH contains some sulfur.

Response: We are very thankful for this suggestion. We have added the following sentence, "According to our previous work, very weak S signal can be observed in the sample (*1*)." in our revised Supporting Information (Line 18, Page 2).

6) "NR-NiOOH under light irradiation exhibited an extremely low overpotential of 135 mV at 10 mA cm-2 (Fig. S5c). This result, to the best of our knowledge, is the best OER performance reported so far (Table. S1)" The overpotential at 10 mA/cm2 is not meaningful without the loading as it can be changed simply by variation of the loading. Are all entries in Table S1 given for the same loading? The statement is not

correct. Lower electrode overpotentials can be found, e.g. here for Ni(Fe) oxides: https://onlinelibrary.wiley.com/doi/10.1002/aenm.201600621

Response: We are very thankful for this insightful comment. We agree that the result can be changed with variation in the loading. As such, we have summarized the respective loading mass for the previous systems in Table R2, (Table S1 in our revised Supporting Information, highlighted in crimson). We acknowledge the different loading mass in these studies, and therefore we would like to change our original statement from "the best OER performance reported so far" into "one of the best OER performances reported so far" in our revised manuscript (Line 16, Page 6, highlighted in crimson). We are thankful for the reference provided by the reviewer, and we found it to be helpful in our study. As such, we have included the catalytic materials with lower potential at a low mass loading from the provided reference (Table S1 in our revised Supporting Information, highlighted in crimson).

Table R2. Comparison of OER catalytic performances of NR-NiOOH under light irradiation and selected previously reported OER catalysts. Table R2 is represented as Table S1 in our revised Supporting Information

Catalyst	Electrolytes	Loading mass (mg)	Overpotential (mV) at 10 mA cm^{-2}	Tafel slope	Ref
G-FeCoW	1 M KOH	0.210	191	-	*Science* **352,** 333-337, 2016
$Ni_xFe_{1-x}Se_2$-DO	1M KOH	4.100	195	28	*Nat. Commun.* **7,** 12324, 2016
Ni_3N COF	1M KOH	0.005	230	79	*Adv. Energy. Mater.* **6,** 1601189, 2016
Co_3O_4/N-rmGO	1 M KOH	0.100	310	67	*Nat. Mater.* **10,** 780-786, 2011
CoZnOOH	1M KOH	0.204	285	35	*Nat. Ener.* **4,** 329-338, 2019
PBSCF-III	0.1M KOH	0.202	358	52	*Nat. Commun.* **8,** 14586, 2017
$Ba_{0.5}Sr_{0.5}Co_{0.8}Fe_{0.2}O_3$	0.1M KOH	0.250	370	-	*Science* **334,** 1383-1385, 2011
$CaFeO_3$	0.1M KOH	0.250	390	47	*Nat. Commun.* **6,** 8249, 2015
NiCo-UMOFENs	1 M KOH	0.200	189	65	*Nat. Ener.* **1,** 16184, 2016
IrO_2	1M KOH	-	325	54	*J. Am. Chem. Soc.* **135,** 16977-16987, 2013
NiFe/NF	1M KOH	0.450	215	28	*Nat. Commun.* **6,** 6616, 2015
FeNi-rGO	1M KOH	0.250	206	39	*Angew. Chem. Int.*

LDH					*Ed.* **53,** 7584, 2014
$NiFeO_x$/C	0.1M KOH	0.008 (only metals)	290	-	*Catal. Today.* **65,** 262, 2016
NiFe LDH	1 M NaOH	0.050	260	21	*Nanoscale Horiz.,* **1,** 156, 2016
NR-NiOOH under light irradiation	1 M KOH	0.420	135	31	Our work

7) P11 “The latter two peaks show that more lattice oxygen atoms participated in OER process as the catalytic reaction proceeded.” Could the latter two peaks be noise? Eventually, the ratio should be constant when 16O diffusion to the surface balances with lattice oxygen evolution. Why are peaks expected?

Response: We are very thankful for this insightful comment. We fully agree with the reviewer’s comment that the latter two peaks may be noise. As the catalytic reaction proceeds, the ratio of $^{18}O/^{16}O$ within the electrocatalyst should continue to decrease, and this would lead to a continuous decrease in the ratio of $^{36}O_2$ to $^{32}O_2$. As such, no more $^{36}O_2$ to $^{32}O_2$ peaks should be observed after the detection of the initial peak. Hence, in our revised manuscript, we have deleted this statement to avoid any misunderstanding.

8) P9 Supplemental. Difference between LOM and COM

Rebuttal P8: The sole oxygen redox activities within LOM in perovskite were verified by another group, using operando oxygen K-edge and metal L-edge X-ray absorption spectra (Nature Communications 6, 6097, 2015).

It would be clearer to include that statement and reference in the manuscript or supplemental as it is important to define the LOM mechanism that the authors use as a reference. As you have seen by all referees’ comments, the LOM mechanism is often not considered as having only oxygen redox. Making this point explicit helps to demarcate the COM from the LOM mechanism.

Response: We are very thankful for this insightful suggestion. We agree with the reviewer that LOM mechanism was defined by other factors in the early stage of LOM. Currently, it is widely known that LOM is a type of oxygen redox reaction. To provide a better clarity in our manuscript, we have defined the LOM mechanism that we have used as a reference. We have added the following sentence in the Supplementary Discussion in our revised Supporting Information. “Currently, it is widely known that LOM is a type of oxygen redox reaction. The sole oxygen redox activities within LOM were verified by researchers in the study of perovskite, using *operando* oxygen *K*-edge and metal *L*-edge X-ray absorption spectra (*3*). The sole oxygen redox activities could be further understood based on the electron transfer process.” (Paragraph 2, Page 8 in our revised Supporting Information).

Meanwhile, to make AEM, LOM and our proposed COM much easier to understand, we have added the redox activities of AEM, LOM and COM routes in our manuscript, as shown in Fig. R4 and R5.

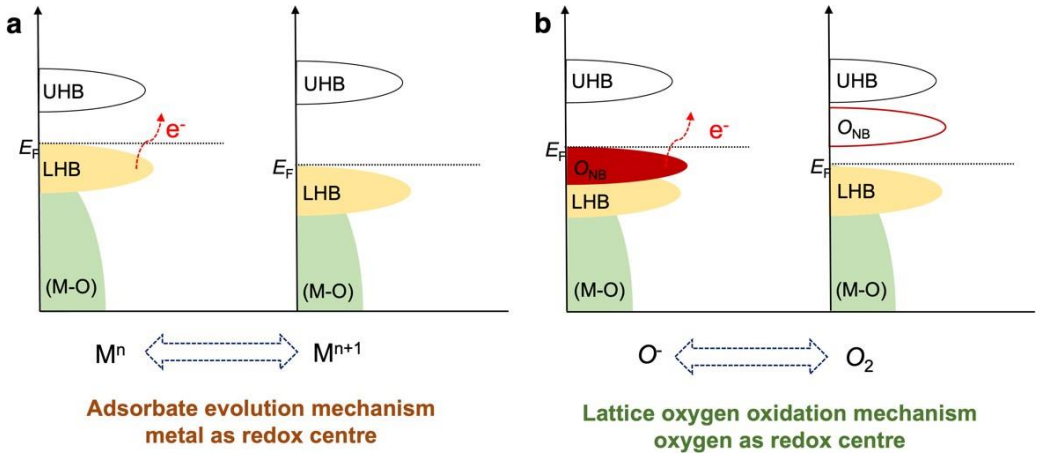

Fig. R4. (a) Schematic illustration of AEM route; (b) schematic illustration of LOM route. Fig. 1 in our revised manuscript. The original Fig. 1 in our previous manuscript has been moved to our revised Supporting Information (Fig. S3).

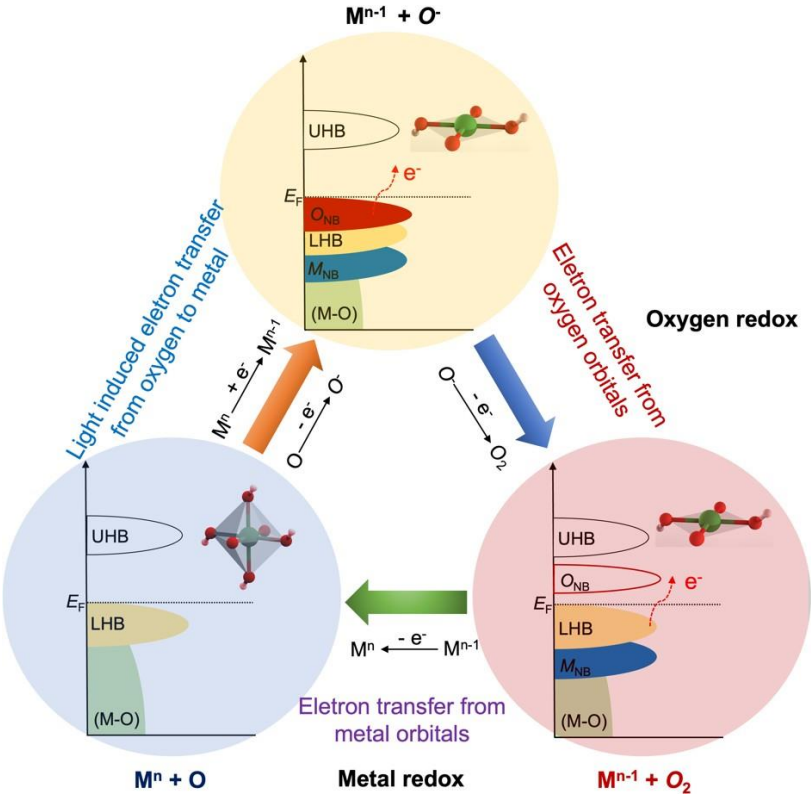

Fig. R5. Schematic illustration of the COM route. Fig. R5 is represented as Fig. 4 in our revised manuscript. The original Fig. 4 in our previous manuscript has been moved to our revised Supporting Information (Fig. S20).

9) Distinction of the COM from other mechanisms

Please address the outstanding comments regarding the DFT calculations fully. I agree that the DFT calculations of all three mechanisms should be performed at an overpotential relevant to the experiments. Since the rate-determining step is discussed, the kinetic barriers should be discussed. These calculations should rigorously support that the COM is a distinctively new mechanism, which the current state of the (DFT) analysis does not.

Response: We are very thankful for these insightful comments We have made vast improvements to our simulations in our revised manuscript by addressing these concerns.

1. Performing the DFT calculations of AEM, LOM and COM at an overpotential relevant to the experiments

Three different biases can be used to display the free energy calculation results for the OER process, *i.e.*, free energies calculation at 0 V, 1.23 V, and the lowest bias potential V vs. RHE. Even though 0 V vs. RHE has been used to express the free energy calculation results in the previous reports (*J. Phys. Chem. C*, 2012, 116, 21077-21082; *Nat. Commun.* 2019, 10, 1711; *J. Mater. Chem. A.*, 2020, 8, 6795), we fully agree with the reviewer that potential at 0 V cannot show the reaction potential in a straightforward manner. Instead, by using the potential at 1.23 V vs. RHE, the overpotential of each step can be clearly shown. On the other hand, by using the potential at the lowest bias potential, the lowest overpotential needed to drive all reactions based on the downhill process can be obtained. As such, to better describe the actual OER process, we have calculated free energies by considering the solvent effect based on U = 0V, 1.23 V and the lowest bias potential vs RHE in the revised manuscript (Fig. R6 to R9, Fig. S23 to 25 in our revised Supporting information).

Here, we performed the calculations for the AEM, LOM, and COM routes based on these 3 biases, i.e., 0 V, 1.23V, and the lowest bias potential vs. RHE, to illustrate the differences in these 3 mechanisms.

a) Calculated reaction free energies of the AEM route

Detailed calculations of the AEM process were provided in our previous work (*Energy Environ. Sci.* 13, 229, (2020)). The calculated free energies of the AEM route in NR-NiOOH based on 0 V, 1.23 V and the lowest bias potential (1.785 V) vs. RHE are provided in Fig. R6 (Fig. S23 in our revised Supporting Information).

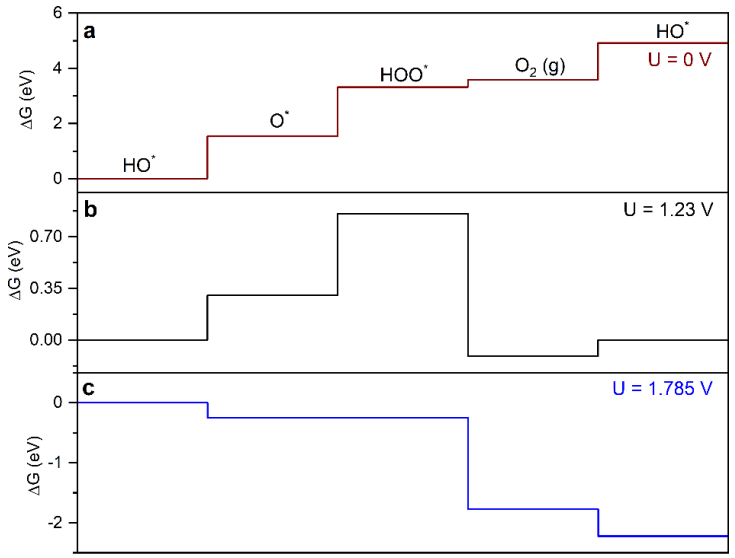

Fig. R6. Calculated reaction free energies of the AEM route in NR-NiOOH based on 0 V, 1.23 V and the lowest bias potential (1.785 V) vs. RHE. Fig. R6 is represented as Fig. S23 in our revised Supporting Information.

b) Calculated reaction free energies of the LOM route

The reaction free energies of the LOM route was calculated with reference to *Nature Energy* 4, 329-338, 2019. The calculated reaction free energies of the LOM route in NR-NiOOH based on 0 V, 1.23 V and the lowest bias potential (1.791 V) vs. RHE are shown in Fig. R7 (Fig. S24 in our revised Supporting Information). The detailed LOM calculation route is provided below:

$\Delta G_{L1} = \Delta G_{[O-O]} - \Delta G_{[OH^*+O^*]} - eU + \Delta G_{pH}$

$\Delta G_{L2} = \Delta G_{[OO^*+OH^*]} - \Delta G_{[O-O]} - eU + \Delta G_{pH}$

$\Delta G_{L3} = 4.92\ eV - \Delta G_{[OO^*+OH^*]} + \Delta G_{[OH^*+OH^*]} - eU + \Delta G_{pH}$

$\Delta G_{L4} = \Delta G_{[OH^*+O^*]} - \Delta G_{[OH^*+OH^*]} - eU + \Delta G_{pH}$

The new LOM route has been added in the theoretical calculation section in our revised Supporting Information (Page 7).

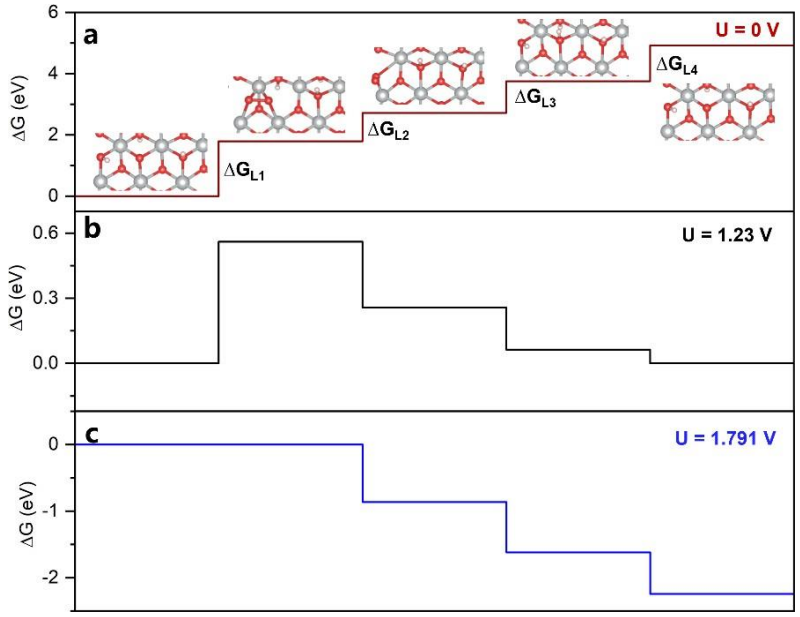

Fig. R7. Calculated reaction free energies of the LOM route in NR-NiOOH based on 0 V, 1.23 V and the lowest bias potential (1.791 V) vs. RHE. Fig. R7 is represented as Fig. S24 in our revised Supporting Information.

c) Calculated reaction free energies of the COM route

In our revised manuscript, we have performed the COM calculations with reference to *Nature Energy* 4, 329-338, 2019. The new COM route has been added in the theoretical calculation section in our revised Supporting Information (Page 7). The detailed COM route is provided below:

$\Delta G_{C1} = \Delta G_{[O^*+O^*]} - \Delta G_{[OH^*+O^*]} - eU + \Delta G_{pH}$

$\Delta G_{C2} = \Delta G_{[O-O]} - \Delta G_{[O^*+O^*]}$ **(light dominated process)**

$\Delta G_{C3} = \Delta G_{[OO^*+OH^*]} - \Delta G_{[O-O]} - eU + \Delta G_{pH}$

$\Delta G_{C4} = 4.92\ eV - \Delta G_{[OO^*+OH^*]} + \Delta G_{[OH^*+OH^*]} - eU + \Delta G_{pH}$

$\Delta G_{C5} = \Delta G_{[OH^*+O^*]} - \Delta G_{[OH^*+OH^*]} - eU + \Delta G_{pH}$

In contrast to the conventional OER process, the (O-O) coupling step in our proposed COM pathway was realized *via* photon-induced geometry conversion from octahedron to square planar. The geometry conversion from octahedron to square planar involved the occurrence of two neighboring (O-O) couplings, and this implies the participation of four oxygen atoms sites during the geometry conversion. Nevertheless, an OER process (with only one O_2 molecule produced) is a four-electron process, and during the OER calculation only one type of O-O bond formation will be considered, *i.e., either* OOH or (O-O) coupling. To demonstrate the geometry conversion from octahedron to square planar during the OER via calculation, a NR-NiOOH with one inner (O-O) coupling was employed in our DFT simulations, whereby it possessed an octahedral configuration with one inner (O-O) coupling. When the OER process follows the COM route, there is a geometry conversion to square planar during the light dominated process. Based on the calculations, the potential limiting step was between C1 to C2, with a calculated overpotential of 0.093 V (Solvent) (Fig. R8, Fig. S25 in our revised Supporting Information).

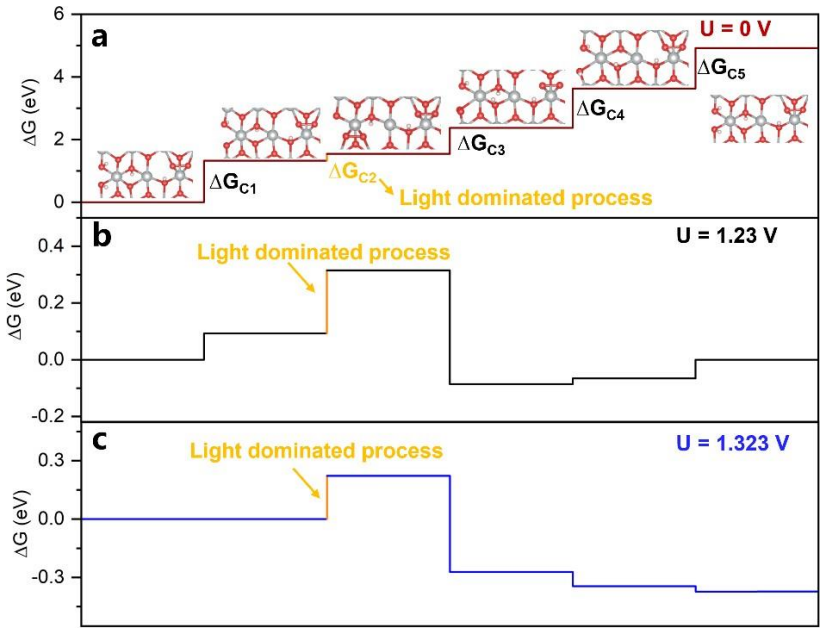

Fig. R8. Calculated reaction free energies of the COM route in NR-NiOOH (with one inner (O-O) coupling as the starting model) based on 0V, 1.23 V and the lowest bias potential (1.323 V) vs. RHE. Fig. R8 is

represented as Fig. S25 in our revised Supporting Information. Here, it is worth noting that the light-dominated process is a potential independent step.

For the calculations based on the COM route, the starting model and OER calculation route were different from those in the AEM route. As such, it would be unfair to directly compare the calculated overpotential value with that based on the AEM route. Thus, we performed DFT simulations using NR-NiOOH, *i.e.*, octahedron, as the initial model based on the same route as COM, *i.e.*, the light provides the energy required for (O-O) coupling. The adsorption configurations for the calculation process were provided in Fig. R9 (Fig. S26 in our revised Supporting Information). It shows that this route follows the same route as COM, while no geometry conversion was demonstrated in the route. In this route, the calculated overpotential was 0.403 V. Since the calculation employed the same model (NR-NiOOH) as that for AEM, we could conclude that it exhibited a lower overpotential (0.403 V) as compared to NR-NiOOH *via* AEM route (0.555 V). Moreover, since the calculation proceeded in the same route as COM, we could conclude that it possessed higher overpotential (0.403 V) as compared to the COM route (0.093 V). Hence, the COM route exhibited a significantly smaller overpotential as compared to the AEM route.

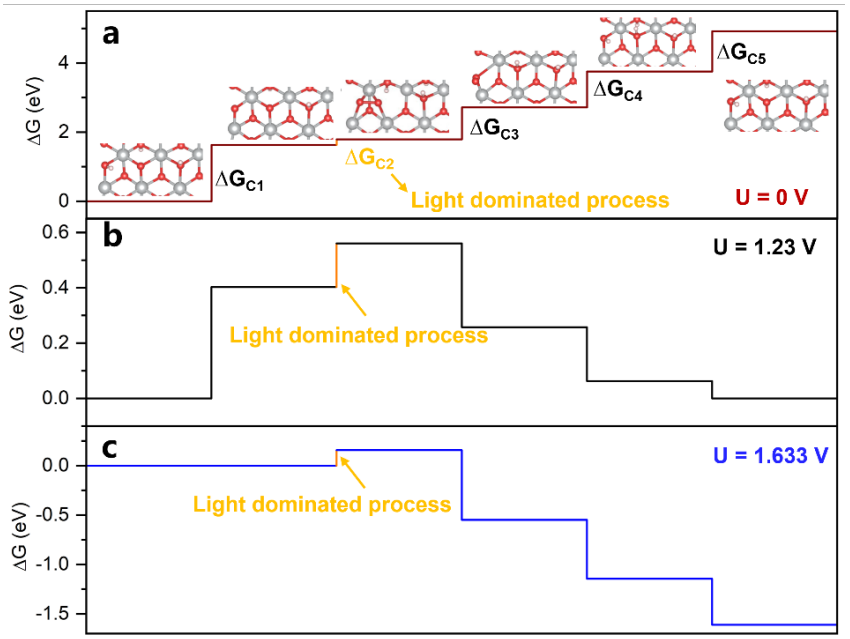

Fig. R9. Calculated reaction free energy (Solvent) of NR-NiOOH following the same route as COM route according to 0V, 1.23 V and the lowest bias potential (1.633 V). Here, it should be noted that light-dominated process is a potential independent step. It shows that this route follows the same route as COM, while no geometry conversion was demonstrated in the route. Fig. R9 is represented as Fig. S26 in our revised Supporting Information.

Thus, based on our revised calculations, the overpotential of COM is lower as compared to those of AEM and LOM. To increase the clarity of our results, we have added Fig. R6 to R9 in our revised Supporting Information (Fig. S23 to S26).

2. The kinetic barriers of AEM, LOM and COM routes were discussed in our revised manuscript.

The main difference among AEM, LOM and COM routes is the types of O-O bond formation, *i.e.* OOH formation in AEM (electrochemical process), direct (O-O) coupling in LOM (chemical process), and (O-O)

coupling in COM *via* photon induced geometry conversion from octahedron to square planar (light dominated process). Thus, in the following section, we will discuss the kinetic barriers of O-O bond formation in AEM, LOM and COM routes.

a) The discussion on OOH formation in AEM route (electrochemical process)

OOH formation is an electrochemical process. The kinetic barrier for OOH formation *via* AEM pathway is more challenging to calculate since it is potential dependent. Based on the previous reports, the kinetic barrier of OOH formation (potential dependent) reduces with increasing applied potential (*Nature* 587, 408, 2020).

b) The discussion on direct (O-O) coupling in LOM route (chemical process)

(O-O) coupling *via* LOM pathway is a chemical process (potential independent), which is typically related to temperature. At room temperature, the hard limit for a surmountable barrier is 0.75 eV (*Chem. Rev.* 2019, 119, 12, 7610–7672). Hence, for (O-O) coupling *via* LOM to proceed, it is necessary to fulfill both conditions; (1) $\Delta G_{[O\text{-}O]}$ must be smaller than $\Delta G_{[O^*]}$ and (2) the activation energy from $\Delta G_{[O^*]}$ to $\Delta G_{[O\text{-}O]}$ (E_a) must be smaller than 0.75 eV (*Nature Energy* 4, 329-338, 2019). To determine the accessibility of O-O coupling, we calculated the free energy of the two isometric intermediates of $\Delta G_{[O^*]}$ and $\Delta G_{[O\text{-}O]}$ (Fig. R10). Based on the calculations results, $\Delta G_{[O\text{-}O]}$ (0.158 eV) is larger than $\Delta G_{[O^*]}$, which indicates that O-O coupling was thermodynamically unfeasible (Fig. R 10, Fig. S22a in our revised Supporting Information). Furthermore, the energy barrier from $\Delta G_{[O^*]}$ to $\Delta G_{[O\text{-}O]}$ was 0.794 eV, which is higher than the activation energy limit for facile kinetics, *i.e.*, 0.75 eV (*Chem. Rev.* 2019, 119, 12, 7610–7672). As such, based on these two conditions, the (O-O) coupling via LOM pathway is not accessible for NR-NiOOH.

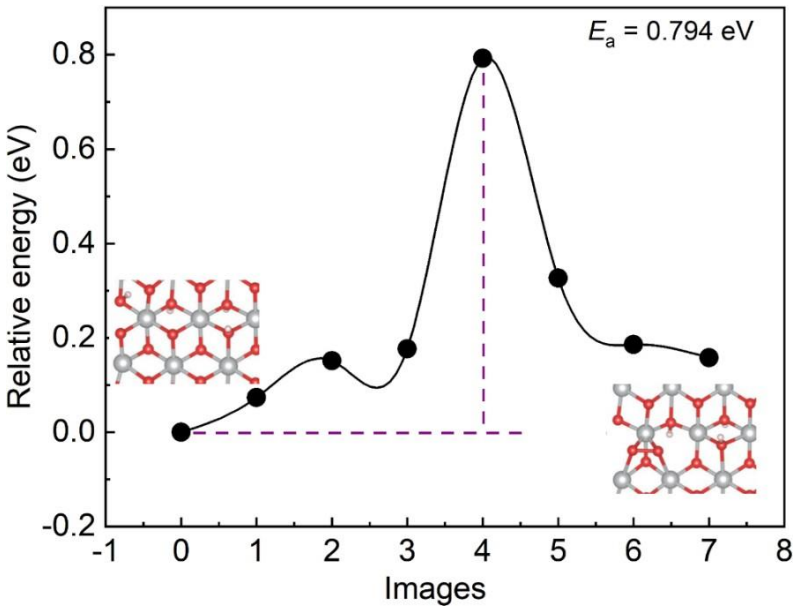

Fig. R10. The energy barrier for (O-O) coupling of LOM process. Based on the calculations, $\Delta G_{[O\text{-}O]}$ (0.158 eV) is larger than $\Delta G_{[O^*]}$, which indicates that O-O coupling was thermodynamically unfeasible. At the same time, the energy barrier from $\Delta G_{[O^*]}$ to $\Delta G_{[O\text{-}O]}$ was 0.794 eV, which is higher than the activation energy limit for facile kinetics. Fig. R10 is represented as Fig. S22a in our revised Supporting Information.

c) The discussion on (O-O) coupling in COM route (light dominated process)

I. Feasibility of (O-O) coupling during COM route based on theoretical standpoint

In contrast to the conventional AEM and LOM routes, the (O-O) coupling step in our proposed COM pathway was realized *via* photon-induced geometry conversion from octahedron to square planar. To realize the geometry conversion from octahedron to square planar, two neighboring (O-O) coupling will have to occur. In this calculation, two possible pathways were considered, *i.e.,* these two (O-O) couplings can occur either asynchronously or simultaneously. The simulation results showed that the calculated kinetic barrier based on asynchronous pathway was 1.741 eV, which is smaller than that of simultaneous pathway (2.148 eV) (Fig. R11 c and d, Fig. S22c and d in our revised Supporting Information). Since the kinetic barrier based on asynchronous pathway is lower than that of simultaneous pathway, the asynchronous pathway was considered, which means that a kinetic energy barrier of 1.741 eV must be overcome to achieve geometry conversion. In our proposed COM route, the geometry conversion from octahedron to square planar was triggered by light, which was realized by the photon-induced ligand-to-metal charge transfer (LMCT), electron transfer from (M-O) (ligand like character) to the non-overlapping region of dd_{z^2} orbitals with a_{1g}^* band (metal like character), as shown in Fig. R12a and b. As shown in our PDOS results, the energy required for this type of electron transfer was 1.85 eV, which is larger than the energy barrier (1.7412 eV) of the geometry conversion from octahedron to square planar (Fig. R12c). This means that such a geometry conversion is feasible as long as the photon can provide sufficient energy to trigger the electron transfer from (M-O) to the non-overlapping region of dd_{z^2} orbitals with a_{1g}* band (despite the high kinetic energy barrier).

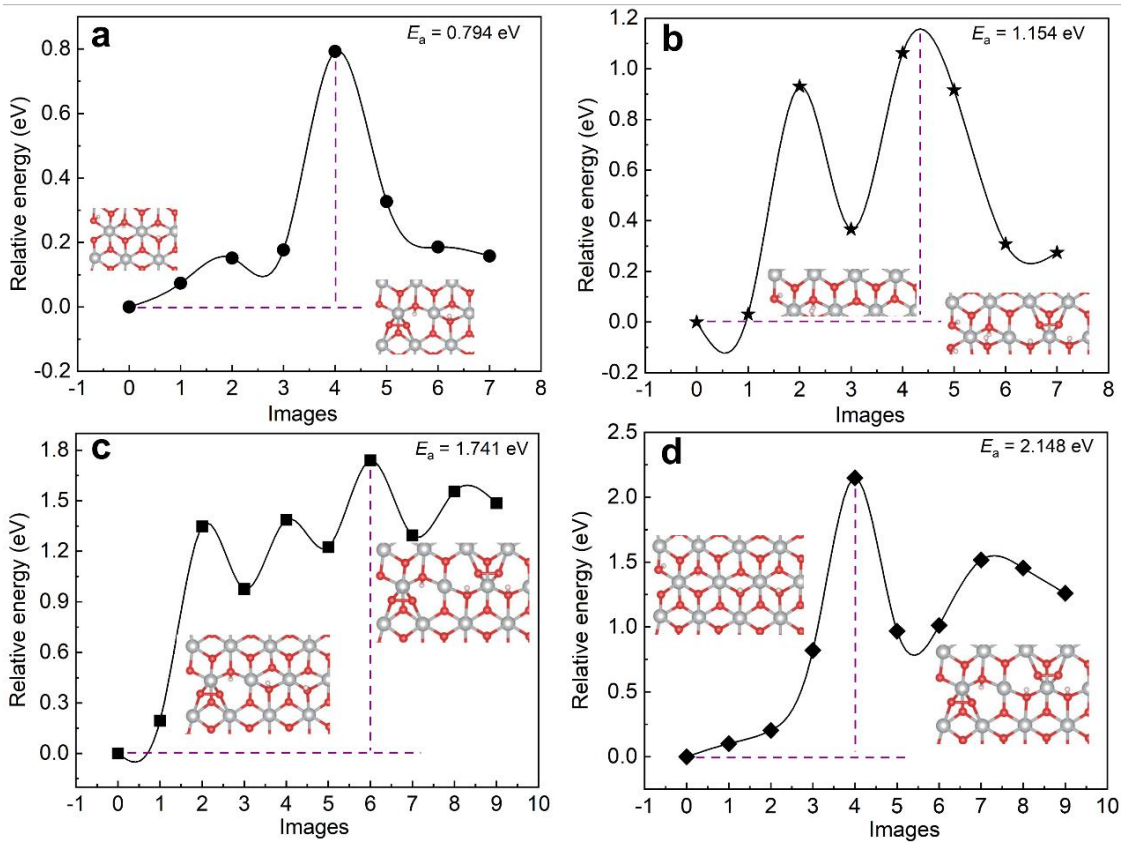

Fig. R11. The energy barrier for geometry conversion from octahedron to square planar. (a) (b) The energy barrier for (O-O) coupling occurring on the edge and inner, respectively; (c)-(d) the energy barrier of asynchronous and simultaneous pathways for geometry conversion from octahedron to square planar, respectively. In the asynchronous pathway, the kinetic energy barriers for (O-O) coupling formation in the edge was 0.794 eV (a) smaller than that of inner (O-O) coupling (b) (1.154 eV). As such, it is believed that

O-O coupling formation at the edge of NR-NiOOH should be formed first. When the edge (O-O) coupling formed, the energy barrier for the inner (O-O) coupling (c) was 1.741 eV, which was the energy barrier for the asynchronous pathway. Fig. R11 is represented as Fig. S22 in our revised Supporting Information.

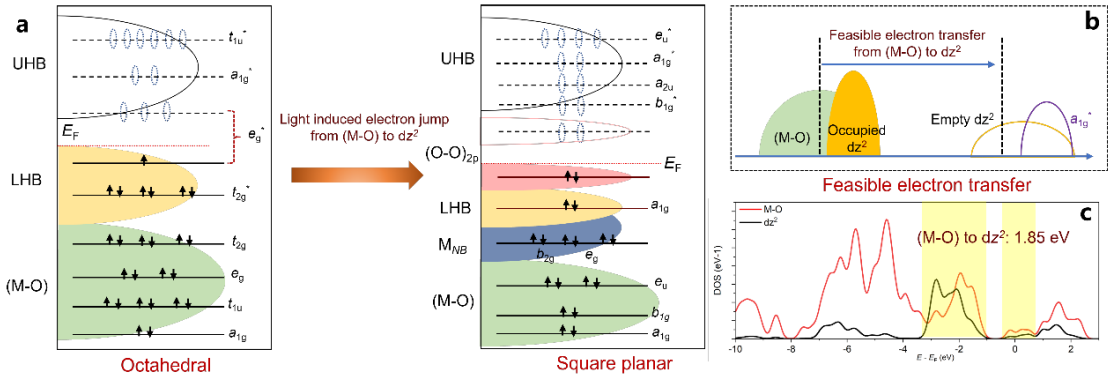

Fig. R12. The electron transfer from (M-O) to the non-overlapping region of dz^2 orbital with a_{1g}* band. (a) The schematic electronic configuration of the induced geometry conversion from octahedron to square planar *via* light irradiation; (b) feasible electron from (M-O) to dz^2 due to the partial overlapping of empty dz^2 orbital and a_{1g}* band; (c) PDOS of dz^2 orbital and (M-O) bands for NR-NiOOH model. Fig. R12 is represented as Fig. S12d and Fig. S28 in our revised Supporting Information.

II. Experimental evidence of O-O coupling during COM under light condition

In our work, a solar simulator (NBeT Solar-500, 300 W) was used as the light source to simulate AM 1.5G, and it could provide sufficient energy to trigger the electron transfer from (M-O) to the non-overlapping region of dd_{z^2} orbitals with a_{1g}* band. To prove the ability of photon in overcoming the high kinetic energy barrier required for geometry conversion, various factors such as electronic states, Ni-O coordinates numbers and Ni-O bond length were considered by conducting *operando* XAFS measurement (Fig. 3a and Fig. S9 to S13 in our revised version). Hence, based on the theoretical and experimental results, we have shown that (O-O) coupling could be triggered by light irradiation, which indicates that our proposed COM route was accessible under light conditions. The accessibility of COM route under light irradiations was further identified using operando XAFS, TMA^+ probe and isotope measurements (Fig. 3 c and d in our revised version).

As such, based on our calculation and experimental results, O-O coupling in COM *via* photon induced geometry conversion from octahedron to square planar was achieved under light condition. Kinetic energy barrier for OOH formation during AEM cannot be precisely determined since it is potential dependent. On the other hand, kinetic energy barrier for direct O-O coupling during LOM was calculated as 0.794 eV, which indicates its inaccessibility without external stimuli. In contrast, a kinetic energy barrier of 1.741eV was determined for O-O coupling during COM *via* photon induced geometry conversion from octahedron to square planar. However, due to the utilization of light, this kinetic barrier could be overcome for COM to process, and this calculation is consistent with our experimental results.

3. The comparison of AEM, LOM and COM routes in NR-NiOOH

Based on the earlier discussion (for (O-O) coupling *via* LOM), direct O-O coupling is thermodynamically unfeasible in NR-NiOOH. This would suggest that LOM route is not likely to occur for our system in dark

condition. Instead, since kinetic barrier for OOH formation via AEM decreases with potential, this would suggest that OOH formation in NR-NiOOH is more likely to occur, especially at high potential. As such, if we consider the operation of our system under dark conditions, the OER process would simply follow the AEM route.

Interestingly, if we were to consider the operation of our system under light conditions, the OER mechanism would change. As mentioned earlier, OOH formation is an electrochemical process that is related to the applied potential, while (O-O) coupling in COM is triggered by light. Since the energy sources for OOH (AEM) and (O-O) coupling (COM) are different, it is difficult to compare which route is favorable based on their activation energy. However, based on the DFT calculations, model proceeding via COM route exhibited a smaller overpotential (0.093 V) as compared to that *via* AEM route (0.555 V) (Fig. R6 to R9). Hence, it is predicted that COM could dominate at the low potential range, while AEM could become accessible at high potential. The actual transition potential depends on the electrocatalyst structure and light irradiation, which will require further studies. In our work, the electrochemical measurement results showed that when NR-NiOOH was irradiated by a solar simulator (100 mW cm^{-2}), the COM route becomes more favorable than the AEM route within the potential range between 1.34 to 1.55 V vs RHE.

Meanwhile, our DFT calculation results shows that the potential limiting step in AEM is the OOH formation process, and the potential limiting step of COM is the deprotonation process. These two potential limiting steps are also likely to be the rate determining steps, as deduced from the Tafel slope analysis.

To increase the clarity of our calculations, we have made the following revisions in our revised version:
1. The discussion on the accessibility of AEM and LOM in NR-NiOOH was added in our revised Supporting Information (Page 16, highlighted in crimson in our revised Supporting Information):
Discussion on the accessibility of AEM and LOM routes in NR-NiOOH
To determine the actual process, *i.e.*, O-O coupling via LOM or OOH formation via AEM, that is more favorable for our NR-NiOOH sample (dark), the kinetics of each process was considered. (O-O) coupling *via* the LOM pathway is a chemical process (potential independent), which is typically related to temperature. At room temperature, the hard limit for a surmountable barrier is 0.75 eV (*4*). Hence, for (O-O) coupling *via* LOM to proceed, it is necessary to fulfill both conditions; (1) $\Delta G_{[O\text{-}O]}$ must be smaller than $\Delta G_{[O^*]}$ and (2) the activation energy from $\Delta G_{[O^*]}$ to $\Delta G_{[O\text{-}O]}$ (E_a) must be smaller than 0.75 eV (*5*). To determine the accessibility of O-O coupling, we calculated the free energy of the two isometric intermediates of $\Delta G_{[O^*]}$ and $\Delta G_{[O\text{-}O]}$ (Fig. S22a). Based on the calculations, $\Delta G_{[O\text{-}O]}$ (0.158 eV) is larger than $\Delta G_{[O^*]}$, which indicates that O-O coupling was thermodynamically unfeasible. Furthermore, the energy barrier from $\Delta G_{[O^*]}$ to $\Delta G_{[O\text{-}O]}$ was 0.794 eV, which is higher than the activation energy limit for facile kinetics, *i.e.*, 0.75 eV (*5*). As such, based on these two conditions, O-O coupling is not accessible for NR-NiOOH without considering the light effect (LOM is inaccessible for NR-NiOOH). On the other hand, OOH formation is an electrochemical process, and the activation energy of OOH formation reduces with increasing applied potentials (*6*).

Thus, by considering the nature of OOH formation (potential dependent) with that of O-O coupling (potential independent), OOH formation will become more accessible in NR-NiOOH during OER without considering light effect. To further verify our conclusion, we have conducted TMA^+ probe and isotope measurement (Fig. 3c and d) and proved the proceeding of AEM route in our NR-NiOOH under dark

conditions. Based on our experimental results, OER process can only proceed via the AEM route in NR-NiOOH under dark conditions, which is consistent with our DFT results that revealed O-O coupling is thermodynamically unfeasible. Thus, by considering the accessibility of O-O coupling, a more meaningful conclusion can be drawn, *i.e.*, O-O coupling is thermodynamically unfeasible in NR-NiOOH under dark conditions, and OOH formation (AEM route) is more likely to occur, especially at high potentials.

2. The discussion on the accessibility of the COM route in NR-NiOOH was added in our revised Supporting Information (Page 15, highlighted in crimson):

Discussion on the accessibility of COM route in NR-NiOOH

In contrast to the conventional OER process, the (O-O) coupling step in our proposed COM pathway was realized *via* photon-induced geometry conversion from octahedron to square planar. To realize the geometry conversion from octahedron to square planar, two neighboring (O-O) coupling will have to occur. In this calculation, two possible pathways were considered, *i.e.,* these two (O-O) couplings can occur either asynchronously or simultaneously. The simulation results showed that the calculated kinetic barrier based on asynchronous pathway was 1.741 eV, which is smaller than that of simultaneous pathway (2.148 eV) (Fig. S22 c and d). Since the kinetic barrier based on asynchronous pathway is lower than that of simultaneous pathway, the asynchronous pathway was considered, which means that a kinetic energy barrier of 1.741 eV must be overcome to achieve geometry conversion. In our proposed COM route, the geometry conversion from octahedron to square planar was triggered by light, which was realized by the photon-induced ligand-to-metal charge transfer (LMCT), electron transfer from (M-O) (ligand like character) to the non-overlapping region of dd_{z^2} orbitals with a_{1g}^* band (metal like character), as shown in in Fig. 5a. As shown in our PDOS results, the energy required for this type of electron transfer was 1.85 eV, which is larger than the energy barrier (1.7412 eV) of the geometry conversion from octahedron to square planar (Fig. S13d). This means that such a geometry conversion is feasible as long as the photon can provide sufficient energy to trigger the electron transfer from (M-O) to the non-overlapping region of dd_{z^2} orbitals with a_{1g}* band (despite the high kinetic energy barrier).

In our work, a solar simulator (NBeT Solar-500, 300 W) was used as the light source to simulate AM 1.5G, and it could provide sufficient energy to trigger the electron transfer from (M-O) to the non-overlapping region of dd_{z^2} orbitals with a_{1g}* band. To prove the ability of photon in overcoming the high kinetic energy barrier required for geometry conversion, various factors such as electronic states, Ni-O coordinates numbers and Ni-O bond length were considered by conducting *operando* XAFS measurement (Fig. 3a and Fig. S9 to S13). Hence, based on the theoretical and experimental results, we have shown that (O-O) coupling could be triggered by light irradiation, which indicates that our proposed COM route was accessible under light conditions. The accessibility of COM route under light irradiations was further identified using operando XAFS, TMA^+ probe and isotope measurements (Fig. 3 c and d).

3. in our revised manuscript, the discussion on the COM calculation is added in our revised manuscript (Page 13 highlighted in crimson):

To gain an in-depth understanding of the COM route, we performed comprehensively theoretical calculations of reaction free energy landscapes. Firstly, we examined the accessibility of the COM route. In our proposed COM pathway, the (O-O) coupling step was realized *via* photon-induced geometry conversion from octahedron to square planar. The calculation results show that a kinetic energy barrier of 1.741 eV must be overcome to achieve geometry conversion (Fig. S22). Such a geometry can be realized

by the electron transfer from (M-O) to dd_{z^2} orbital (1.85 eV), which can be satisfied by natural light (Fig. S13d) (Detailed discussion on the accessibility of COM is provided in Supplementary Discussions). Then, the calculated overpotentials of AEM and COM routes were compared to determine the favorable route under light conditions (the discussion on dark conditions was provided in Supplementary Discussions) (Fig. S23 to S26) (*36*). COM route exhibited a smaller overpotential as compared to AEM route, with proton transfer as the potential limiting step (Fig. S25). Here, it should be noted that the proton transfer step is also likely to be the rate determining step, as deduced from the Tafel slope (Fig. S5d, detailed discussion is provided in Supplementary Text) (*37-38*). Hence, it is predicted that COM could dominate at the low potential range, while AEM could become accessible at a high potential range. The actual transition potential depends on the electrocatalyst structure and light irradiation, which will require further studies. In our work, the electrochemical measurement results showed that when NR-NiOOH was irradiated by a solar simulator (100 mW cm^{-2}), the COM route becomes more favorable than the AEM route within the potential range between 1.34 to 1.55 V vs RHE (Fig. 2c).

Referee #2 (Remarks to the Author):

The authors did a lengthy and diligent revision of the paper, mainly on the experimental part. However, I am now convinced that this paper does not warrant publication in Nature. Mainly because the DFT modelling is unclear, inconclusive, and incomplete, which prevents the authors from validating the hypothesis drawn from their experiments. I would advise a referral to Nature Communications.

Response: We sincerely appreciate the reviewer for the time and efforts in assessing our manuscript, together with very valuable comments. In our revised version, we have fully and faithfully addressed all the reviewer's concerns. We would like to summarize the novelty of our proposed COM and our redesigned DFT calculations to provide more meaningful conclusions.

Novelty: In conventional OER routes, the types of electronic states around the Fermi level in electrocatalysts are fixed. Hence, as a result of this constraint, the OER mechanisms reported in previous studies proceed either solely *via* a metal redox chemistry (AEM, with metal bands around the Fermi level) or an oxygen redox chemistry (LOM, with oxygen bands around the Fermi level). However, in our proposed COM pathway, the electronic states around the Fermi level are able to exhibit alternative metal/oxygen characters throughout the oxygen evolution process, which results from a reversible geometry conversion between octahedron to square planar in the electrocatalyst. Therefore, our proposed COM pathway involves both metal redox (octahedron) and oxygen redox (square planar) chemistries, which contrasts with all known OER routes, and to the best of our knowledge, has yet to be reported in the field of OER. To make our proposed COM easier to understand, the Figure 1 and 4 in the revised manuscript have been simplified to illustrate the view of redox activities.

We have also made vast improvements to our simulations in our revised manuscript by addressing the concerns. We have highlighted some of the key improvements as below:

1) **The simulations of LOM and COM routes are redesigned.**

   (i) As suggested in Q4, the deprotonation steps of two OH have been decoupled in the simulations of both LOM and COM, with reference to *Nature Energy* 4, 329-338, 2019. As a result, the accurate overpotentials of the potential limiting steps (deprotonation) can be obtained.

   (ii) As suggested in Q5, the O_2 desorption energy was excluded in the energy calculation. As a result, the overall free energies of both LOM and COM are 4.92 eV.

   (iii) As suggested in Q1, the reaction free energies of AEM, LOM and COM routes considering solvent effect based on U=0, 1.23 V and the lowest bias potentials have been recalculated

2) **The accessibility of (O-O) coupling in LOM route of NR-NiOOH without the light effect was re-evaluated.**

As pointed out in Q2, to understand which process, i. e. O-O coupling of LOM and OOH formation of AEM, is more favorable for NR-NiOOH without the light effect, both potential and kinetics shall be evaluated. However, we would like to point out that the kinetic barrier for OOH formation via AEM pathway

is hard to calculate since it is potential dependent. Thus, the direct comparison of potential and kinetics barriers between O-O coupling (LOM) and OOH formation (AEM) is not feasible. Therefore, we evaluate the accessibility of O-O coupling via LOM for NR-NiOOH. To make the O-O coupling via LOM accessible, it is necessary to fulfill both conditions; (1) $\Delta G_{[O-O]}$ must be smaller than $\Delta G_{[O^*]}$ and (2) the activation energy from $\Delta G_{[O^*]}$ to $\Delta G_{[O-O]}$ (E_a) must be smaller than 0.75 eV (*Nature Energy* 4, 329-338, 2019). Based on our calculation results, (O-O) coupling via LOM for NR-NiOOH is unfeasible in the absence of light due to its high kinetic energy barrier. This result is consistent with our TMA^+ probe and the isotope measurement result.

3) The kinetic barrier of the transformation from octahedral to square planar has been recalculated, by comparing with the light induced electron transfer from (M-O) to dd_{z^2} orbital.

As pointed out in Q3, the required kinetic barrier of the transformation from octahedral to square planar is beyond the surmountable barrier limit (0.75 eV), thus such a transformation is not feasible. However, we would like to clarify that geometry conversion from octahedron to square planar is triggered by light instead of thermal energy at room temperature in our proposed COM pathway. To overcome the geometry conversion, a kinetic energy barrier of 1.741 eV must be overcome, which can be realized by the electron transfer from (M-O) to dd_{z^2} orbital (1.85 eV). This process can be satisfied by natural light.

4) The overpotentials of COM and AEM for NR-OOH are compared.

As pointed out in Q4, to understand whether COM is more favorable than AEM or not, both potential and kinetics shall be evaluated. Since the energy sources for OOH (AEM, electrochemical process) and (O-O) coupling (COM, light induced process) are different, it is difficult to compare their activation energies. However, based on the simulation results, the kinetic energy barrier of O-O coupling via COM can be easily overcome by light, which is also confirmed by the experiment results. Furthermore, it was shown in our new calculation result that COM route exhibits a much smaller overpotential than AEM route. These results suggest that COM route is the favorable route under light conditions, which is predominant at the low potential range.

Q1- The authors did not address my comments in full. Let me be specific: I said that the authors are making claims based on plots at 0 V vs RHE, whereas the potentials of the reaction are no less than 1.23 V vs RHE (plus the usual overpotential).

Response: We agree with the reviewer that the potentials of the reaction were no less than 1.23 V vs. RHE, and therefore making our conclusions based on the plots at 0V vs. RHE could be misleading. To address the reviewer's comment, we like to point out that three different biases can be used to display the free energy calculation results for the OER process, i.e., free energies calculation at 0 V, 1.23 V, and the lowest bias potential V vs. RHE. Even though 0V vs. RHE has been used to express the free energy calculation results in previous reports (*J. Phys. Chem. C*, 2012, 116, 21077-21082; *Nat. Commun.* 2019, 10, 1711; *J. Mater. Chem. A.*, 2020, 8, 6795), we fully agree with the reviewer that potential at 0 V cannot straightforwardly show the reaction potential. Instead, by using the potential at 1.23 V vs. RHE, overpotential of each step can be clearly shown. On the other hand, by using the potential at the lowest

bias potential, the lowest overpotential needed to drive all reactions based on the downhill process can be obtained. Therefore, we acknowledge that different expressions of the result can be obtained by using different potentials, i.e., U=0 V, 1.23 V, or the lowest bias potential V vs. RHE. As such, to better describe the actual OER process, we have calculated free energies considering the solvent effect based on U=0V, 1.23 V and the lowest bias potential vs RHE in the revised manuscript (Fig. R2-1 to R2-3, Fig. S23 to 25 in our revised Supporting information).

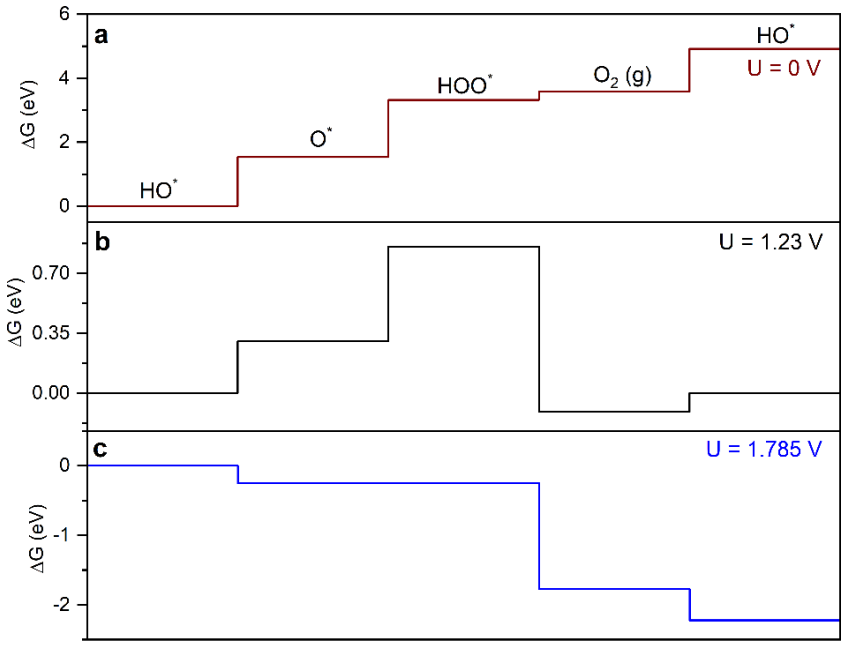

Fig. R2-1. Calculated reaction free energies of the AEM route in NR-NiOOH based on 0 V, 1.23 V and the lowest bias potential (1.785 V) vs. RHE. Fig. R2-1 is represented as Fig. S23 in our revised Supporting Information. Detailed calculations process was provided in our previous work (*Energy Environ. Sci.* 13, 229, (2020)).

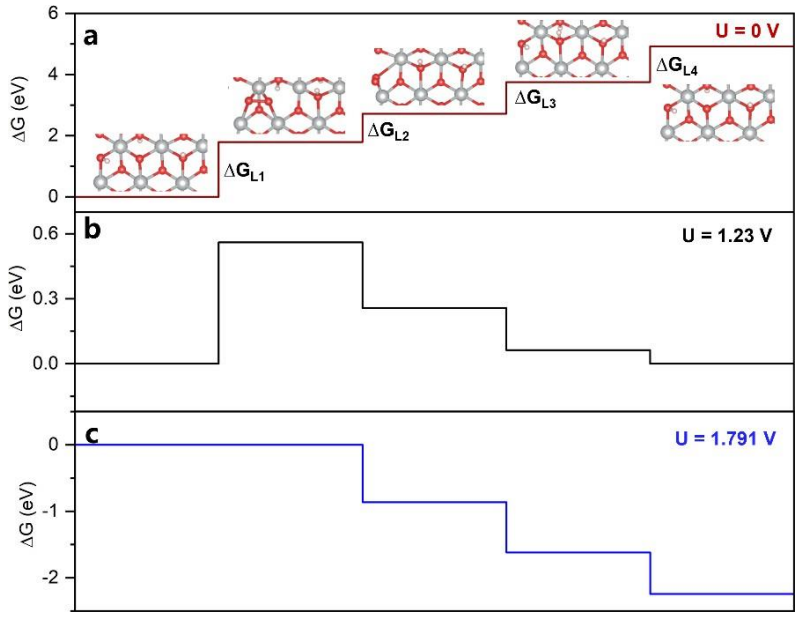

Fig. R2-2. Calculated reaction free energies of the LOM route in NR-NiOOH based on 0V, 1.23 V and the lowest bias potential (1.791 V) vs. RHE. The LOM calculated was reconducted with reference to *Nature*

Energy 4, 329-338, 2019. Fig. R2-2 is represented as Fig. S24 in our revised Supporting Information.

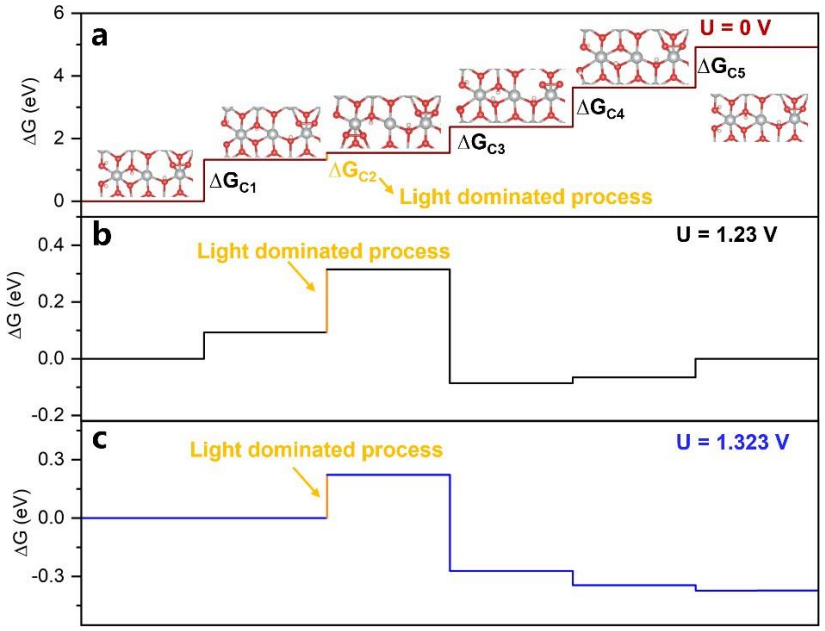

Fig. R2-3. Calculated reaction free energies of the COM route in NR-NiOOH (with one inner (O-O) coupling as the starting model) based on 0V, 1.23 V and the lowest bias potential (1.323 V) vs. RHE. Detailed calculation process is shown in the response to Q4. Here, it is worth noting that the light-dominated process is a potential independent step. Fig. R2-3 is represented as Fig. S25 in our revised Supporting Information.

Q2- The authors say that OOH formation takes 1.59 eV, which leads to an overpotential of 0.36 eV. This low overpotential would be located at the very top of the volcano in Norskov's pathway (AEM in the authors' notation. See e.g. ChemCatChem 3 (7), 1159-1165, Journal of Electroanalytical Chemistry 2007, 607 (1-2), 83-89). In addition, a favorable formation energy for O-O coupling does not imply that the kinetics will be low. Such a chemical barrier (potential independent) should have been calculated and compared to the electrochemical barrier (potential dependent) for OOH formation to arrive at sound conclusions.

Response: We are very thankful for this insightful suggestion. We agree with the reviewer that the overpotential of AEM route *via* OOH formation for our NR-NiOOH is already very low, i.e., at the top of the volcano plot in the Norskov's pathway. As such this makes it less likely that the overpotential of LOM route *via* O-O coupling for our NR-NiOOH can be lower than that of AEM route since AEM route can already proceed with a very low overpotential. Furthermore, we agree that a favorable formation energy for O-O coupling does not necessary result in that the kinetics of (O-O) coupling for NR-NiOOH will be low. We acknowledge that to arrive at sound conclusions, the kinetic barriers of both OOH formation and O-O coupling should be compared instead.

Firstly, we apologize for our improper wording in our previous manuscript, which may have caused this misunderstanding. In our introduction, the statement "(O-O) coupling was favorable than OOH formation" is a generally accepted concept that has been widely indicated in previous reports (*Nature Energy* 4, 329-338, 2019; *ACS Catal*. 8, 4628-4636, 2018, *etc.*). It is noteworthy that when non-bonding oxygen states

become accessible, (O-O) coupling will become more favorable than OOH formation (*Nature Energy* 4, 329-338, 2019). As such, this statement is generalized and dependent on the accessibility of the non-bonding oxygen states, and therefore we should not use our NR-NiOOH structure as the example in our introduction.

Secondly, we agree on the importance of considering both potential and kinetics in determining the actual process, i.e., O-O coupling via LOM or OOH formation via AEM, that is more favorable for our NR-NiOOH sample (dark). (O-O) coupling *via* LOM pathway is a chemical process (potential independent), which is typically related to temperature. At room temperature, the hard limit for a surmountable barrier is 0.75 eV (*Chem. Rev.* 2019, 119, 12, 7610–7672). Hence, for (O-O) coupling *via* LOM to proceed, it is necessary to fulfill both conditions; (1) $\Delta G_{[O-O]}$ must be smaller than $\Delta G_{[O^*]}$ and (2) the activation energy from $\Delta G_{[O^*]}$ to $\Delta G_{[O-O]}$ (E_a) must be smaller than 0.75 eV (*Nature Energy* 4, 329-338, 2019). To determine the accessibility of O-O coupling, we calculated the free energy of the two isometric intermediates of $\Delta G_{[O^*]}$ and $\Delta G_{[O-O]}$ (Fig. R2-4). Based on the calculations results, $\Delta G_{[O-O]}$ (0.158 eV) is larger than $\Delta G_{[O^*]}$, which indicates that O-O coupling was thermodynamically unfeasible. Furthermore, the energy barrier from $\Delta G_{[O^*]}$ to $\Delta G_{[O-O]}$ was 0.794 eV, which is higher than the activation energy limit for facile kinetics, *i.e.*, 0.75 eV (*Chem. Rev.* 2019, 119, 12, 7610–7672). As such, based on these two conditions, O-O coupling is not accessible for NR-NiOOH without considering external environment factors such as light (LOM is inaccessible for NR-NiOOH). On the other hand, OOH formation is an electrochemical process. The kinetic barrier for OOH formation *via* AEM pathway is more challenging to calculate since it is potential dependent. Based on the previous reports, the activation energy of OOH formation (potential dependent) reduces with increasing applied potential (*Nature* 587, 408, 2020).

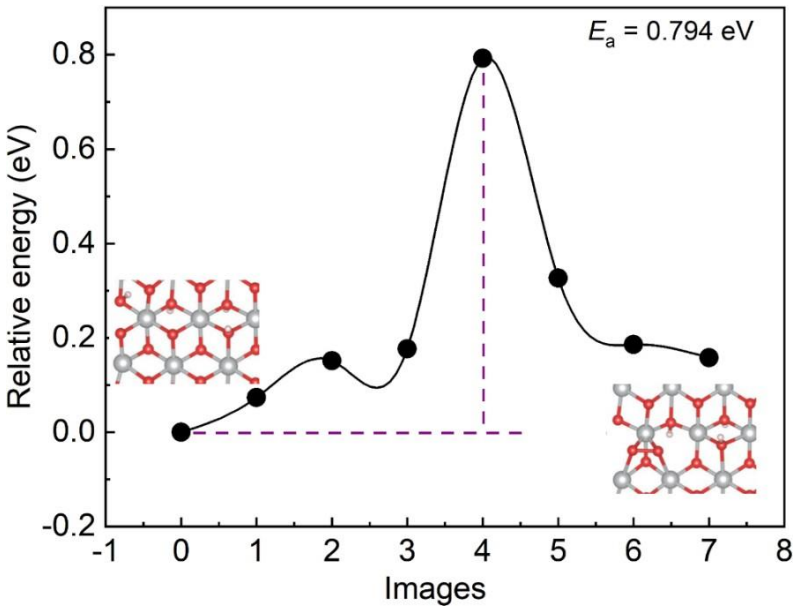

Fig. R2-4. The energy barrier for (O-O) coupling of LOM process. Based on the calculations, $\Delta G_{[O-O]}$ (0.158 eV) is larger than $\Delta G_{[O^*]}$, which indicates that O-O coupling was thermodynamically unfeasible. At the same time, the energy barrier from $\Delta G_{[O^*]}$ to $\Delta G_{[O-O]}$ was 0.794 eV, which is higher than the activation energy limit for facile kinetics. Fig. R2-4 is represented as Fig. S21a in our revised Supporting Information.

Thus, by considering the nature of OOH formation (potential dependent) with that of O-O coupling (potential independent), OOH formation would be more accessible in NR-NiOOH during OER. To further

verify our conclusion, we have conducted TMA^+ probe and isotope measurement (Fig. 3c and d, in our previous and revised manuscript) and proved the proceeding of AEM route in our NR-NiOOH under dark conditions. Based on our experimental results, OER process can only proceed via AEM route in NR-NiOOH under dark conditions, which is consistent with our calculations that revealed O-O coupling is thermodynamically unfeasible. Thus, by considering the accessibility of O-O coupling, a more meaningful conclusion can be drawn, i.e., O-O coupling is thermodynamically unfeasible in NR-NiOOH under dark conditions, and OOH formation (AEM route) is more likely to occur, especially at high potentials.

To increase the clarity of our calculations, we have made the following revisions in our revised manuscript:

1. We have revised the statement in our introduction (Line 5, Page 4, highlighted in crimson in our revised manuscript):

In AEM routes, the existence of potential-limiting step (PLS), *i.e.*, O-O bonding, can cause the overall process to become sluggish (*1-2, 7-10, 14*). Hence, O-O bonding step in the AEM route is often considered as one of the main culprits behind the poor OER performance exhibited by AEM-based electrocatalysts. Unlike AEM, LOM involves a direct oxygen-oxygen (O-O) bond, which can bypass the limitation of AEM, and this highlights the merit of LOM as compared to AEM (*2*, *8-12*). When the non-bonding oxygen states become accessible, the OER process would proceed *via* the LOM pathway (*2*, *8*, *9*) (Fig. S2). Even though LOM is able to avoid the potential-limiting step of AEM, the deprotonation step during LOM is still an energy-demanding process, and therefore it is considered as the PLS for LOM (*7*, *10-11*).

2. The discussion on the accessibility of AEM and LOM in NR-NiOOH was added in our revised Supporting Information (Page 16, highlighted in crimson in our revised Supporting Information):

Discussion on the accessibility of AEM and LOM routes in NR-NiOOH

To determine the actual process, *i.e.*, O-O coupling via LOM or OOH formation via AEM, that is more favorable for our NR-NiOOH sample (dark), the kinetics of each process was considered. (O-O) coupling *via* the LOM pathway is a chemical process (potential independent), which is typically related to temperature. At room temperature, the hard limit for a surmountable barrier is 0.75 eV (*4*). Hence, for (O-O) coupling *via* LOM to proceed, it is necessary to fulfill both conditions; (1) $\Delta G_{[O\text{-}O]}$ must be smaller than $\Delta G_{[O^*]}$ and (2) the activation energy from $\Delta G_{[O^*]}$ to $\Delta G_{[O\text{-}O]}$ (E_a) must be smaller than 0.75 eV (*5*). To determine the accessibility of O-O coupling, we calculated the free energy of the two isometric intermediates of $\Delta G_{[O^*]}$ and $\Delta G_{[O\text{-}O]}$ (Fig. S21a). Based on the calculations, $\Delta G_{[O\text{-}O]}$ (0.158 eV) is larger than $\Delta G_{[O^*]}$, which indicates that O-O coupling was thermodynamically unfeasible. Furthermore, the energy barrier from $\Delta G_{[O^*]}$ to $\Delta G_{[O\text{-}O]}$ was 0.794 eV, which is higher than the activation energy limit for facile kinetics, *i.e.*, 0.75 eV (*5*). As such, based on these two conditions, O-O coupling is not accessible for NR-NiOOH without considering the light effect (LOM is inaccessible for NR-NiOOH). On the other hand, OOH formation is an electrochemical process, and the activation energy of OOH formation reduces with increasing applied potentials (*6*).

Thus, by considering the nature of OOH formation (potential dependent) with that of O-O coupling (potential independent), OOH formation will become more accessible in NR-NiOOH during OER without considering light effect. To further verify our conclusion, we have conducted TMA^+ probe and isotope measurement (Fig. 3c and d) and proved the proceeding of AEM route in our NR-NiOOH under dark conditions. Based on our experimental results, OER process can only proceed via the AEM route in NR-NiOOH under dark conditions, which is consistent with our DFT results that revealed O-O coupling is

thermodynamically unfeasible. Thus, by considering the accessibility of O-O coupling, a more meaningful conclusion can be drawn, *i.e.*, O-O coupling is thermodynamically unfeasible in NR-NiOOH under dark conditions, and OOH formation (AEM route) is more likely to occur, especially at high potentials.

Q3- Figure R49 shows that the transformation from octahedral to square planar complexes requires na large kinetic barrier of 0.79 eV. Based on simple considerations, Chorkendorff et al (Chem. Rev. 2019, 119, 12, 7610–7672) established that the hard limit for a surmountable barrier at room temperature is 0.75 eV.

Response: We are very grateful for this suggestion. In our previous version, 0.794 eV was the kinetic energy barrier for (O-O) coupling at the edge of NR-NiOOH (Figure R2-5a), instead of the kinetic energy barrier for the geometry conversion from octahedron to square planar. To realize the geometry conversion from octahedron to square planar, two neighboring (O-O) coupling will have to occur. In our revised manuscript, we have recalculated the kinetic energy barrier for the geometry conversion from octahedron to square planar by considering the occurrence of two neighboring (O-O) couplings (Fig. R2-5, Fig. S21 in our revised Supporting Information). For this calculation, two possible pathways were considered, *i.e.,* these two (O-O) couplings occur asynchronously or simultaneously. The simulation results showed that the calculated kinetic barrier based on asynchronous pathway was 1.741 eV, which is smaller than that of the simultaneous pathway 2.148 eV. Since the kinetic barrier based on asynchronous pathway is lower than that of the simultaneous pathway, the asynchronous pathway was considered in our further study, which means a kinetic energy barrier of 1.741 eV must be overcome for the geometry conversion to occur. Based on the result, we agreed with the reviewer that it would be difficult for this process to proceed in dark conditions due to this significantly high kinetic energy barrier (1.741 eV), which is much higher than the surmountable barrier limit (0.75 eV) as proposed by Chorkendorff et al (*Chem. Rev.* 2019, 119, 12, 7610–7672).

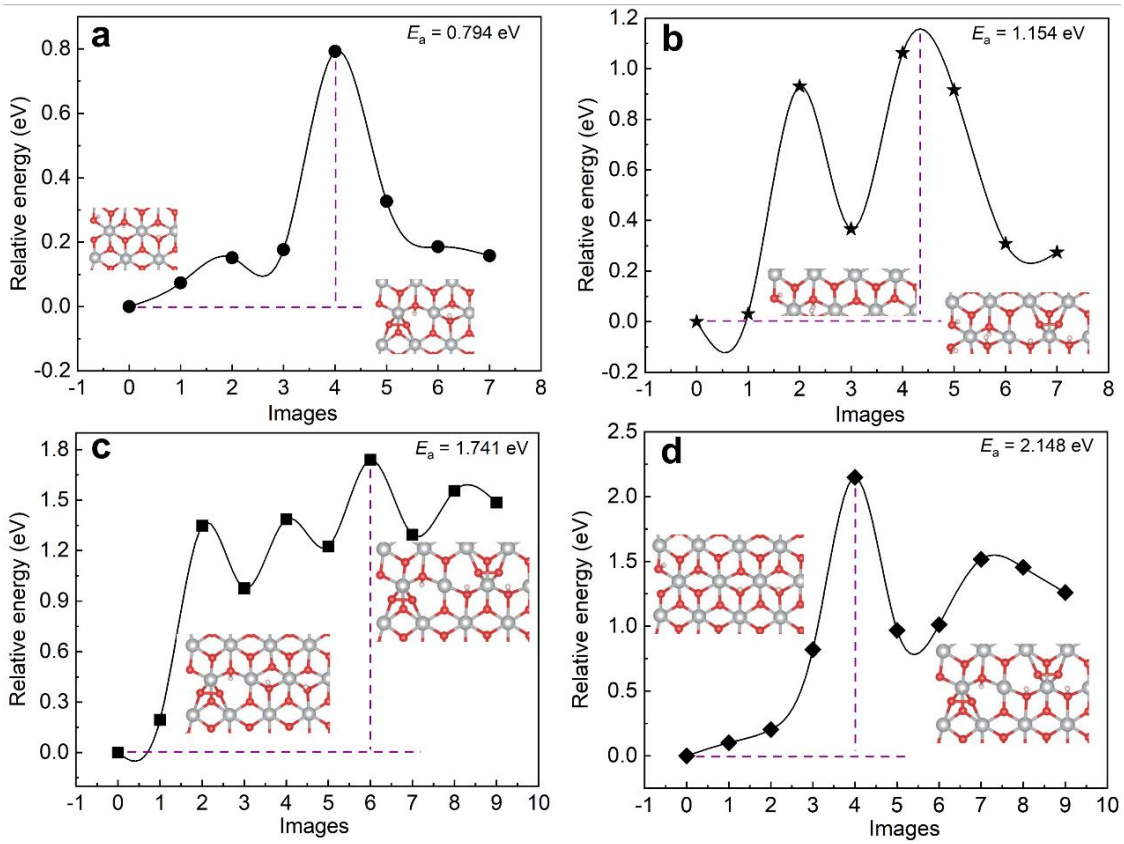

Fig. R2-5. The energy barrier for geometry conversion from octahedron to square planar. (a) (b) The energy barrier for (O-O) coupling occurring on the edge and inner, respectively; (c)-(d) the energy barrier of asynchronous and simultaneous pathways for geometry conversion from octahedron to square planar, respectively. In the asynchronous pathway, the kinetic energy barriers for (O-O) coupling formation in the edge was 0.794 eV (a) smaller than that of inner (O-O) coupling (b) (1.154 eV). As such, it is believed that O-O coupling formation at the edge of NR-NiOOH should be formed first (Fig. R2-5). When the edge (O-O) coupling formed, the energy barrier for the inner (O-O) coupling (c) was 1.741 eV, which was the energy barrier for the asynchronous pathway. Fig. R2-5 is represented as Fig. S21 in our revised Supporting Information. The detailed calculations process was provided as the MP4 file in Supplementary Movie 1-4.

We acknowledge that the kinetic energy barrier for the geometry conversion *via* asynchronous pathway is much higher than the theoretical limit, i.e., 0.75 eV. However, in our proposed COM route, the geometry conversion from octahedron to square planar was triggered by light, which was realized by the photon-induced ligand-to-metal charge transfer (LMCT), electron transfer from (M-O) (ligand like character) to the non-overlapping region of dz^2 orbital with a_{1g}* band (metal like character), as shown in Fig. R2-6a and b. According to our PDOS results, the energy required for such an electron transfer was 1.85 eV, which is larger than the energy barrier (1.7412 eV) of the geometry conversion from octahedron to square planar. This means that such a geometry conversion is possible as long as the photon could provide sufficient energy to trigger the electron transfer from (M-O) to the non-overlapping region of dz^2 orbital with a_{1g}* band (despite the high kinetic energy barrier).

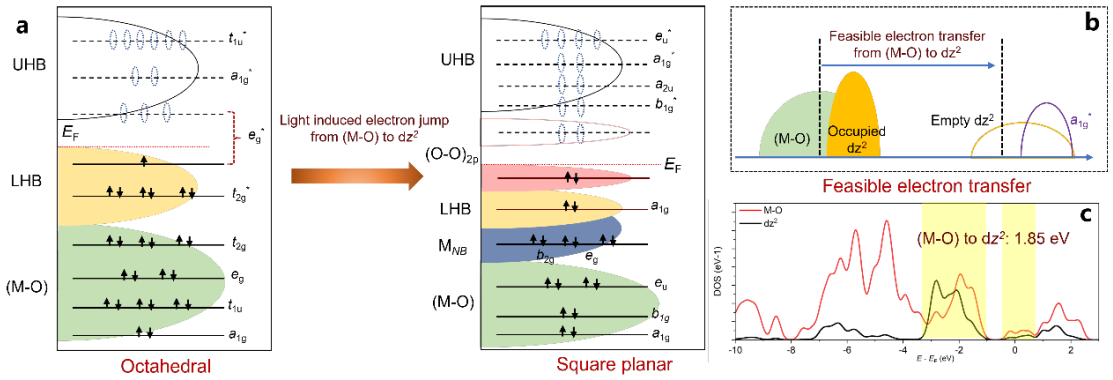

Fig. R2-6. The electron transfer from (M-O) to the non-overlapping region of dz^2 orbital with a_{1g}* band. (a) The schematic electronic configuration of the induced geometry conversion from octahedron to square planar *via* light irradiation; (b) feasible electron from (M-O) to dz^2 due to the partial overlapping of empty dz^2 orbital and a_{1g}* band; (c) PDOS of dz^2 orbital and (M-O) bands for NR-NiOOH model. Fig. R2-6 is represented as Fig. S12d and Fig. S29 in our revised Supporting Information.

In our work, a solar simulator (NBeT Solar-500, 300 W) was used as the light source to simulate AM 1.5G, and this source could provide sufficient energy for electrons from (M-O) to transfer to the non-overlapping region of dz^2 orbital with a_{1g}* band. To prove the ability of the photon in overcoming the high kinetic energy barrier required for geometry conversion, various factors such as electronic states, Ni-O coordinates numbers and Ni-O bond length were considered by conducting *operando* XAFS measurement (Fig. 3a and Fig. S9 to S13 in our revised version). Furthermore, we employed two wavelengths with filters (575 nm ~ 2.16 eV and 625 nm ~ 1.98 eV) during the photon-response measurement, and the results are shown in Fig. R2-7a and b (Fig. S22 in our revised Supporting Information). Based on our experimental results, both wavelengths could trigger COM, which further supports the hypothesis of which the ability of light in triggering the geometry conversion from octahedron to square planar based on an asynchronous pathway.

Thus, based on the above discussion, (O-O) coupling in NR-NiOOH is unfeasible in the absence of light due to its significant kinetic energy barrier. As such, NR-NiOOH does not exhibit COM under dark conditions, i.e., geometry conversion. However, when light is introduced, NR-NiOOH is able to proceed with COM that indicates the ability of the incorporated photon in overcoming this high kinetic energy barrier. At the same time, the AEM route on the dark conditions and COM route on the light conditions were verified with TMA^+ probe and isotope technique (Fig. 3c and d).

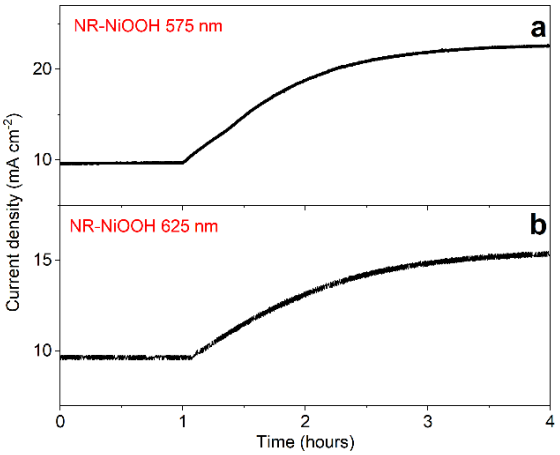

Fig. R2-7. (a) and (b) photon response measurement with two wavelength filters (575 nm ~ 2.16 eV and 625 nm ~ 1.98 eV). Fig. R2-7 is represented as Fig. S22 in our revised Supporting Information.

To enhance the clarity of our calculations, we have made the following revisions in our revised version:

1. We have added Fig. R2-5. (The energy barrier for geometry conversion from octahedron to square planar) in our revised Supporting Information (Fig. S21). At the same time, the photon response measurement with two wavelength filters (575 nm ~ 2.16 eV and 625 nm ~ 1.98 eV) was added in our revised Supporting Information (Fig. S22).

2. The discussion on the accessibility of the COM route in NR-NiOOH was added in our revised Supporting Information (Page 15, highlighted in crimson):

Discussion on the accessibility of COM route in NR-NiOOH

In contrast to the conventional OER process, the (O-O) coupling step in our proposed COM pathway was realized *via* photon-induced geometry conversion from octahedron to square planar. To realize the geometry conversion from octahedron to square planar, two neighboring (O-O) coupling will have to occur. In this calculation, two possible pathways were considered, *i.e.,* these two (O-O) couplings can occur either asynchronously or simultaneously. The simulation results showed that the calculated kinetic barrier based on asynchronous pathway was 1.741 eV, which is smaller than that of simultaneous pathway (2.148 eV) (Fig. S21 c and d). Since the kinetic barrier based on asynchronous pathway is lower than that of simultaneous pathway, the asynchronous pathway was considered, which means that a kinetic energy barrier of 1.741 eV must be overcome to achieve geometry conversion. In our proposed COM route, the geometry conversion from octahedron to square planar was triggered by light, which was realized by the photon-induced ligand-to-metal charge transfer (LMCT), electron transfer from (M-O) (ligand like character) to the non-overlapping region of dd_{z^2} orbitals with a_{1g}^* band (metal like character), as shown in in Fig. 5a. As shown in our PDOS results, the energy required for this type of electron transfer was 1.85 eV, which is larger than the energy barrier (1.7412 eV) of the geometry conversion from octahedron to square planar (Fig. S13d). This means that such a geometry conversion is feasible as long as the photon can provide sufficient energy to trigger the electron transfer from (M-O) to the non-overlapping region of dd_{z^2} orbitals with a_{1g}* band (despite the high kinetic energy barrier).

In our work, a solar simulator (NBeT Solar-500, 300 W) was used as the light source to simulate AM 1.5G, and it could provide sufficient energy to trigger the electron transfer from (M-O) to the non-overlapping region of dd_{z^2} orbitals with a_{1g}* band. To prove the ability of photon in overcoming the high kinetic energy barrier required for geometry conversion, various factors such as electronic states, Ni-O coordinates

numbers and Ni-O bond length were considered by conducting *operando* XAFS measurement (Fig. 3a and Fig. S9 to S13). Furthermore, we employed two wavelengths with filters (575 nm ~ 2.16 eV and 625 nm ~ 1.98 eV) during the photon-response measurement, and the results are shown in Fig. S22. Based on our experimental results, both wavelengths could trigger COM, which further supports the hypothesis that the geometry conversion from octahedron to square planar was triggered by light based on asynchronous pathway. Hence, based on the theoretical and experimental results, we have shown that (O-O) coupling could be triggered by light irradiation, which indicates that our proposed COM route was accessible under light conditions. The accessibility of COM route under light irradiations was further identified using operando XAFS, TMA^+ probe and isotope measurements (Fig. 3 c and d).

Q4- Besides, in Figure S21 the potential limiting step takes 3.00 eV for the COM to happen. This step has to be decoupled for the pathway to be meaningful. Assuming it is fully symmetric (which would be the best-case scenario), the overpotential would be 3 eV/2e- -1.23 V = 0.27 V vs RHE. This value is not so different compared to the value of 0.36 V vs RHE obtained in Norskov's pathway, which again calls for the assessment of the barriers.

Response: We are very thankful for this insightful suggestion. In our previous calculations, the deprotonation step involves two OH deprotonation which was calculated to take 3.00 eV. We agree with the reviewer that we should decouple these two OH deprotonation since their positions were asymmetric. As such, we have recalculated the process by decoupling the OH deprotonation step. Below show the detailed COM route used in the calculation:

$\Delta G_{C1} = \Delta G_{[O^*+O^*]} - \Delta G_{[OH^*+O^*]} - eU + \Delta G_{pH}$

$\Delta G_{C2} = \Delta G_{[O-O]} - \Delta G_{[O^*+O^*]}$ **(light dominated process)**

$\Delta G_{C3} = \Delta G_{[OO^*+OH^*]} - \Delta G_{[O-O]} - eU + \Delta G_{pH}$

$\Delta G_{C4} = 4.92\ eV - \Delta G_{[OO^*+OH^*]} + \Delta G_{[OH^*+OH^*]} - eU + \Delta G_{pH}$

$\Delta G_{C5} = \Delta G_{[OH^*+O^*]} - \Delta G_{[OH^*+OH^*]} - eU + \Delta G_{pH}$

The theoretical overpotential of COM was calculated based on the revised pathway as shown above. In contrast to the conventional OER process, the (O-O) coupling step in our proposed COM pathway was realized *via* photon-induced geometry conversion from octahedron to square planar. As mentioned in response to Q3, the geometry conversion from octahedron to square planar involved the occurrence of two neighboring (O-O) couplings, and this implies the participation of four oxygen atoms sites during the geometry conversion. Nevertheless, an OER process (with only one O_2 molecule produced) is a four-electron process, and during the OER calculation only one type of O-O bond formation will be considered, *i.e., either* OOH or (O-O) coupling. To demonstrate the geometry conversion from octahedron to square planar during the OER via calculation, the following models was employed in our DFT simulations.

A NR-NiOOH with one inner (O-O) coupling was used as the model (Fig. R2-8), whereby it possessed an octahedral configuration with one inner (O-O) coupling. When the OER process follows the COM route, there is a geometry conversion to square planar during the light dominated process. Based on the calculations, the potential limiting step was between C1 to C2, with a calculated overpotential of 0.093 V (Solvent). For the calculations based on the COM route, the starting model and OER calculation route were different from those in the AEM route. As such, it would be unfair to directly compare the calculated

overpotential value with that based on the AEM route.

Thus, we performed DFT simulations using NR-NiOOH, i.e., octahedron, as the initial model based on the same route as COM, i.e., the light provides the energy required for (O-O) coupling. The adsorption configurations for the calculation process were provided in Fig. R2-9a. It shows that this route follows the same route as COM, while no geometry conversion was demonstrated in the route. In this route, the calculated overpotential was 0.403 V (Fig. R2-9). Since the calculation employed the same model (NR-NiOOH) as that for AEM, we could conclude that it exhibited a lower overpotential (0.403 V) as compared to NR-NiOOH via AEM route (0.555 V). Moreover, since the calculation proceeded in the same route as COM, we could conclude that it possessed higher overpotential (0.403 V) as compared to the COM route (0.093 V). Hence, the COM route exhibited a significantly smaller overpotential as compared to the AEM route.

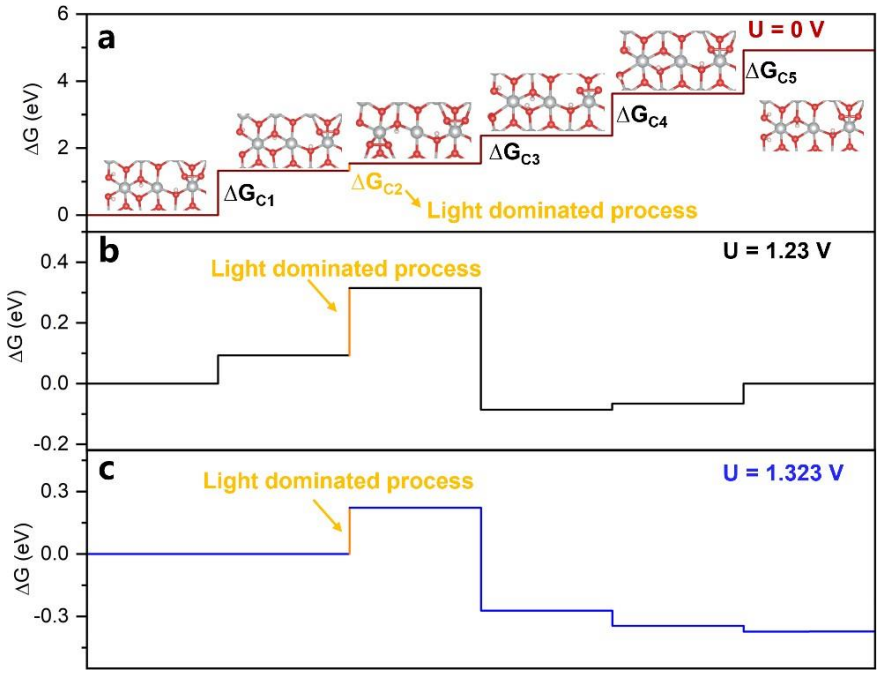

Fig. R2-8. Calculated reaction free energy change (Solvent) of COM based on NR-NiOOH with one inner (O-O) coupling as starting models, according to 0V, 1.23 V and the lowest bias potential (1.323 V) vs. RHE. Here, it should be noted that light-dominated process is a potential independent step. Fig. R2-8 is represented as Fig. S25 in our revised Supporting Information.

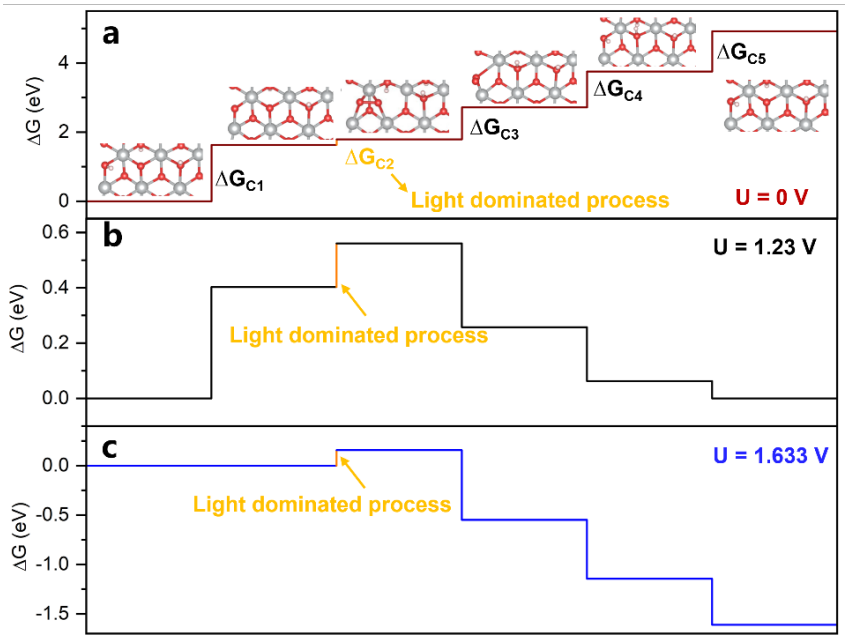

Fig. R2-9. Calculated reaction free energy (Solvent) of NR-NiOOH following the same route as COM route according to 0V, 1.23 V and the lowest bias potential (1.633 V). Here, it should be noted that light-dominated process is a potential independent step. It shows that this route follows the same route as COM, while no geometry conversion was demonstrated in the route. Fig. R2-9 is represented as Fig. S26 in our revised Supporting Information.

Next, we examined the accessibility of the COM route. In response to Q3, based on the calculation and experimental results, we have shown that (O-O) coupling could be triggered by light irradiation. This indicates that our proposed COM route was accessible under light condition. The accessibility of COM route under light irradiation was further identified experimentally using operando XAFS, TMA+ probe and isotope measurements (Figure 3 in our revised version).

OOH formation is an electrochemical process that is related to the applied potential, while (O-O) coupling in COM is triggered by light. Since the energy sources for OOH (AEM) and (O-O) coupling (COM) are different, it is difficult to compare which route is favorable based on their activation energy. However, based on the DFT calculations, model proceeding via COM route exhibited a smaller overpotential (0.093 V) as compared to that via AEM route (0.555 V). Hence, it is predicted that COM could dominate at the low potential range, while AEM could become accessible at high potential. The actual transition potential depends on the electrocatalyst structure and light irradiation, which will require further studies. In our work, the electrochemical measurement results showed that when NR-NiOOH was irradiated by a solar simulator (100 mW cm^{-2}), the COM route becomes more favorable than the AEM route within the potential range between 1.34 to 1.55 V vs RHE.

To enhance the clarity of our calculations, we have made the following revisions in our revised version:
1, in our revised manuscript, the discussion on the COM calculation is added in our revised manuscript (Page 13 highlighted in crimson):
To gain an in-depth understanding of the COM route, we performed comprehensively theoretical calculations of reaction free energy landscapes. Firstly, we examined the accessibility of the COM route.

In our proposed COM pathway, the (O-O) coupling step was realized *via* photon-induced geometry conversion from octahedron to square planar. The calculation results show that a kinetic energy barrier of 1.741 eV must be overcome to achieve geometry conversion (Fig. S21). Such a geometry can be realized by the electron transfer from (M-O) to dd_{z^2} orbital (1.85 eV), which can be satisfied by natural light (Fig. S13d) (Detailed discussion on the accessibility of COM is provided in Supplementary Discussions). Then, the calculated overpotentials of AEM and COM routes were compared to determine the favorable route under light conditions (the discussion on dark conditions was provided in Supplementary Discussions) (Fig. S23 to S26) (*36*). COM route exhibited a smaller overpotential as compared to AEM route, with proton transfer as the potential limiting step (Fig. S25). Here, it should be noted that the proton transfer step is also likely to be the rate determining step, as deduced from the Tafel slope and reaction orders (Fig. S5d and S27, detailed discussion is provided in Supplementary Text) (*37-38*). Hence, it is predicted that COM could dominate at the low potential range, while AEM could become accessible at a high potential range. The actual transition potential depends on the electrocatalyst structure and light irradiation, which will require further studies. In our work, the electrochemical measurement results showed that when NR-NiOOH was irradiated by a solar simulator (100 mW cm^{-2}), the COM route becomes more favorable than the AEM route within the potential range between 1.34 to 1.55 V vs RHE (Fig. 2c).

2. Fig. R2-8 and 2-9 were added in our revised Supporting Information as Fig. S25 and S26, respectively.

Q5- About Figures S3d and S21a: there must be something wrong, as the total energy of the reaction is in the range of 5-6 eV, while it should be 4.92 eV. This questions the whole modelling.

Response: We are very thankful for this insightful suggestion. We have mistakenly included O_2 desorption energy in the energy calculations, and this caused the total energy of our LOM and COM to be more than 4.92 eV. Since 4.92 eV refers to the total energy required to convert from H_2O to O_2 in the electrochemical overall reactions, we acknowledged that the extra energy needed for the desorption of O_2 should not be involved (*Nature Communications*, 10, 4993, 2019; *Nature Energy* 4, 329-338, 2019). In our revised manuscript, we have performed the LOM and COM calculations with reference to *Nature Energy* 4, 329-338, 2019. According to the new LOM and COM routes, the overall free energy required was 4.92 eV. The detailed LOM calculations and COM routes are provided below:

LOM:

$\Delta G_{L1} = \Delta G_{[O\text{-}O]} - \Delta G_{[OH^*+O^*]} - eU + \Delta G_{pH}$

$\Delta G_{L2} = \Delta G_{[OO^*+OH^*]} - \Delta G_{[O\text{-}O]} - eU + \Delta G_{pH}$

$\Delta G_{L3} = 4.92\ eV - \Delta G_{[OO^*+OH^*]} + \Delta G_{[OH^*+OH^*]} - eU + \Delta G_{pH}$

$\Delta G_{L4} = \Delta G_{[OH^*+O^*]} - \Delta G_{[OH^*+OH^*]} - eU + \Delta G_{pH}$

COM:

$\Delta G_{C1} = \Delta G_{[O^*+O^*]} - \Delta G_{[OH^*+O^*]} - eU + \Delta G_{pH}$

$\Delta G_{C2} = \Delta G_{[O\text{-}O]} - \Delta G_{[O^*+O^*]}$ **(light dominated process)**

$\Delta G_{C3} = \Delta G_{[OO^*+OH^*]} - \Delta G_{[O\text{-}O]} - eU + \Delta G_{pH}$

$\Delta G_{C4} = 4.92\ eV - \Delta G_{[OO^*+OH^*]} + \Delta G_{[OH^*+OH^*]} - eU + \Delta G_{pH}$

$\Delta G_{C5} = \Delta G_{[OH^*+O^*]} - \Delta G_{[OH^*+OH^*]} - eU + \Delta G_{pH}$

In our revised version, we have performed the DFT calculations based on the new LOM and COM routes

as shown above (Fig. S24 to S26 in our revised Supporting Information). At the same time, the new LOM and COM routes have been added in the theoretical calculation section in our revised Supporting Information (Page 7).

Q6- Finally, about Figure R37: it is not just a mechanism based on metal sites only, as the authors claim. The bridge sites on the rutile oxide are made of oxygen. Although the authors made long summaries of the articles I mentioned in the rebuttal letter, the discussion in the paper is too simplistic.

Response: We are very thankful for this comment. Figure R37 mentioned by the referee was from *Energy Environ. Sci.*, 2017,10, 2626-2637 (Figure 4 in their paper). In their work, the participation of bridge sites in the OER process was found during the steps from OOH to -OO, as shown in Fig. R2-10 (V and VI). They proposed that "Following this step, we propose the adsorption and deprotonation of an additional water molecule to form a precursor state of an -OOH group on the oxygen adsorbed on the Ru_{CUS} site (V), which was immediately followed by the proton transfer step, resulting in a hydrogen-bond-stabilized -OO group on the Ru_{CUS} site (VI). Lastly, the removal of the final proton destabilized the -OO group, leading to the release of oxygen gas (VII).". Based on their description, the bridge oxygen provided the adsorption site for proton, which was to stabilize the -OO group.

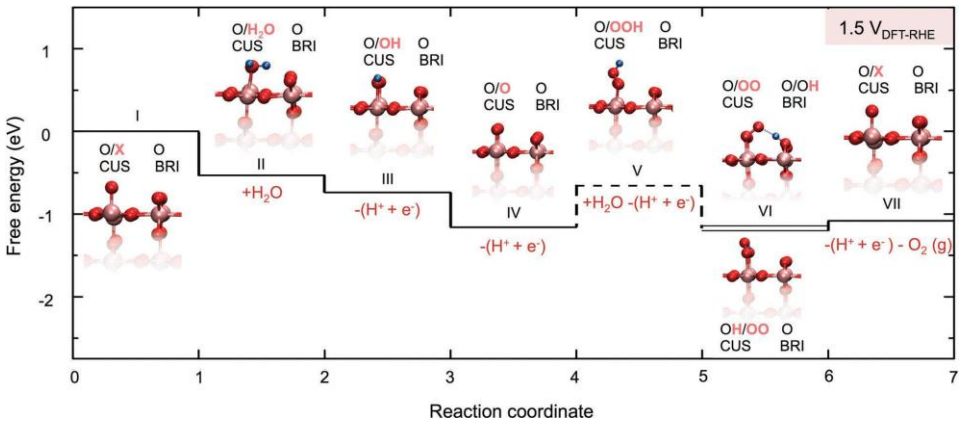

Fig. R2-10. OER scheme provided in *Energy Environ. Sci.*, 2017,10, 2626-2637.

In this work, the authors did not mention the feasibility of electron being transferred from the bridge oxygen site to the external circuit. However, the role of bridge oxygen site could be distinguished from the electron transfer route. As shown in their OER scheme, no electron transfer to the external circuit was observed from V to VI; an electron transfer was observed from VI to VII, which was attributed by the conversion from -OO to oxygen gas. Hence, the bridge oxygen site only provided an adsorption site for proton without electron transfer to the external circuit.

To provide in-depth understanding of the OER mechanism, this work was analyzed with respects to the oxygen redox activities. The emergence of oxidized oxygen states and participation of lattice oxygen atoms are characteristics of oxygen redox activities. According to their work, "No evidence was found to support lattice oxygen involvement reported previously for RuO_2, which is agreement with recent online electro-chemical mass spectrometry (OLEMS) measurement on oriented RuO_2 films and powders, showing no measurable oxygen exchange unlike Co-base perovskite", "The binding of oxygenated species on the Ru bridge sites on RuO_2 (110) is too strong to generate -OO, which is considered as the

surface precursor of molecular oxygen release". Hence, based on these discussions, we could conclude that their proposed OER mechanism was still solely based on metal redox activity.

To provide a more comprehensive understanding of our proposed COM route, we would like to give a summary of the reported OER mechanism and compare it with our proposed COM mechanism. In a conventional OER route, the types of electronic states around the Fermi level in the electrocatalyst are fixed. When the electronic states around Fermi level are metal bands, the OER would proceed via AEM route, with the variation of metal valence (Fig. R2-11a). The AEM route is widely known to solely involve metal redox. When the electronic states around Fermi level are oxygen orbitals, OER process would follow the LOM route as the sole oxygen redox activity (Fig. R2-11b). The oxygen redox activities within LOM were verified by researchers based on perovskite, and various techniques such as *operando* oxygen *K*-edge and metal *L*-edge X-ray absorption spectroscopy were used (Nature Communications 6, 6097, 2015).

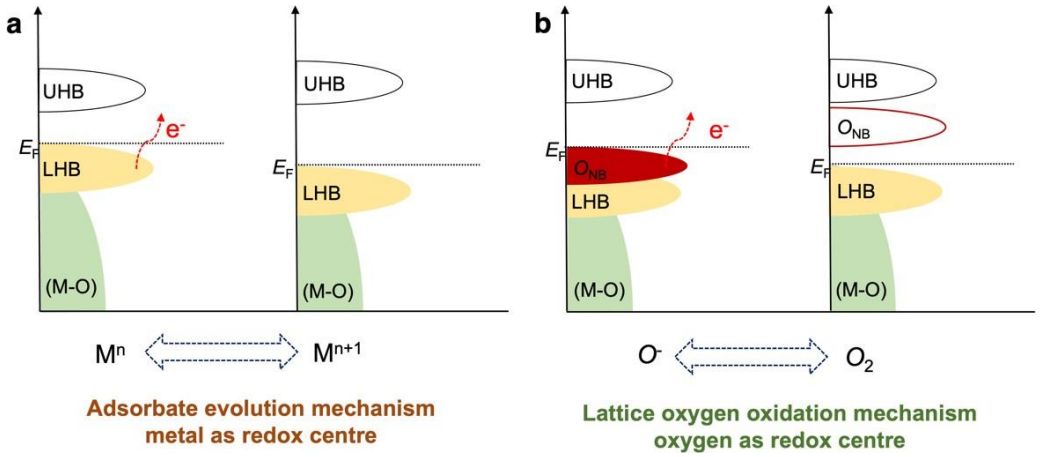

Fig. R2-11. (a) Schematic illustration of AEM route; (b) schematic illustration of LOM route. Fig. 1 in our revised manuscript.

In contrast to the conventional OER process, a reversible geometry conversion between octahedron to square planar arises in our proposed COM pathway. Three types of electron transfer processes are involved: 1, light-induced electron transfer from oxygen atom to metal atoms, with the decrease of Ni valence and appearance of non-bonding oxygen states (O_{NB}); 2, two-electron transfer from the non-bonding oxygen states (O_{NB}) to an external circuit (oxygen redox), with oxygen release; 3, another two-electron transfer from the metal orbital to an external circuit (metal redox), with metal valence increased and geometry back to octahedron (Fig. R2-12). The variations of geometry lead to the electronic states around the Fermi level exhibiting alternative metal/oxygen characters throughout the oxygen evolution process. This is the key reason behind the switchable metal and oxygen redox chemistry in our proposed COM route, i.e., octahedron (metal redox) and square planar (oxygen redox).

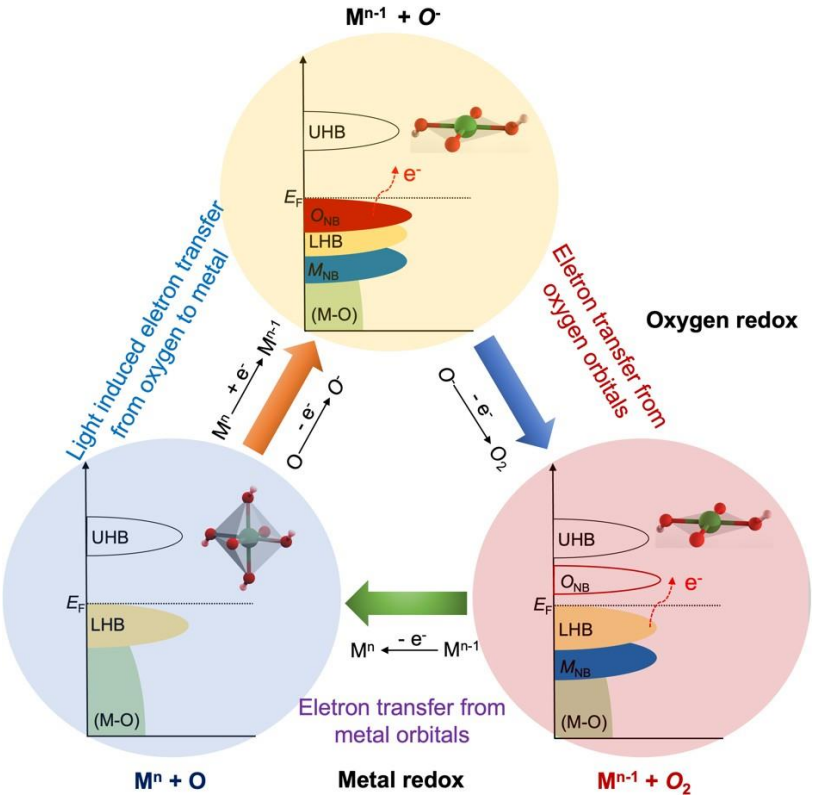

Fig. R2-12. Schematic illustration of the COM route. Fig. R2-12 is represented as Fig. 4 in our revised manuscript.

To make our proposed COM route much easier to understand, we have done the following revisions:

1, The redox activities of AEM and LOM routes (Fig. R2-11) have been added in our revised manuscript (Fig. 1). The original Fig. 1 in our previous manuscript has been moved to our revised Supporting Information (Fig. S3).

2, The redox activities of COM route (Fig. R2-12) were added to our revised manuscript (Fig. 4). The original Fig. 4 in our previous manuscript has been moved to our revised Supporting Information (as Fig. S20).

3, We have added the following paragraph in our revised manuscript (Page 13):

Thus, our OER route, termed as coupled oxygen evolution mechanism (COM), involves both oxygen and metal redox reactions. The variations of geometry lead to the electronic states around the Fermi level exhibiting alternative metal/oxygen characters throughout the oxygen evolution process. This is the key reason behind the switchable metal and oxygen redox chemistry in our proposed COM route, i.e., the octahedron (metal redox) and square planar (oxygen redox). Hence, our proposed COM is different from the OER mechanisms reported in previous studies, *i.e.*, partaking of metal and oxygen sites, OER process on square-planar configurations, interchange of high spin and low spin configurations, *etc.,* which proceeds either solely *via* a metal redox chemistry or an oxygen redox chemistry (*30-35*).

Q7- Still no coordinates of the simulated slabs with and without the adsorbates were given.

Response: We are very thankful for this insightful suggestion. All coordinates of the simulated slabs with and without adsorbates (POSCAR) have been provided in our revised Supporting Information (Page 77

to Page 102).

Q8- No description whatsoever to the method used to calculate the data labelled as “solvent” was provided

Response: We are very thankful for this insightful suggestion. In this work, the solvent effect was considered using the implicit solvation model implemented in the vasp code (*J. Chem. Phys.* 140, 084106 (2014). We have added this in our revised Supporting Information (Page 7).

Reviewer Reports on the Second Revision:

----- Referees' comments -----

Referee #1 (Remarks to the Author):

Wang et al. have further revised their manuscript to address outstanding issues, mostly relating to the DFT calculations. New DFT calculations were performed and photon response measurements. The revised presentation and new DFT calculations support that the COM is distinct from the other discussed mechanisms. The revised figures 1 and 4 help to better illustrate the differences among the mechanisms which further corroborates the distinction of the proposed COM. I find the conclusion significant that the dominant mechanism may change with applied potential.

The LOM mechanism and its benefits are now clearly defined. Additionally, the revised electrochemical analysis, incl. determination of the double layer capacitance, is state-of-the art. The supporting tables include all information to make fair comparisons.

Two points should be further strengthened prior to publication:

1) Performing DFT calculations at an overpotential relevant to experiments
The authors have shown the effective barrier height with applied potential, which is visually helpful. Was the structure relaxed at the applied potential before the calculations of the barrier height? Asked differently: is the surface at 0 V the same as compared to 1.785 V in the used implicit electrolyte? This would be surprising for an oxide.

2) Accessibility of the COM route
The calculated kinetic barrier is 1.741 eV which is about 720 nm. Both experiments were performed at lower wavelength / higher energy. An additional control experiment at a wavelength above 720 nm would help to bracket the calculated value and thereby further link experiment and calculations.

Overall, the novel mechanism has been supported better by revision. The use of light to induce a coordination change a highly interesting and very general approach to optimize electrocatalysts that are limited in darkness. I expect that the study would spark much fundamental to exploit the new mechanism in the context of the OER and many other electrochemical reactions. If the transition between the COM and AEM can be understood better, electrocatalysts operating by the COM may also be an option for applied research at high current density. I think a new mechanism of the important oxygen evolution reaction is

exciting and could be published in Nature.

Referee #2 (Remarks to the Author):

The authors addressed my comments and I have no further questions. I only ask the authors to note in the manuscript that implicit solvation as implemented in vasp is not able to capture hydrogen bonding (see Catalysis Today 323, 2019, 35-43) and, thus, the energy diagrams presented are merely indicative rather than conclusive.

Author Rebuttals to Second Revision:

Referee #1 (Remarks to the Author):

Wang et al. have further revised their manuscript to address outstanding issues, mostly relating to the DFT calculations. New DFT calculations were performed and photon response measurements. The revised presentation and new DFT calculations support that the COM is distinct from the other discussed mechanisms. The revised figures 1 and 4 help to better illustrate the differences among the mechanisms which further corroborates the distinction of the proposed COM. I find the conclusion significant that the dominant mechanism may change with applied potential.

The LOM mechanism and its benefits are now clearly defined. Additionally, the revised electrochemical analysis, incl. determination of the double layer capacitance, is state-of-the art. The supporting tables include all information to make fair comparisons.

Response: We sincerely appreciate the reviewer for the time and efforts in assessing our manuscript, together with very valuable comments. In our revised version, we have faithfully addressed all the reviewer's concerns.

Two points should be further strengthened prior to publication:

1) Performing DFT calculations at an overpotential relevant to experiments
The authors have shown the effective barrier height with applied potential, which is visually helpful. Was the structure relaxed at the applied potential before the calculations of the barrier height? Asked differently: is the surface at 0 V the same as compared to 1.785 V in the used implicit electrolyte? This would be surprising for an oxide.

Response: We appreciate the reviewer for the valuable comment. According to the reviewer's suggestion, the structure was relaxed under the applied potential of 1.412 V (the potential of 10 mA cm^{-2} under light irradiation) and 1.785 V, respectively. The simulation results showed that the surface structure at 0 V is the same as those at 1.412 V and 1.785 V (Fig. R1 and detailed coordination information is provided in Table R1). Hence, the applied potential does not affect the optimized model and has negligible influence on the DFT calculations.

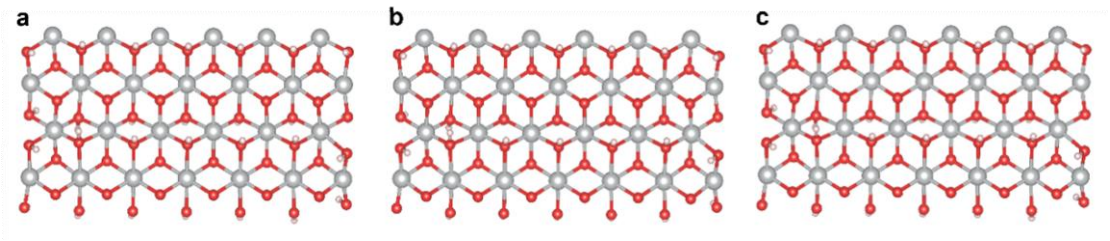

Fig. R1. The relaxed NR-NiOOH structure under the potential of 0 V (a), 1.412 V (b) and 1.785 V (c). Fig. S28 in our revised Supporting Information.

Table R1. The coordination information of NR-NiOOH structure under the potential of 0 V, 1.412 V and 1.785 V. The differences between U=1.412 V or 1.785 V and U=0 are highlighted in crimson. It can be seen that the difference ($\Delta_{x,y,x}$) between U=1.412 V or 1.785 V and U=0 is nearly zero.

ion	U= 0			U= 1.412			U=1.785			Difference ($U_{1.412}$-U_0)			Difference ($U_{1.785}$-U_0)		
	x	y	z	x	y	z	x	y	z	Δ_x	Δ_y	Δ_z	Δ_x	Δ_y	Δ_z
Ni1	0.2199	0.2567	0.1365	0.2209	0.2594	0.1357	0.2199	0.2563	0.1366	0.0010	0.0027	-0.0008	-0.0001	-0.0004	0.0001
Ni2	0.2210	0.7555	0.1445	0.2214	0.7537	0.1415	0.2209	0.7554	0.1445	0.0004	-0.0017	-0.0030	-0.0001	-0.0001	-0.0001
Ni3	0.2618	0.0058	0.1396	0.2627	0.0049	0.1400	0.2617	0.0059	0.1397	0.0008	-0.0009	0.0004	-0.0002	0.0001	0.0001
Ni4	0.2642	0.5056	0.1403	0.2647	0.5058			0.5055	0.1403	0.0005	0.0002	-0.0006	-0.0001	-0.0001	0.0000
Ni5	0.3125	0.2519	0.1385	0.3127	0.2510	0.1388	0.3126	0.2520	0.1387	0.0002	-0.0009	0.0002	0.0001	0.0001	0.0001
Ni6	0.3134	0.7575	0.1409	0.3137	0.7552	0.1415	0.3133	0.7574	0.1408	0.0003	-0.0023	0.0006	-0.0001	-0.0001	0.0000
Ni7	0.3605	0.0040	0.1393	0.3604	0.0025	0.1393	0.3605	0.0041	0.1394	-0.0001	-0.0015	0.0000	0.0000	0.0001	0.0001
Ni8	0.3606	0.5041	0.1395	0.3608	0.5018	0.1396	0.3606	0.5042	0.1395	0.0002	-0.0024	0.0001	0.0000	0.0000	0.0000
Ni9	0.4094	0.2522	0.1395	0.4095	0.2497	0.1397	0.4094	0.2521	0.1395	0.0001	-0.0025	0.0002	0.0000	0.0000	0.0000
Ni10	0.4097	0.7534	0.1390	0.4098	0.7508	0.1392	0.4097	0.7534	0.1390	0.0001	-0.0026	0.0002	0.0000	0.0000	-0.0001
Ni11	0.4581	0.0016	0.1392	0.4579	0.0003	0.1389	0.4581	0.0016	0.1392	-0.0002	-0.0013	-0.0003	0.0001	0.0000	0.0000
Ni12	0.4577	0.5019	0.1391	0.4577	0.5004	0.1389	0.4577	0.5019	0.1390	-0.0001	-0.0014	-0.0002	0.0000	0.0000	-0.0001
Ni13	0.5069	0.2505	0.1395	0.5068	0.2483	0.1397	0.5068	0.2504	0.1394	-0.0001	-0.0021	0.0002	-0.0001	0.0000	-0.0001
Ni14	0.5065	0.7505	0.1392	0.5063	0.7484	0.1393	0.5066	0.7507	0.1392	-0.0002	-0.0021	0.0001	0.0001	0.0002	0.0000

Ni15	0.5555	0.9992	0.1401	0.5554	0.9975	0.1399	0.5555	0.9993	0.1400	-0.0001	-0.0017	-0.0002	0.0000	0.0001	-0.0001
Ni16	0.5553	0.4992	0.1391	0.5552	0.4979	0.1389	0.5552	0.4993	0.1392	-0.0001	-0.0013	-0.0002	0.0000	0.0001	0.0001
Ni17	0.6042	0.2484	0.1398	0.6038	0.2459	0.1399	0.6043	0.2485	0.1398	-0.0004	-0.0025	0.0001	0.0001	0.0001	0.0000
Ni18	0.6034	0.7485	0.1399	0.6032	0.7460	0.1402	0.6035	0.7486	0.1399	-0.0003	-0.0025	0.0003	0.0000	0.0001	0.0000
Ni19	0.6529	0.9968	0.1412	0.6528	0.9948	0.1409	0.6530	0.9968	0.1413	-0.0001	-0.0019	-0.0003	0.0000	0.0001	0.0000
Ni20	0.6528	0.4978	0.1389	0.6528	0.4968	0.1390	0.6529	0.4978	0.1389	-0.0001	-0.0010	0.0001	0.0000	0.0000	0.0000
Ni21	0.7014	0.2474	0.1397	0.7009	0.2457	0.1401	0.7015	0.2474	0.1397	-0.0005	-0.0017	0.0004	0.0001	0.0001	0.0000
Ni22	0.7002	0.7474	0.1399	0.7002	0.7461	0.1405	0.7003	0.7475	0.1399	-0.0001	-0.0013	0.0006	0.0000	0.0001	0.0000
Ni23	0.7507	0.9949	0.1381	0.7504	0.9976	0.1369	0.7507	0.9951	0.1382	-0.0003	0.0027	-0.0012	0.0001	0.0002	0.0001
Ni24	0.7508	0.4986	0.1406	0.7505	0.4978	0.1413	0.7509	0.4984	0.1405	-0.0003	-0.0007	0.0006	0.0001	-0.0002	-0.0001
Ni25	0.7925	0.2466	0.1385	0.7922	0.2486	0.1368	0.7926	0.2464	0.1385	-0.0002	0.0020	-0.0017	0.0001	-0.0001	0.0000
Ni26	0.7932	0.7471	0.1389	0.7920	0.7479	0.1366	0.7932	0.7471	0.1389	-0.0012	0.0009	-0.0023	0.0000	0.0000	0.0000
H1	0.2095	0.0950	0.0987	0.2113	0.1022	0.1003	0.2093	0.0947	0.0988	0.0018	0.0072	0.0016	-0.0002	-0.0003	0.0001
H2	0.2179	0.5863	0.1012	0.2187	0.5867	0.1011	0.2181	0.5867	0.1010	0.0008	0.0005	-0.0001	0.0001	0.0004	-0.0002
H3	0.2662	0.1646	0.1765	0.2654	0.1655	0.1772	0.2662	0.1648	0.1767	-0.0008	0.0008	0.0007	0.0000	0.0002	0.0002
H4	0.2691	0.6612	0.1797	0.2683	0.6593	0.1803	0.2690	0.6611	0.1798	-0.0008	-0.0019	0.0005	-0.0001	-0.0002	0.0000
H5	0.2184	0.4261	0.1804	0.2185	0.4200	0.1793	0.2181	0.4260	0.1801	0.0001	-0.0061	-0.0011	-0.0003	-0.0001	-0.0003

H6	0.2140	0.9209	0.1827	0.2144	0.9181	0.1811	0.2139	0.9205	0.1829	0.0004	-0.0028	-0.0016	-0.0001	-0.0003	0.0002
H7	0.3098	0.0784	0.0954	0.3095	0.0783	0.0960	0.3097	0.0785	0.0955	-0.0003	-0.0001	0.0007	-0.0001	0.0001	0.0001
H8	0.3085	0.5710	0.0949	0.3092	0.5720	0.0965	0.3085	0.5706	0.0949	0.0007	0.0011	0.0016	0.0000	-0.0004	-0.0001
H9	0.2681	0.3504	0.1008	0.2686	0.3496	0.1010	0.2681	0.3502	0.1009	0.0004	-0.0008	0.0001	0.0000	-0.0002	0.0000
H10	0.2668	0.8460	0.1034	0.2678	0.8468	0.1042	0.2666	0.8457	0.1032	0.0010	0.0008	0.0008	-0.0001	-0.0003	-0.0002
H11	0.3606	0.1654	0.1740	0.3601	0.1637	0.1745	0.3607	0.1655	0.1741	-0.0005	-0.0018	0.0005	0.0001	0.0001	0.0001
H12	0.3613	0.6656	0.1736	0.3612	0.6629	0.1744	0.3613	0.6658	0.1736	-0.0001	-0.0027	0.0007	0.0000	0.0002	0.0000
H13	0.3096	0.4395	0.1843	0.3092	0.4388	0.1853	0.3096	0.4392	0.1843	-0.0004	-0.0006	0.0009	0.0000	-0.0003	-0.0001
H14	0.3138	0.9320	0.1839	0.3135	0.9309	0.1851	0.3139	0.9319	0.1838	-0.0002	-0.0010	0.0013	0.0001	0.0000	-0.0001
H15	0.4076	0.0756	0.0950	0.4072	0.0742	0.0953	0.4075	0.0757	0.0950	-0.0004	-0.0014	0.0002	-0.0001	0.0000	0.0000
H16	0.4077	0.5753	0.0944	0.4075	0.5740	0.0947	0.4076	0.5755	0.0943	-0.0002	-0.0013	0.0003	-0.0002	0.0002	-0.0001
H17	0.3609	0.3422	0.1056	0.3608	0.3396	0.1065	0.3610	0.3422	0.1056	-0.0001	-0.0026	0.0010	0.0001	-0.0001	0.0000
H18	0.3613	0.8425	0.1048	0.3610	0.8405	0.1059	0.3613	0.8425	0.1048	-0.0003	-0.0020	0.0011	0.0000	0.0000	0.0000
H19	0.4579	0.1636	0.1736	0.4577	0.1620	0.1740	0.4579	0.1637	0.1737	-0.0003	-0.0016	0.0004	-0.0001	0.0001	0.0000
H20	0.4577	0.6636	0.1733	0.4575	0.6621	0.1736	0.4577	0.6638	0.1732	-0.0002	-0.0016	0.0003	0.0000	0.0001	-0.0001
H21	0.4097	0.4318	0.1837	0.4097	0.4306	0.1843	0.4099	0.4321	0.1836	0.0000	-0.0012	0.0006	0.0002	0.0004	-0.0001
H22	0.4110	0.9302	0.1835	0.4107	0.9297	0.1839	0.4112	0.9302	0.1835	-0.0003	-0.0005	0.0003	0.0001	0.0000	-0.0001

H23	0.5057	0.0724	0.0953	0.5055	0.0711	0.0956	0.5055	0.0726	0.0952	-0.0002	-0.0013	0.0003	-0.0001	0.0002	-0.0001
H24	0.5050	0.5726	0.0946	0.5049	0.5714	0.0950	0.5048	0.5728	0.0945	-0.0001	-0.0011	0.0004	-0.0002	0.0002	-0.0001
H25	0.4582	0.3393	0.1053	0.4580	0.3371	0.1062	0.4582	0.3392	0.1053	-0.0002	-0.0022	0.0009	-0.0001	-0.0002	0.0000
H26	0.4584	0.8401	0.1047	0.4581	0.8382	0.1055	0.4585	0.8401	0.1047	-0.0003	-0.0019	0.0008	0.0001	-0.0001	0.0000
H27	0.5553	0.1617	0.1740	0.5552	0.1599	0.1743	0.5553	0.1619	0.1739	-0.0001	-0.0018	0.0003	0.0000	0.0002	-0.0001
H28	0.5545	0.6608	0.1736	0.5545	0.6593	0.1740	0.5546	0.6610	0.1737	0.0000	-0.0014	0.0004	0.0000	0.0002	0.0001
H29	0.5080	0.4290	0.1835	0.5081	0.4282	0.1840	0.5082	0.4288	0.1835	0.0001	-0.0008	0.0005	0.0002	-0.0001	0.0000
H30	0.5077	0.9278	0.1840	0.5076	0.9271	0.1844	0.5078	0.9277	0.1840	-0.0001	-0.0007	0.0005	0.0001	-0.0002	0.0000
H31	0.6041	0.0697	0.0964	0.6040	0.0678	0.0967	0.6041	0.0697	0.0964	-0.0001	-0.0018	0.0003	0.0000	0.0000	0.0000
H32	0.6022	0.5707	0.0948	0.6024	0.5697	0.0952	0.6020	0.5707	0.0948	0.0002	-0.0010	0.0004	-0.0002	0.0000	0.0001
H33	0.5558	0.3367	0.1052	0.5558	0.3348	0.1060	0.5559	0.3366	0.1052	0.0000	-0.0019	0.0008	0.0001	-0.0001	0.0000
H34	0.5554	0.8379	0.1054	0.5553	0.8356	0.1063	0.5555	0.8380	0.1054	0.0000	-0.0024	0.0008	0.0001	0.0001	-0.0001
H35	0.6531	0.1606	0.1745	0.6529	0.1580	0.1749	0.6532	0.1607	0.1745	-0.0002	-0.0026	0.0004	0.0001	0.0000	0.0000
H36	0.6516	0.6585	0.1740	0.6519	0.6573	0.1748	0.6517	0.6586	0.1739	0.0003	-0.0012	0.0008	0.0000	0.0001	0.0000
H37	0.6060	0.4262	0.1835	0.6063	0.4255	0.1840	0.6063	0.4263	0.1835	0.0003	-0.0007	0.0005	0.0003	0.0000	0.0000
H38	0.6043	0.9247	0.1852	0.6047	0.9234	0.1857	0.6043	0.9248	0.1851	0.0004	-0.0013	0.0006	0.0000	0.0001	0.0000
H39	0.7024	0.0670	0.0965	0.7015	0.0684	0.0966	0.7024	0.0669	0.0965	-0.0008	0.0014	0.0001	0.0001	-0.0001	0.0000

H40	0.6998	0.5723	0.0952	0.7000	0.5727	0.0967	0.6996	0.5720	0.0951	0.0002	0.0003	0.0015	-0.0002	-0.0003	-0.0001
H41	0.6533	0.3343	0.1051	0.6532	0.3329	0.1062	0.6534	0.3344	0.1051	-0.0001	-0.0014	0.0011	0.0001	0.0001	-0.0001
H42	0.6519	0.8368	0.1059	0.6522	0.8337	0.1067	0.6520	0.8368	0.1059	0.0002	-0.0030	0.0008	0.0000	0.0001	0.0000
H43	0.7487	0.1537	0.1765	0.7491	0.1521	0.1766	0.7487	0.1542	0.1766	0.0004	-0.0016	0.0000	0.0000	0.0004	0.0001
H44	0.7462	0.6549	0.1779	0.7475	0.6561	0.1793	0.7462	0.6549	0.1779	0.0013	0.0012	0.0013	0.0000	0.0001	-0.0001
H45	0.7039	0.4250	0.1833	0.7042	0.4238	0.1847	0.7042	0.4249	0.1834	0.0002	-0.0012	0.0014	0.0002	-0.0001	0.0001
H46	0.7015	0.9197	0.1848	0.7025	0.9190	0.1845	0.7015	0.9198	0.1849	0.0010	-0.0007	-0.0003	0.0000	0.0001	0.0001
H47	0.7981	0.1113	0.0913	0.7966	0.1080	0.0928	0.7983	0.1113	0.0913	-0.0015	-0.0034	0.0015	0.0001	0.0000	0.0000
H48	0.8007	0.5752	0.1033	0.7984	0.5864	0.1030	0.8007	0.5754	0.1032	-0.0023	0.0111	-0.0004	-0.0001	0.0002	-0.0002
H49	0.7482	0.3401	0.1018	0.7476	0.3426	0.1030	0.7483	0.3397	0.1017	-0.0006	0.0025	0.0012	0.0001	-0.0004	-0.0001
H50	0.7457	0.8388	0.1007	0.7459	0.8389	0.1004	0.7458	0.8387	0.1008	0.0002	0.0001	-0.0003	0.0000	-0.0001	0.0001
H51	0.7998	0.3818	0.1853	0.8000	0.3840	0.1843	0.8001	0.3816	0.1852	0.0002	0.0022	-0.0010	0.0003	-0.0002	-0.0001
H52	0.8019	0.9192	0.1736	0.8011	0.9086	0.1727	0.8018	0.9191	0.1738	-0.0007	-0.0107	-0.0009	0.0000	-0.0001	0.0002
O1	0.2140	0.1016	0.0602	0.2114	0.1037	0.0609	0.2139	0.1019	0.0603	-0.0025	0.0022	0.0007	-0.0001	0.0003	0.0001
O2	0.2308	0.6091	0.0665	0.2263	0.5986	0.0631	0.2313	0.6103	0.0665	-0.0045	-0.0106	-0.0034	0.0005	0.0012	0.0001
O3	0.3072	0.0520	0.0581	0.3071	0.0597	0.0577	0.3072	0.0528	0.0582	-0.0001	0.0076	-0.0004	-0.0001	0.0007	0.0000
O4	0.3069	0.5099	0.0645	0.3069	0.5306	0.0610	0.3068	0.5086	0.0647	0.0000	0.0207	-0.0034	0.0000	-0.0013	0.0002

O5	0.2229	0.9149	0.2201	0.2235	0.9098	0.2185	0.2229	0.9141	0.2203	0.0006	-0.0052	-0.0016	0.0000	-0.0009	0.0001
O6	0.4053	0.0528	0.0574	0.4055	0.0589	0.0567	0.4050	0.0534	0.0573	0.0002	0.0061	-0.0006	-0.0004	0.0006	-0.0001
O7	0.4062	0.5512	0.0568	0.4063	0.5586	0.0561	0.4059	0.5519	0.0567	0.0001	0.0074	-0.0007	-0.0003	0.0007	-0.0001
O8	0.3157	0.9600	0.2210	0.3161	0.9616	0.2219	0.3156	0.9593	0.2210	0.0004	0.0016	0.0009	-0.0001	-0.0007	0.0000
O9	0.5042	0.0476	0.0578	0.5042	0.0543	0.0572	0.5040	0.0479	0.0577	0.0000	0.0067	-0.0006	-0.0002	0.0003	-0.0001
O10	0.5030	0.5490	0.0570	0.5031	0.5557	0.0565	0.5026	0.5494	0.0569	0.0002	0.0067	-0.0005	-0.0003	0.0004	-0.0001
O11	0.4108	0.4596	0.2209	0.4113	0.4627	0.2210	0.4111	0.4603	0.2208	0.0004	0.0032	0.0000	0.0003	0.0008	-0.0001
O12	0.4131	0.9532	0.2212	0.4131	0.9564	0.2211	0.4133	0.9533	0.2212	0.0000	0.0032	-0.0001	0.0002	0.0001	0.0000
O13	0.6038	0.0428	0.0590	0.6038	0.0503	0.0582	0.6038	0.0428	0.0590	0.0000	0.0075	-0.0008	0.0001	0.0000	0.0000
O14	0.5999	0.5476	0.0571	0.6004	0.5545	0.0567	0.5995	0.5478	0.0572	0.0005	0.0070	-0.0005	-0.0004	0.0002	0.0000
O15	0.5099	0.4543	0.2209	0.5104	0.4565	0.2211	0.5102	0.4542	0.2209	0.0004	0.0022	0.0002	0.0003	-0.0001	0.0000
O16	0.5094	0.9507	0.2217	0.5094	0.9534	0.2218	0.5094	0.9504	0.2217	0.0000	0.0027	0.0001	0.0001	-0.0003	0.0000
O17	0.7026	0.0269	0.0610	0.7021	0.0449	0.0585	0.7028	0.0262	0.0611	-0.0006	0.0179	-0.0025	0.0001	-0.0007	0.0001
O18	0.6981	0.5511	0.0573	0.6991	0.5591	0.0579	0.6978	0.5498	0.0573	0.0010	0.0080	0.0006	-0.0003	-0.0013	0.0000
O19	0.6082	0.4504	0.2210	0.6086	0.4525	0.2212	0.6087	0.4502	0.2211	0.0004	0.0021	0.0002	0.0004	-0.0002	0.0001
O20	0.6048	0.9458	0.2231	0.6048	0.9478	0.2233	0.6048	0.9455	0.2231	0.0000	0.0020	0.0003	0.0000	-0.0003	0.0000
O21	0.7845	0.1380	0.0575	0.7901	0.1271	0.0552	0.7845	0.1380	0.0577	0.0056	-0.0109	-0.0024	0.0000	0.0000	0.0001

O22	0.7947	0.5773	0.0651	0.7972	0.5848	0.0637	0.7945	0.5778	0.0649	0.0026	0.0075	-0.0014	-0.0001	0.0005	-0.0001
O23	0.7054	0.4602	0.2195	0.7052	0.4589	0.2210	0.7057	0.4603	0.2195	-0.0002	-0.0013	0.0014	0.0003	0.0001	0.0000
O24	0.7013	0.9358	0.2231	0.7015	0.9371	0.2226	0.7011	0.9365	0.2232	0.0002	0.0013	-0.0005	-0.0002	0.0006	0.0001
O25	0.7873	0.3554	0.2198	0.7866	0.3553	0.2180	0.7874	0.3554	0.2196	-0.0007	-0.0001	-0.0018	0.0001	0.0000	-0.0002
O26	0.7970	0.9183	0.2121	0.7953	0.9015	0.2111	0.7968	0.9179	0.2122	-0.0017	-0.0168	-0.0011	-0.0001	-0.0004	0.0001
O27	0.2314	0.4031	0.2150	0.2314	0.3963	0.2140	0.2308	0.4039	0.2151	0.0000	-0.0069	-0.0011	-0.0007	0.0008	0.0000
O28	0.3085	0.4997	0.2151	0.3088	0.5028	0.2149	0.3085	0.4989	0.2153	0.0002	0.0031	-0.0003	-0.0001	-0.0008	0.0001

2) Accessibility of the COM route

The calculated kinetic barrier is 1.741 eV which is about 720 nm. Both experiments were performed at lower wavelength / higher energy. An additional control experiment at a wavelength above 720 nm would help to bracket the calculated value and thereby further link experiment and calculations.

Response: We are very thankful for this insightful suggestion. We agree with the reviewer that using wavelengths of above 720 nm would help to validate the calculated value. As such, we have conducted additional photon response measurements using four wavelength filters, i.e., 700 nm ~ 1.771 eV; 750 nm ~ 1.653 eV; 800 nm ~ 1.550 eV; 900 nm ~ 1.378 eV. Generally, with higher wavelength (lower energy), the distinct stages (effects on current density with the light source switched on and off) were less obvious. Specifically, it is shown that with wavelength of 575 nm (Fig. R2a) and 625 nm (Fig. R2b), the current increased significantly when light was switch on. As the wavelength used increased to 700 nm (Fig. R2c), an increase in the current can still be observed. Since the calculated kinetic barrier is about 720 nm, it is expected that the current increment with light source of 750 nm to be greatly weakened. As shown in Fig. R2d, the current increment can be barely observed when a light source of 750 nm was used. This result suggests that the wavelength of 750 nm could trigger COM minimally, which is in good agreement with our calculations. Interestingly, switching on the light source with higher wavelength of 800 nm (Fig. R2e) to 900 nm (Fig. R2f) did not trigger any observable change in the current, which suggests the inability of these wavelengths in triggering COM. This result further validates our calculation of the kinetic energy barrier needed to overcome to trigger COM.

Thus, based on these results, it can be concluded that the lowest wavelength that can trigger COM is around 750 nm (1.653 eV), which is relatively close to our calculations (1.741 eV). We have included these results in Fig. S23 of our revised Supporting Information (Page 53, highlighted in yellow).

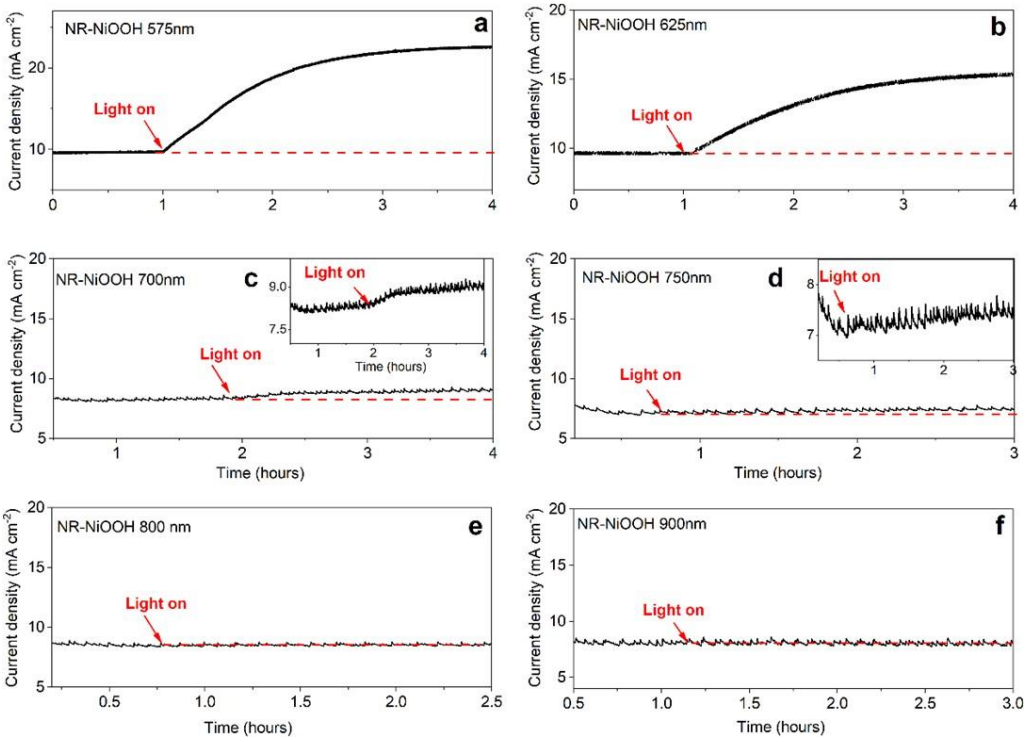

Fig. R2. Photon response measurement. The photon response measurement was equipped with the wavelength filter of 575 nm (a), 625 nm (b), 700 nm (c), 750 nm (d) 800 nm (e) and 900 nm (f), respectively. Fig. S23 in our revised Supporting Information.

Overall, the novel mechanism has been supported better by revision. The use of light to induce a coordination change a highly interesting and very general approach to optimize electrocatalysts that are limited in darkness. I expect that the study would spark much fundamental to exploit the new mechanism in the context of the OER and many other electrochemical reactions. If the transition between the COM and AEM can be understood better, electrocatalysts operating by the COM may also be an option for applied research at high current density. I think a new mechanism of the important oxygen evolution reaction is exciting and could be published in Nature.

Response: We thank the reviewer for the time and efforts in assessing our manuscript and their positive remarks.

Referee #2 (Remarks to the Author):

The authors addressed my comments and I have no further questions. I only ask the authors to note in the manuscript that implicit solvation as implemented in vasp is not able to capture hydrogen bonding (see Catalysis Today 323, 2019, 35-43) and, thus, the energy diagrams presented are merely indicative rather than conclusive.

Response: We are very thankful for this insightful suggestion. We have added the following sentence "It should be noted that the implicit solvation implemented in the VASP is unable to capture hydrogen bonding (33). Hence, the energy diagrams and energy barrier presented in this study are indicative rather than conclusive." in our revised manuscript (Paragraph 2, Page 7 highlighted in yellow). Meanwhile, we have included this reference in our revised manuscript (see reference 33, highlighted in yellow).